Dissertation zur Erlangung des Doktorgrades
der Fakultät für Chemie und Pharmazie
der Ludwig-Maximilians-Universität München

Functional Investigation of the Lanthanide-Dependent Methanol Dehydrogenase from *Methylacidiphilum fumariolicum* SolV

Bérénice Olivia Gea Jahn
aus
München, Deutschland

2020

Erklärung

Diese Dissertation wurde im Sinne von § 7 der Promotionsordnung vom 28. November 2011 von Frau Prof. Dr. Lena J. Daumann betreut.

Eidesstattliche Versicherung

Diese Dissertation wurde eigenständig und ohne unerlaubte Hilfe erarbeitet.

München, 08.07.2020

_____

Bérénice Jahn

Dissertation eingereicht am	08.07.2020
1. Gutachterin:	Prof. Dr. Lena J. Daumann
2. Gutachter:	PD Dr. Dietmar Martin
Mündliche Prüfung am	27.08.2020

Diese Arbeit wurde in der Zeit von Januar 2017 bis Juli 2020 am Department für Chemie der Ludwig-Maximilians-Universität München unter Anleitung von Frau Prof. Dr. Lena J. Daumann durchgeführt.

Meinen Eltern & Max

„W życiu nie ma rzeczy, których należy się bać, są tylko rzeczy, które trzeba zrozumieć. Musimy zrozumieć więcej, aby móc bać się mniej.”

[Nothing in life is to be feared, it is only to be understood. Now is the time to understand more, so that we may fear less.]

Maria Skłodowska-Curie

Contents

Table of Contents

Summary

I. Summary

The biological relevance of lanthanides remained long unknown. However, recent research has shown that lanthanides are utilized by a variety of methanotrophs and methylotrophs. These bacteria carry lanthanides as central metal ions in the active sites of methanol dehydrogenases (MDH) to metabolize methanol and thereby generate energy. MDH enzymes contain two cofactors: a metal ion and the prosthetic group pyrroloquinoline quinone (PQQ). Lanthanides are potent Lewis acids and were recently discovered to serve as central metal ion in MDH enzymes, a role which is commonly fulfilled by Ca^{2+} ions.

Although the lanthanide-dependent XoxF-type MDH enzyme is evolutionarily older and more widespread in nature than its Ca^{2+}-dependent MxaF counterpart, its mechanism and the reason why lanthanides are preferred over Ca^{2+} in these enzymes is not fully understood. Therefore, this work studies a lanthanide-dependent MDH that originates from the extremophilic methanotroph *Methylacidiphilum fumariolicum* SolV, which is strictly dependent on lanthanides for growth on methanol and was discovered in 2007 by the Dutch research group of Prof. H. J. M. Op den Camp from the Radboud University in Nijmegen, Netherlands.

Different lanthanide derivatives of the MDH enzyme were purified and analyzed. It was found that early lanthanides such as La^{3+} and Pr^{3+}, that promote fast exponential growth rates of *M. fumariolicum* SolV, also favor a high metalation state of the active sites and a high metal to PQQ ratio. These early lanthanides lead to high enzymatic activities, whereas later lanthanides such as Eu^{3+} occupy the active sites to a lesser extent and cause decreased enzymatic activities. This finding correlates with the growth of *M. fumariolicum* SolV. Further, the SolV MDH derivatives exhibited differential stabilities, which was also dependent on the buffer system or storage condition, and a loss of both, the central metal ion and the prosthetic group PQQ were observed.

A dye-coupled assay, consisting of a primary electron acceptor (phenazine methosulfate or ethosulfate) and a dye (dichlorophenol indophenol), was applied to study the mechanism of SolV MDH, yet was found to be highly error-prone. Therefore, the single components of the assay were analyzed individually. Additionally, a second assay system was tested and the used dye, Wurster´s blue, was synthesized. It was found that the choice of the buffer system, the pH and temperature of the assay as well as the additives significantly influence MDH activity. Both primary electron acceptors and dyes are strongly light- and temperature-sensitive and decompose over time. Based on these findings, the assay was optimized for the kinetic investigation of SolV MDH to ensure a high reproducibility of measured data.

To understand the role of the lanthanide ion in the active site, metal binding studies were conducted using the partial apo-enzyme Eu-MDH. Metal titrations and competition experiments were performed. The optimized assay system was used to measure SolV MDH activity. Additionally, more sensitive techniques, such as isothermal titration calorimetry or luminescence spectroscopy, were applied. The latter makes use of the attractive photophysical properties of the well-studied luminescent probe Eu^{3+}. It was found that the early lanthanides La^{3+} and Pr^{3+} promote high enzymatic activity and bind with high affinity to the active site, whereas MDH activity in the presence of Eu^{3+} and the affinity of Eu^{3+} for the active site are lower compared to La^{3+}. The late lanthanide Lu^{3+} showed the lowest binding affinity for SolV MDH. Ca^{2+} and Ba^{2+} did not promote activity of this lanthanide-dependent XoxF-type MDH.

Kinetic parameters of the Eu-MDH derivative were determined to further characterize SolV MDH and better understand the role of the lanthanide metal. It was found that short-chain primary alcohols and aldehydes are successfully oxidized by the Eu-MDH derivative and that its affinity and number of substrates is more limited compared to a mixed early lanthanide MDH enzyme from the same organism. The cyclic alcohol cyclopropanol was additionally found to deactivate SolV MDH. Further, the known MDH activator glycine ethyl ester (GEE) was shown to decompose under assay conditions and is itself used as substrate by the enzyme, exhibiting a Michaelis-Menten-like behavior.

Additional insights into the mechanism of SolV MDH were gained by investigating the deuterium isotope effect. Both substrate and solvent isotope effects were analyzed. SolV MDH shows small temperature- and pH-dependent kinetic isotope effects. Moreover, further studies suggest a competitive binding of PES, which is the primary electron acceptor in MDH assays, and the substrate methanol at the same enzymatic site.

In conclusion, this work provides deeper insights into the mode of action of lanthanide-dependent MDH enzymes and the role of the lanthanide ion in the active site. Further, it provides a kinetic characterization of the first Eu^{3+}-utilizing enzyme.

Introduction

II. Introduction

1 Methanotrophy

Methanotrophy is the ability of microorganisms to use methane as a sole carbon and energy source.[1] Methane is a potent greenhouse gas and a major contributor to climate change. Its estimated annual global emissions are approximately 570 million tons and it has a global warming power (GWP) that is about 28 – 36 times greater than that of carbon dioxide over a 100-year timeframe.[2] Methanotrophs are capable of assimilating methane and concurrently produce methanol as an intermediate of their carbon metabolism, making them interesting targets for biotechnological and environmental applications.[3,4] Interestingly, recent studies showed that methanotrophs can be applied for the degradation of waste plastics[5], the detoxification of such neurotoxins as methylmercury[6] or for the bioremediation of environmentally persistent organic compounds (aliphatics, alkanes, aromatics, halogenated hydrocarbons)[7–9]. Further, the production of biodegradable alternatives for plastics has been reported.[10]

Methanotrophs are Gram-negative bacteria and a subclass of methylotrophs.[1] Methylotrophic organisms are able to grow on reduced organic compounds without carbon-carbon bonds, such as methane, methanol or methylamine.[11] Methylotrophs are predominantly aerobic organisms that colonize a variety of aquatic and terrestrial ecosystems.[1,12] In 1906, the first methylotroph, *Bacillus methanicus*, was reported by Söhngen and the research on these microorganisms began.[13] Today, *Methylorubrum extorquens* AM1 is one of the most prominent representatives and a well-studied model organism for methylotrophy that has been investigated for nearly 60 years.[12,14]

Methane oxidation takes place in both anoxic and oxic environments.[15] Anoxic methane assimilation, a recent discovery, is performed by anaerobic methanotrophic archaea and non-methanotrophic bacteria.[16] Here, the methane oxidation is coupled to the reduction of sulfate, nitrite, iron or manganese.[9] On the other site, the oxic methane consumption is carried out by aerobic bacteria. The latter methanotrophs were characterized in the 1970s by Whittenbury and colleagues.[11,17] Based on their findings, aerobic methane-oxidizing bacteria can be categorized into three types, dependent on their metabolic pathways (Scheme 1).

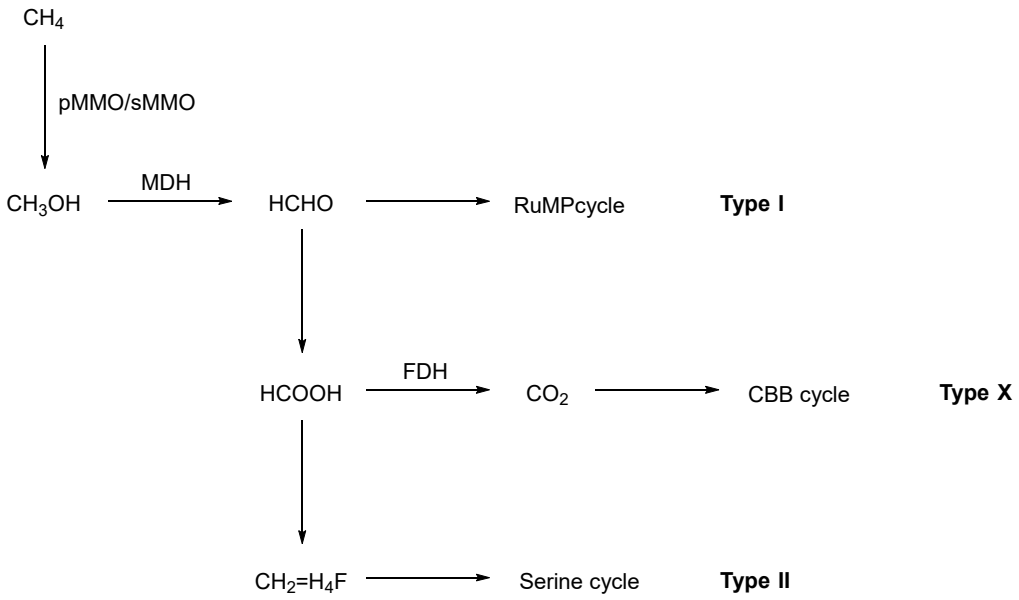

Scheme 1 Simplified methane oxidation by methanotrophs and subsequent metabolic pathways of the ribulose monophosphate (RuMP) cycle, serine cycle and Calvin-Benson-Bassham (CBB) cycle. Key enzymes are particulate or soluble methane monooxygenase (pMMO/sMMO), methanol dehydrogenase (MDH) and formate dehydrogenase (FDH). Adapted from S. Park & C. Kim (2019).[4]

Aerobic methanotrophs assimilate methane, which is oxidized to methanol by the particulate methane monooxygenase (pMMO). Some methanotrophs also utilize a soluble methane monooxygenase (sMMO) under copper-limiting conditions. The oxidation of methanol to formaldehyde is further catalyzed by a methanol dehydrogenase (MDH).[1,18] This core methane assimilation is common to all aerobic methanotrophs, whereas the subsequent metabolic pathways divide these bacteria into three types.[1,4,16] Type I methanotrophs are comprised of γ-proteobacteria, such as the *Methylococcus*, *Methylomonas*, *Methylomicrobium* and *Methylobacter* genera. These microbes directly use formaldehyde that is transformed by the ribulose monophosphate cycle.[4,19] The carbon assimilation of type II methanotrophs, classified as α-proteobacteria, such as the *Methylosinus*, *Methylocystis* and *Methylocella* genera, proceeds via the serine cycle.[4,19] Type X methanotrophs are distinguished from type I methanotrophs as they use the Calvin-Benson-Bassham (CBB) cycle,[1] as do the recently discovered species of methane-utilizing Verrucomicrobia *Methylacidiphilum infernorum* or *Methylacidiphilum fumariolicum*.[20–23]

2 Metals in Methanotrophy

Metals play an important role in various biological processes such as the metabolism, homeostasis or cell signaling. Although their occurrence in living organisms is low compared to the abundant and biologically relevant elements carbon, hydrogen, oxygen or nitrogen, these elements are essential components. Calcium, for example, acts as a second messenger, while magnesium is responsible for *inter alia* RNA stability and function, as well as ATP production. The trace element iron is found as a cofactor in cytochromes.[24,25]

In methanotrophy, copper, calcium and lanthanides play important roles in the central carbon metabolism. Methanotrophs exhibit multiple so-called “metal switches”, controlling the gene expression of key enzymes by the availability of metals.[26] Cu^{2+} is found as a cofactor in the membrane-bound pMMO, which catalyzes the oxidation of methane in the majority of aerobic methanotrophic bacteria. In contrast, the less common sMMO is iron-dependent. Some methanotrophs express both types of MMO enzymes and were found to be subject to the “copper-switch” that promotes the expression of pMMO over sMMO when Cu^{2+} is available.[27–29]

Calcium is the cofactor of the second enzyme in the methane assimilation pathway, a methanol dehydrogenase, which catalyzes the oxidation of methanol to formaldehyde or formate.[30] Ca^{2+}-dependent MDH enzymes have been identified nearly 60 years ago and these enzymes constitute about 15% of soluble protein in methylotrophs.[30] When the biological role of lanthanides was discovered a few years ago, it was found that these metal ions are used instead of Ca^{2+} in an alternative MDH enzyme.[31] Studies with *Methylorubrum extorquens* AM1 and *Methylosinus trichosporium* OB3b showed that both methylo- and methanotrophs present a “lanthanide-switch”, allowing the regulation of MDH availability. The investigations exhibited a differential gene expression; expression of the lanthanide-dependent MDH was upregulated if lanthanides were present, whereas the gene coding for the Ca^{2+}-dependent MDH was repressed.[32,33]

3 Rare-Earth Elements

Rare earth elements were first discovered at the beginning of the 19th century. In 1787, Carl Axel Arrhenius found an unidentified black rock near the village of Ytterby, Sweden. A few years later, Johan Gadolin analyzed the composition of this rock, and the discovered element was afterward named yttrium. Later, in 1803, cerium was isolated from a heavy rock found in the Bastnas mine in Sweden.[34] Rare earth elements (REE) are a group of 17 metals consisting of the d-block element lanthanum and the subsequent lanthanides (f-block) cerium to lutetium (Ln), as well as the group III elements scandium and yttrium.[35] REE are commonly divided into two distinct groups. The light REE (LREE), which are also called cerium group, are comprised of La, Ce, Pr, Nd, Sm and Eu. The heavy REE (HREE) or yttrium group contain Gd, Tb, Dy, Ho, Er, Tm, Yb and Lu.[36] REE were long thought to be scarce since their extraction was difficult and only low amounts of their oxides ("earth" being an early name for oxides) were obtained. Yet, their naming is misleading because REE are neither rare nor solely occurring as oxides. The abundance of REE in the earth's crust is similar to that of other common elements (Figure 1). Cerium, for example, is the most abundant REE (66 ppm) and its abundancy lays between that of copper (50 ppm) and zinc (75 ppm). Also, REE that are found in smaller concentrations, such as thulium (0.5 ppm) or lutetium (0.8 ppm), are still more abundant than the noble metals silver (0.07 ppm) and platinum (0.001 ppm).[34,37] The radioactive Pm, however, is present in only miniscule amounts in nature and is formed by e.g. spontaneous fission.[35,38]

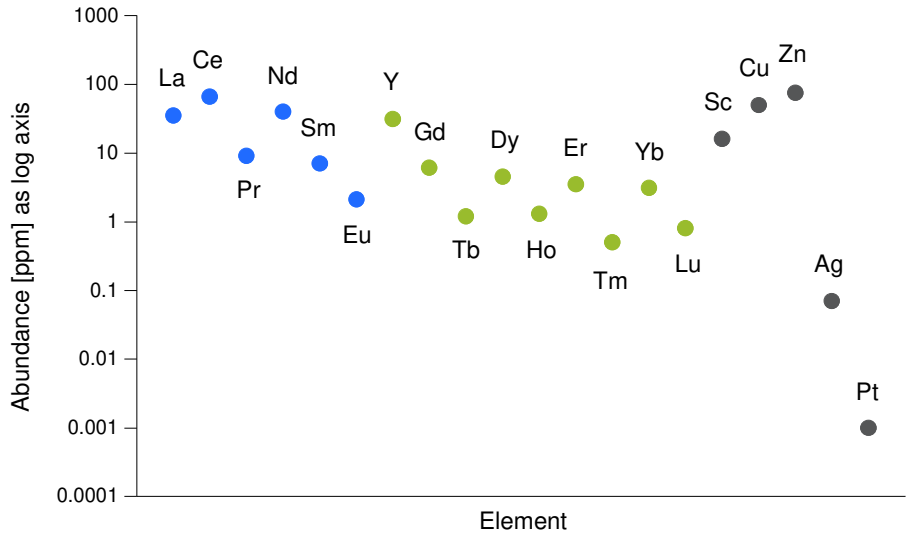

Figure 1 Abundance of REE and selected metals in the earth's crust in ppm. Data from S. Cotton (2006).[35] Light REE are shown in blue and heavy REE in green. Other metals are presented in grey.

The separation of REE is difficult. At the beginning of the 20th century, REE were separated in a time-consuming process called fractionized crystallization, which makes use of slight solubility differences between lanthanide salts. During World War II, ion exchange chromatography was developed under the Manhattan Project. Today, along with liquid-liquid extraction, it is used to separate REE.[35]
Lanthanides are chemically very similar. The valence electrons of all lanthanides except lanthanum are localized in the 4f shell, which is well-shielded by the 5s and 5p orbitals. Therefore, these electrons do not participate significantly in bonding and their spectroscopic and magnetic properties are largely independent of the chemical environment. On the other hand, the valence electrons are less well-shielded from the nucleus. Therefore, the ionic radii (Table 1) decrease to an unexpectedly high extent with increasing nuclear charge from La to Lu. This phenomenon, which is to some extent also caused by relativistic effects, is termed lanthanide contraction.[35]

Table 1 Properties of calcium and the lanthanides compared. Data from C.H. Evans 1983.[39]

Element	Atomic number	Outer electronic configuration (4f)	Ionic radius (Å)	
			CN = 6	CN = 9
Ca	20	-	1.00	1.18
La	57	-	1.03	1.22
Ce	58	2	1.01	1.20
Pr	59	3	0.99	1.18
Nd	60	4	0.98	1.16
Sm	62	6	0.96	1.13
Eu	63	7	0.95	1.12
Gd	64	7	0.94	1.11
Tb	65	9	0.92	1.10
Dy	66	10	0.91	1.08
Ho	67	11	0.90	1.07
Er	68	12	0.89	1.06
Tm	69	13	0.88	1.05
Yb	70	14	0.87	1.04
Lu	71	14	0.86	1.03

The prevalent oxidation state of the lanthanides is +3. It results from the release of two electrons from the s-shell and one electron from the d-shell. Exceptions can be found for e.g. Eu, which exhibits also a divalent oxidation state Eu^{2+} or Ce with an additional tetravalent state Ce^{4+}.[36] The trivalent

lanthanides La^{3+} to Gd^{3+} present a high similarity to the divalent Ca^{2+}. Due to the similar ionic radii of 1.00-1.18 Å for Ca^{2+} and 0.86-1.22 Å for Ln^{3+} with coordination numbers (CN) of 6-9 (Table 1), Ca^{2+} can be replaced by lanthanides in the active site of enzymes, thereby allowing the use of their spectroscopic properties in the investigation of metalloenzymes.[39–41] Further, all lanthanides exhibit hydrolytic activity because of their strong Lewis acidity and possess, with the exception of La (empty f-shell) and Lu (full f-shell), paramagnetic properties.[35,42] All of these features enable the manifold use of REE in modern technology, industry and medicine (Figure 2).[43–45]

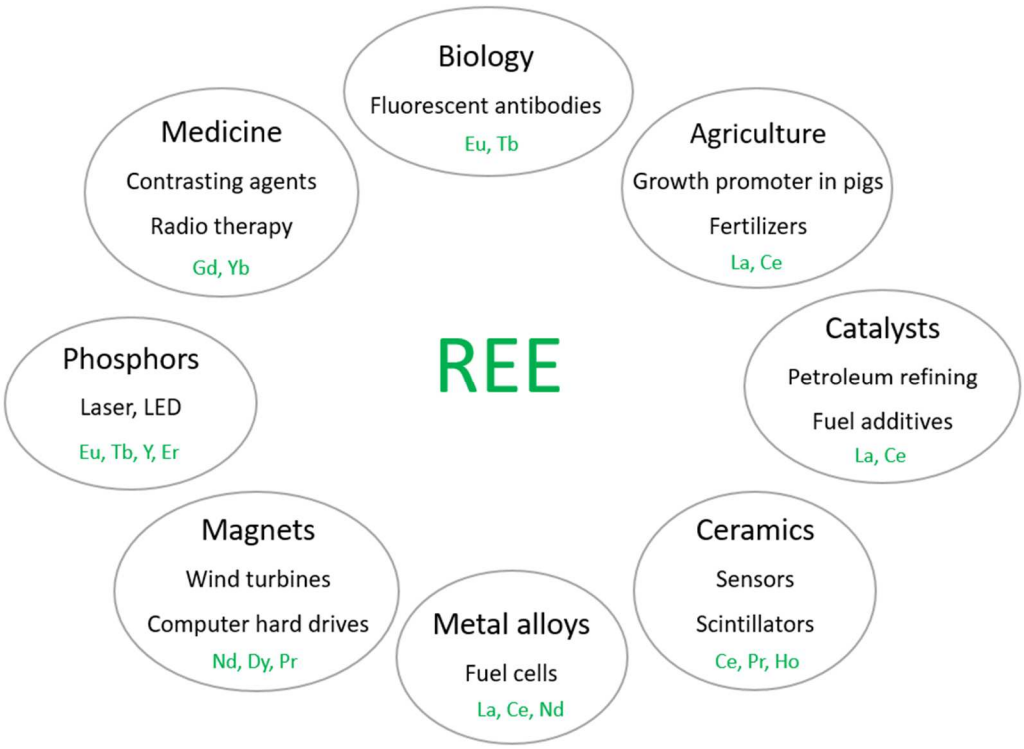

Figure 2 Examples for applications of REE in modern technology, research and medicine.

4 Lanthanide-Dependent Bacteria

In 2010, the explosion of the offshore drilling rig Deepwater Horizon resulted in the worst oil spill in U.S. history.[46] Released natural gas and crude oil accumulated in submerged plumes in the ocean and the concentration of methane increased up to five magnitudes. At the same time, a bloom of methanotrophic bacteria and a concurrent depletion of light REE from methane-rich water was observed.[46–48] Yet, the biological role of lanthanides had not been discovered at that time. Although it was hypothesized that REE are superior to calcium in enzymes, the assumption that the bioavailability of these elements was too low long prevented further research in this field.[42]

In 2011, Hibi *et al.* reported the first bacterium that uses lanthanum in its methanol metabolism.[31] This finding, however, remained widely unnoticed. It took another two years until, in 2014, Pol *et al.* reported the first crystal structure of a lanthanide-dependent MDH, which ultimately raised the interest for the research on these "new life metals".[49]

Methanol dehydrogenases catalyze the oxidation of methanol to formaldehyde. At least three different types of these alcohol dehydrogenases must be distinguished in methylotrophic organisms: cytoplasmic $NAD(P)^+$-dependent nicotinoproteins in Gram-positive bacteria[50], peroxisomal FAD-dependent flavoproteins in yeast[51] and periplasmic PQQ-dependent quinoproteins in Gram-negative bacteria[52]. The latter MDH, which is expressed by methanotrophs and Gram-negative methylotrophs[11], was first investigated in *M. extorquens* (formerly *Pseudomonas* sp. M27).[53] The genes for this MDH are localized in the *mxa* operon. This MDH consist of the large MxaF (α) and the small MxaI (β) subunit, which are assembled to a $\alpha_2\beta_2$ tetrameric structure. The active site, which is located in the α subunit, contains pyrroloquinoline quinone (PQQ) as a cofactor, which is tightly but non-covalently bound, and a Ca^{2+} ion as the central metal that acts as a Lewis acid.[30] The *mxa* operon further consists of *mxa*G, which codes for the primary electron acceptor cytochrome c_L (a specific highly acidic ferricytochrome), and genes for calcium insertion or other proteins of partially unknown function.[30,54,55] The oxidation of methanol (Scheme 2) proceeds in the periplasm and is coupled to the reduction of the prosthetic group PQQ to its quinol form. This is followed by a two-step electron transfer to cytochrome c_L. The methanol oxidase transport chain further involves a secondary electron acceptor cytochrome c_H, which is in turn oxidized by a membrane-bound oxidase.[30,56]

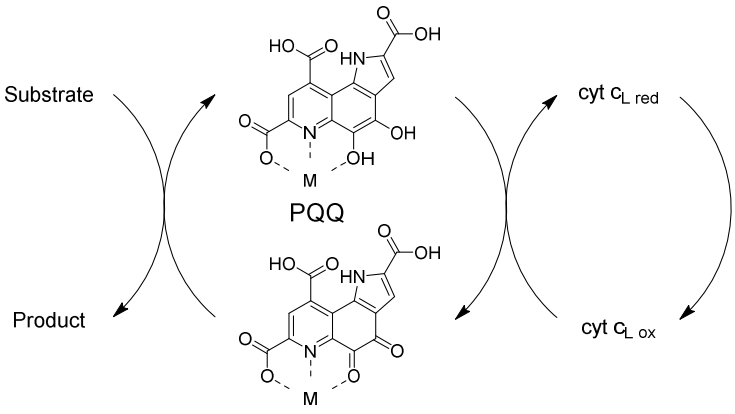

Scheme 2 Methanol oxidation by PQQ-dependent methanol dehydrogenases. M stands for Ca^{2+} in the case of MxaF and for Ln^{3+} in the case of XoxF.

The Ca-enzyme was long thought to be the only PQQ-dependent MDH in methano- and methylotrophs. In 1995, the *xox*F gene was discovered[57] which shares 50% amino acid identity with the sequence of the large subunit MxaF of the extensively studied Ca^{2+}-dependent MDH.[58] Its function, however, remained unknown for years until the discovery of lanthanide-dependent bacteria.[59] The name XoxF of the alternative MDH therefore historically derives from the original designation of the large subunit of the Ca^{2+}-dependent MDH (MoxF), and the "X" stands for the at that time unknown function.[60] XoxF, which is more widespread than MxaF and also evolutionarily older, has been classified into five different clades XoxF1 – 5; however, recent research suggests a more widespread distribution of the XoxF-like sequence among bacterial taxa.[54,59,61]

XoxF-expressing bacteria are ubiquitous in a variety of natural habitats, such as coastal ocean waters[62], soil[12], lake sediments[63] or the plant phyllosphere (external leaf surface)[64,65], and were recently even found in hostile environments like geothermal areas[66]. The latter is the natural habitat of the extremophilic genus *Methylacidiphilum*, which belongs to the phylum Verrucomicrobia.[67] Three representatives have been isolated in the years 2007 and 2008: *M. infernorum* strain V4 from a steaming soil at Hell's Gate, New Zealand[23], *M. fumariolicum* strain SolV from a volcanic mudpot in the Solfatara crater, Italy[68] and *M. kamchatkense* strain Kam1 from an acidic hot spring in Uzon Caldera, Kamchatka, Russia[22]. These extremophilic methanotrophs thrive at low pH (2 – 3.5) and high temperatures (55 – 60 °C).[21,67] *M. fumariolicum* strain SolV was found to express the XoxF-type MDH and to be strictly dependent on lanthanides for growth.[49]

XoxF is found in an operon along with genes coding for its natural electron acceptor cytochrome c_L (XoxG) and an accessory protein, whose function is not exactly known (XoxJ).[69,70] Although the XoxF-type MDH is extensively studied today, crystal structures are only available for three organisms: the two methanotrophs *M. fumariolicum* SolV[49,71] and *M. buryatense* 5GB1C[72] and one methylotroph

M. extorquens AM1[73]. XoxF MDH is a periplasmic homodimer (α_2) lacking the small subunit of the Ca-MDH. Its active site (Figure 3) is comprised of the prosthetic group PQQ and a lanthanide ion instead of Ca^{2+}.[61] Catalytically and structurally important amino acids such as Asn, Glu, and Asp are highly conserved in the active site of MxaF and XoxF. However, XoxF has an additional catalytically active aspartate (Asp^{301} in *M. fumariolicum* strain SolV), most probably due to the higher demand of coordination partners of the lanthanides compared to calcium. The Asp replaces an Ala residue that is found in all MxaFs. Further, two more amino acid substitutions were found in XoxF MDH: the replacement of Pro by the smaller Thr and that of Ala by Gly.[49,61,73]

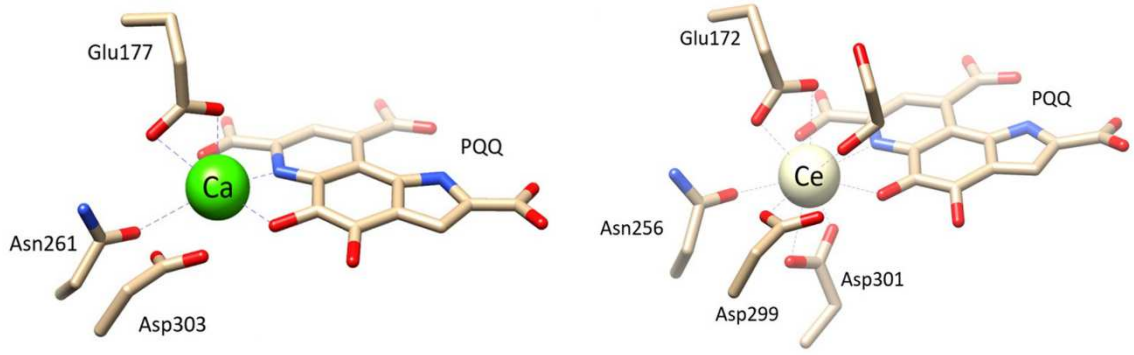

Figure 3 Active sites of Ca^{2+}-dependent MDH from M. extorquens strain AM1 (PDB: 1W6S) and Ce^{3+}-dependent MDH from M. fumariolicum strain SolV (PDB: 4MAE). Figure from Jahn et al. (2018).[71] Reprinted with kind permission of John Wiley and Sons.

As in MxaF, the PQQ cofactor of XoxF MDH acts as an electron acceptor and is reduced upon the two-electron oxidation of methanol. The lanthanide ion acts as a Lewis acid by activating the coordinating C=O group of PQQ, facilitating the addition of the substrate's hydrate to the C5 atom of PQQ.[49,61] However, the exact catalytic mechanism of MDH enzymes is still not fully understood. Several approaches including model compound, crystallographic or DFT studies were applied to elucidate if methanol oxidation proceeds via a hydrate transfer from methanol to the C5 of PQQ or if methanol acts as a nucleophile attacking the C5 atom (hemiketal mechanism).[73–75]

While lanthanide-dependent bacteria such as *M. extorquens* carry both MDH genes, *mxa*F and *xox*F, from which *xox*F is preferentially expressed, *M. fumariolicum* SolV lacks the gene for MxaF and is thus strictly dependent on lanthanides.[49,76] Besides MDH enzymes, an ethanol dehydrogenase was also found that carries a rare earth ion in its active site.[73,77] Lanthanide-dependent bacteria show a clear preference for the early, light lanthanides. The growth of *M. extorquens*, *P. putida*, *M. mobilis* or *M. fumariolicum* and their alcohol dehydrogenase (ADH) activity was shown to be affected by the lanthanides in the growth medium: La^{3+}, Ce^{3+} and Nd^{3+} promote exponential growth, whereas no

growth was observed in the presence of Yb^{3+}.[76] Also, it was demonstrated that microorganisms are capable of accumulating rare earths from mining sites or harvesting these elements from computer hard drive magnets.[78,79] These findings suggest that there must be efficient uptake and transport mechanisms for lanthanides. The existence of small chelators called lanthanophores (lanthanide carriers) was postulated[76,80] and recently the lanthanide binding protein, lanmodulin, has been discovered.[81] Yet, the research on lanthanide biochemistry is just beginning and many questions remain that have to be answered.

5 Aim of The Study

Methanotrophs present several interesting properties for environmental and industrial applications. These include bioremediation, the degradation of harmful pollutants from soil or the ocean, as well as biological denitrification and the recovery of sulfur compounds or metals. Yet most importantly, methanotrophs can regulate the emission of the greenhouse gas methane that these microbes convert to methanol.[9] Besides the methane monooxygenase, MDH is a key enzyme in the methane metabolism. The study of the mechanism of MDH is therefore of great interest since, by tuning its activity, the production of methanol can be controlled.

The aim of this study was to better understand the mechanism of methanol oxidation. The extremophilic bacterium *M. fumariolicum* SolV was chosen because of its strict REE-dependency. REE were recently discovered to be biologically active and to be better Lewis acids than Ca^{2+} in the active site of MDH enzymes. REE possess unique spectroscopic properties, allowing the study of the methanol oxidation process. Different REE-derivatives of this enzyme were analyzed to learn if MDH activity is dependent on the type of lanthanide. In this way, MDH activity and therefore methanol production can be tuned without the need for mutagenesis. Also, as SolV growth is dependent on the lanthanide in the cultivation medium, it was necessary to analyze whether the growth rate is correlated to MDH activity.

The present study contains:

- the characterization of different REE-derivatives of the MDH enzyme from SolV
- the optimization of the dye-couple assay used for the measurement of enzymatic activity
- metal titration experiments and substrate kinetics
- studies of the deuterium isotope effect.

Due to the attractive photophysical features of Eu^{3+}, one of the most informative luminescent probes among the lanthanide series, the Eu-MDH derivative was examined in more detail.

Results & Discussion

III. Results & Discussion

1 SolV MDH Derivatives

1.1 Introduction

The biological role of rare earth elements (REE) remained long unknown until the first reports about the relevance of lanthanides for microorganisms appeared ten years ago. In 2011, Hibi *et al.* reported the first lanthanide-dependent methanol dehydrogenase (MDH) which they found in *Methylobacterium radiotolerans*.[31] Until then, only a calcium-dependent MDH had been known.[60,76,82] This finding was followed by two further rare earth element-dependent MDH enzymes from *Bradyrhizobium* sp. MAFF211645[83] and *Methylorubrum* (former *Methylobacterium*) *extorquens* AM1[84]. The Ln^{3+}-dependent MDH was assigned as XoxF, a homologue of the Ca^{2+}-dependent MxaF MDH.[57,85] In 2007, Pol *et al.* discovered an extremophilic microorganism in a volcanic mudpot close to the volcano Vesuvius in Italy[68], which later, in 2014, was shown to be strictly REE-dependent.[49,61] The cultivation of this microorganism, *Methylacidiphilum fumariolicum* SolV, under laboratory conditions was unsuccessful for a long time. Only the addition of mudpot water or a mixture of early lanthanides (lanthanum to neodymium) promoted exponential growth.[49]

In the course of this work, mechanistic studies of the XoxF-type MDH from *Methylacidiphilum fumariolicum* SolV (SolV) were conducted. The MDH dimer with a molecular mass of 127 kDa was purified from cells cultivated at the Radboud University Nijmegen, Netherlands, by Prof. Dr. Lena Daumann and Dr. Arjan Pol according to a published procedure.[49,71] The cells were grown in the presence of micromolar concentrations of different lanthanides. Since the growth of SolV is poor with late lanthanides, La^{3+}, Pr^{3+} and Eu^{3+} were used as single lanthanides per batch to obtain the respective MDH enzyme derivative.[49,71] A mixed REE-MDH has been characterized prior to this work[49], yet the effect of a specific lanthanide metal on the activity of SolV MDH was not examined at that time. To gain deeper insights into the mechanism of SolV MDH, we purified different Ln^{3+}-derivatives of this enzyme from frozen cell pellets. These MDH enzymes and other previously purified derivatives were used for the subsequent optimization of a dye-coupled assay employed for the kinetic investigation of the first Eu^{3+}-dependent MDH enzyme.

1.2 Characterization of SolV XoxF Ln^{3+}-Derivatives

In the course of this work, three different Ln^{3+}-derivatives of SolV XoxF were examined: a La^{3+}, a Pr^{3+} and an Eu^{3+}-dependent MDH. The latter two derivatives were purified from frozen cell pellets, whereas the La^{3+}-dependent and another Eu^{3+}-dependent MDH fraction (assigned as Eu-MDH 4th) were received as already purified samples. We purified Pr-MDH in one fraction while Eu-MDH was obtained in two fractions: a onefold (Eu-MDH 1st) and a twofold (Eu-MDH 2nd) purified enzyme. The MDH monomer was visible on the SDS-PAGE gel as a prominent band at 63.5 kDa. Eu-MDH 2nd showed high purity whereas Eu-MDH 1st and particularly Pr-MDH exhibit minor impurities (Figure S1 to Figure S3).
In a first step, the folding, metal content and PQQ signature of each MDH derivative were analyzed. A comparison of the CD spectra with the calculated spectrum (DichroCalc[86], sequence from PDB: 4MAE[87]) showed a proper folding of the enzyme with approximately 10% α-helices and 36% β-sheets (Figure 4A). Minor shifts were observed upon the change of the buffer system, suggesting that small conformational changes were caused by re-buffering. The slight difference to the calculated spectrum could be a result of either impurities, different peptide backbone conformations or the applied calculation method.[88,89] The metal content of the enzyme fractions was determined with ICP-OES (Table 2) and gave a similar lanthanide metal occupation of about 70% for freshly purified Pr-MDH and all Eu-MDH purifications. In contrast, the 80% La^{3+} content in La-MDH was significantly higher most likely due to the size of the ionic radius that affects the incorporation of the metal in the active site.[90]

Table 2 REE content in purified MDH as analyzed by ICP-OES after digestion with nitric acid.

MDH derivative	La [mol%]	Pr [mol%]	Eu [mol%]
La-MDH	80	-	-
Pr-MDH	-	70	-
Eu-MDH	-	-	70

UV-visible absorption spectra of the MDH derivatives (Figure 4B) exhibit a PQQ signature with a maximum at 355 nm and a shoulder at 405 nm.[49] This is consistent with the UV-visible absorption spectrum of the mixed REE-dependent MDH from SolV, as well as with those of other PQQ-containing quinoproteins, having a maximum around 345 – 350 nm.[30,49,82,91] Interestingly, variations in the peak ratios at 355 nm and 405 nm have been observed for the three Ln^{3+}-MDH derivatives. Surprisingly, La-MDH is missing a pronounced PQQ signature, which is probably a result of the buffer system since a deactivation of MDH was observed if the enzyme was stored in phosphate buffer (KP) for some time.

Also, a loss of the PQQ cofactor was observed with storage time leading to a decrease or complete loss of enzymatic activity. A comparison of Pr-MDH and Eu-MDH showed that the shoulder is strongly pronounced in the Eu^{3+}-containing derivative. Goodwin and Anthony reported that the ratio of the two absorbance maxima at 345 nm and 400 nm can help to distinguish between the oxidized and reduced forms of PQQ. A higher peak at 345 nm was ascribed to the reduced, active state of PQQ.[92,93] A observed higher activity of Pr-MDH compared to the Eu^{3+}-derivative of the enzyme is in good accordance. The tighter binding of larger central metal ions seems to additionally support the active form of the cofactor PQQ. This finding is consistent with the preference of SolV for early lanthanides.[49]

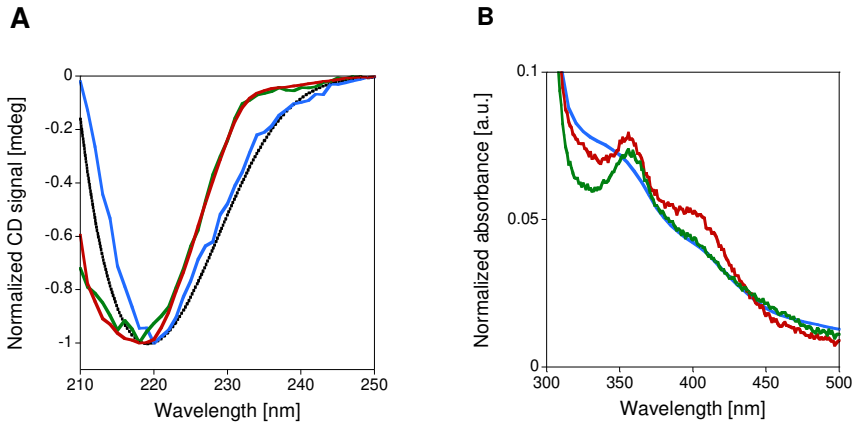

Figure 4 Characterization of MDH derivatives. A: Normalized CD spectra recorded at a Jasco J-810 CD spectrometer at RT: La-MDH in PIPES (blue), Pr-MDH in KP (green), Eu-MDH in KP (red) and the calculated spectrum in black. B: PQQ fingerprint of La-MDH (blue), Pr-MDH (green) and Eu-MDH (red) in PIPES buffer, recorded at a Cary60 spectrophotometer. Spectra were normalized to the A_{280nm} peak.

The PQQ content of each MDH derivative (Table 3) was calculated from UV-visible absorption spectra using the molar extinction coefficient of PQQ (9,620 $M^{-1} \cdot cm^{-1}$)[94]. An occupation of 70% of active sites with PQQ was found for fresh La-MDH samples, which decreased gradually over storage time as described above. Eu-MDH shows a content of 80 – 90% PQQ in the enzyme fractions. The metal content, however, is lower; with only 70% Eu^{3+} in the active sites, it can be supported that some active sites occupied with the cofactor PQQ are missing Eu^{3+}. This could be a result of a weaker binding of Eu^{3+} due to its smaller ionic radius.[95] This finding gives a further explanation for the slower growth rate of SolV in the presence of Eu^{3+} compared to La^{3+}-grown cells.[71] Surprisingly, Pr-MDH exhibits a PQQ content of only 70%. This value is consistent with the metalation state of this MDH fraction and indicates a 1:1 metal to cofactor ratio. The low PQQ content is most probably caused by contaminations of this MDH fraction with other proteins such as its natural electron acceptor

cytochrome c_L. The SDS-PAGE gel (Figure S3) shows various lower molecular and some higher molecular weight bands, and the purified fraction displays a yellowish color.[70]

Table 3 PQQ content of the MDH derivatives. The absorbance at 280 nm and 355 nm was extracted from UV-visible absorption spectra. Conditions: 1 cm cuvette (La-MDH) or 1 mm CD-cuvette (Pr-MDH, Eu-MDH), Cary60 spectrophotometer, RT.

MDH derivative	A_{280}	A_{355}	A_{280}/A_{355}	PQQ per MDH monomer
La-MDH	0.053	0.006	8.8	0.7
Pr-MDH	0.146	0.011	13.3	0.7
Eu-MDH	0.245	0.026	9.4	0.8 - 0.9

The total protein to PQQ ratio (A_{280}/A_{355}; Table 3) was further determined since it is a measure for the purity of MDH fractions[96,97] and, consequently, for MDH activity in the sample. A small value indicates high enzymatic activity and low amount of impurities in the sample. Overall, La-MDH shows the best total protein to PQQ ratio. Eu-MDH presents a slightly increased value, while Pr-MDH exhibits the highest value. These results are consistent with the SDS-PAGE gel and the PQQ content of the sample. The A_{280}/A_{355} ratios differ slightly between the different Eu-MDH purification fractions. The smallest value was found for Eu-MDH 2nd. This fraction displays a very high activity and was therefore chosen for metal studies. The A_{280}/A_{355} ratio of the Eu-MDH 1st and 4th fraction was similar and somewhat lower. The latter fractions were therefore chosen for Michaelis-Menten kinetic studies with dye-coupled assays, where a dye is linked to the consumption of substrate and used as read-out.[53] Since MDH is stored in the presence of methanol for stability[49], residual methanol must first be consumed before substrate is added. Lower activity MDH fractions were best suited, as the conversion of the dye proceeds at a slower rate and a sufficient amount of the dye is therefore left to study kinetics with the intended substrate.

1.3 Stability of SolV XoxF MDH

The mechanistic investigation of SolV MDH throughout this work was predominantly conducted with a dye-coupled assay designed by Anthony and Zatman including a two-electron acceptor and a redox-active dye.[53] Prior to kinetic measurements, SolV MDH was analyzed for stability and handling. As aforementioned, MDH must be stored in the presence of its substrate, methanol. A washing procedure was applied to remove the substrate methanol and its likely formed products

(formaldehyde and formate) to prevent a distortion of the assay outcome. Protein integrity and activity remained even after repeated washing, and two washing steps were found to give best results along with sufficient substrate removal. Additionally, the washing procedure was applied for re-buffering purposes. In the case of La-MDH, phosphate buffer had to be replaced by PIPES buffer to eliminate the observed inactivation of SolV MDH.

A concentration-dependent inactivation of MDH enzymes by the electron acceptor, a phenazine dye, which is routinely used in artificial MDH assays, has been described.[30,98] During kinetic investigations, a decline in enzymatic activity in long-term measurements at elevated temperatures was observed. The stability of SolV MDH was therefore examined under conditions that are applied during kinetic measurements. MDH was incubated in either 20 mM PIPES buffer pH 7.2 or buffered assay mix containing the electron acceptor phenazine ethosulfate (PES) and the dye 2,6-dichlorophenol indophenol (DCPIP) at either 4 °C, room temperature or 45 °C to simulate storage, handling and assay conditions. The enzymatic activity was analyzed at intervals of 15 min.

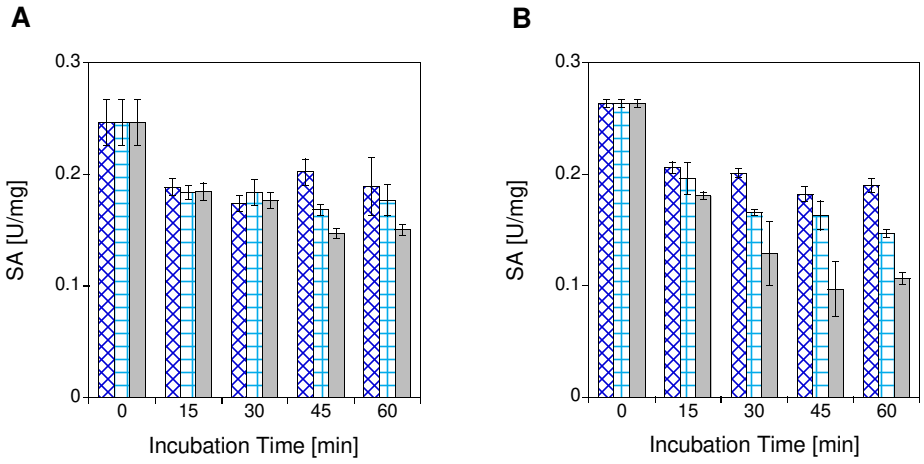

Figure 5 Enzymatic activity of SolV MDH under assay conditions: 200 nM Eu-MDH 1st, 20 mM PIPES pH 7.2, 1 mM PES, 100 µM DCPIP, 50 mM MeOH, 45 °C, n = 3. MDH was stored in either PIPES buffer (A) or assay mix containing buffer, PES and DCPIP (B) at 4 °C (dark blue), room temperature (light blue) or 45 °C (grey) before measurement.

PIPES buffer and assay mix influence MDH activity differently (Figure 5). Although the enzymatic activity drops already after 15 min in both solutions, PIPES buffer shows only a slight effect during the incubation period and only at elevated temperatures (heating at 45 °C). The strong decrease in both solutions at the beginning might be explained by the lack of stabilizing methanol due to the washing step. The assay mix, however, leads to a considerable decline in enzymatic activity, which is more pronounced if MDH is heated. After 45 min at elevated temperatures, the enzyme exhibits only 40% of its initial activity. These results were verified by UV-visible and CD spectroscopy (Figure S4, Figure

S5). Due to the high absorbance of the assay mix and a possible oxidation of PQQ by PES[30], only the PIPES-buffered MDH has been analyzed with the latter two methods. The PQQ signature (Table 4) changes only slightly at room temperature, which is in good agreement with the activity assay (Figure 5A). The heating effect on the PQQ content in SolV MDH, however, is similarly small. CD spectroscopy further showed that the folding of SolV MDH does not change upon heating and short-term storage. Therefore, high temperatures seem to have a minor influence on MDH integrity during a short time span. PES, however, might inhibit MDH to some extent even at low concentrations and especially at assay conditions with elevated temperatures applied. This is particularly troublesome for substrate conversion studies, because residual methanol necessitates longer measurements. To further elucidate the effect of the electron acceptor on MDH, PES-dependence studies (III.2 Assay Optimization and III.5.5 Influence of PES on the KIE) were performed.

Table 4 PQQ fingerprint of Eu-MDH 1st incubated under different conditions. The absorbance at 280 nm and 355 nm was extracted from UV-visible absorption spectra at the respective temperature recorded in a 1 mm-path length CD cuvette on a Cary60 spectrophotometer.

Condition	0 min	15 min	30 min	45 min	60 min
4 °C	9.4	9.4	9.5	9.2	9.1
Room temperature	9.6	9.7	9.7	10.6	11.0
45 °C	9.4	10.1	11.2	10.3	10.7

Besides the short-term, assay-related storage, an effect of long-term storage on MDH activity was observed. The stability of SolV MDH varies between derivatives. Pr-MDH can be easily stored at 4 °C for days whereas Eu-MDH loses activity even if supplemented with methanol. Also, Pr-MDH remains highly active for years when stored at - 80 °C whereas Eu-MDH is stable for only a short time. A possible explanation might be the differences in the properties of the lanthanides (predominantly the radius or Lewis acidity)[35,95] that differently stabilize the enzyme as described above. A diverse interaction of the lanthanide with residues and water molecules in the active site due to its size has also been discussed.[99] In addition to the central metal ion, buffers influence MDH activity differently. MDH samples that have been stored in phosphate buffer showed dramatically decreased levels of PQQ and a loss of activity although CD spectroscopy confirmed a proper folding. Since phosphates are known to readily precipitate metal ions like lanthanides[100,101], a removal of the rare earth ion from the active site is likely. We therefore decided to purify SolV MDH in PIPES buffer. The same effect as described for phosphate buffer was also observed for long-term storage at temperatures other than - 80 °C. SolV MDH lost PQQ

over the storage and a substitution of the isolated enzyme with its cofactor was not successful although some alcohol dehydrogenase (ADH) assays are supplemented with additional PQQ to recover enzymatic activity.[91] Recently, a crystal structure of MDH missing PQQ was published.[73] Although PQQ was no longer part of the cofactor complex, the lanthanide in this enzyme, La^{3+}, was present in the active site and was coordinated to a water molecule instead of PQQ. This effect is also conceivable for SolV MDH, since fresh La-MDH samples showed a slightly higher metal content compared to that of PQQ, indicating that although PQQ is lost over time, the metalation state will most probably persist.

1.4 Conclusion

SolV MDH derivatives were purified and analyzed with regard to their purity, metal content and PQQ fingerprint. The MDH activity was mostly dependent on the properties of the central metal ion, whereas the purity and PQQ content of the enzyme had a smaller effect. In contrast to the Eu^{3+}-containing enzyme, Pr-MDH is fairly stable and show a balanced PQQ to lanthanide ratio. Eu-MDH was obtained in different fractions and showed diverse activities. The highly active Eu-MDH 2nd purification fraction was used for metal-binding studies and Eu-MDH 1st was analyzed regarding substrate affinity. Pr-MDH was applied for assay optimization due to its high activity. Additionally, at the beginning of this work, La-MDH and Eu-MDH 4th were used for metal binding and methanol-dependent kinetic studies as well as for assay optimization.

The stability of SolV MDH was investigated under assay and storage conditions. The success of long-term storage is not only dependent on the MDH derivative, but also on storage buffer and temperature. SolV Eu-MDH easily loses its cofactor PQQ upon storage, resulting in a loss of enzymatic activity. In terms of the assay procedure, the incubation of MDH with assay mix caused a large decrease of enzymatic activity. This finding shows that long-term measurements will distort the outcome of such dye-coupled MDH assays and thus make results difficult to compare.

2 Assay Optimization

2.1 Introduction

The kinetic parameters of methanol dehydrogenases are routinely measured using dye-coupled assays in which the conversion of the substrate is linked to artificial electron acceptors (Scheme 3).[27,33] Although the physiological electron acceptor of MDH enzymes, cytochrome c_L,[56,70,103] can be applied for the electron transfer in the assay,[69,104,105] artificial components are utilized predominantly. In 1964, Anthony and Zatman described a convenient method for the analysis of MDH enzymes, which is now widely used.[53] This artificial assay system consists of the primary electron acceptor phenazine and the dye DCPIP. The substrate methanol or another primary alcohol is converted to its corresponding aldehyde by the enzyme.[106] This reaction involves the transfer of two electrons and two protons to the cofactor PQQ. The latter undergoes a ping-pong reaction by a subsequent transfer of the electrons to the primary electron acceptor phenazine methosulfate (PMS) or phenazine ethosulfate (PES) that further reduces the dye DCPIP. The uptake of electrons by DCPIP results in its decoloration.[30,102,107] Therefore, the colorimetric read-out can be monitored at 600 nm, the absorbance maximum of DCPIP.[108] Additionally, another assay system involving only one component is utilized in the investigation of MDH enzymes. Here, the electron acceptor couple phenazine/DCPIP is replaced by the combined one-electron acceptor and dye Wurster's blue (WB).[109–111]

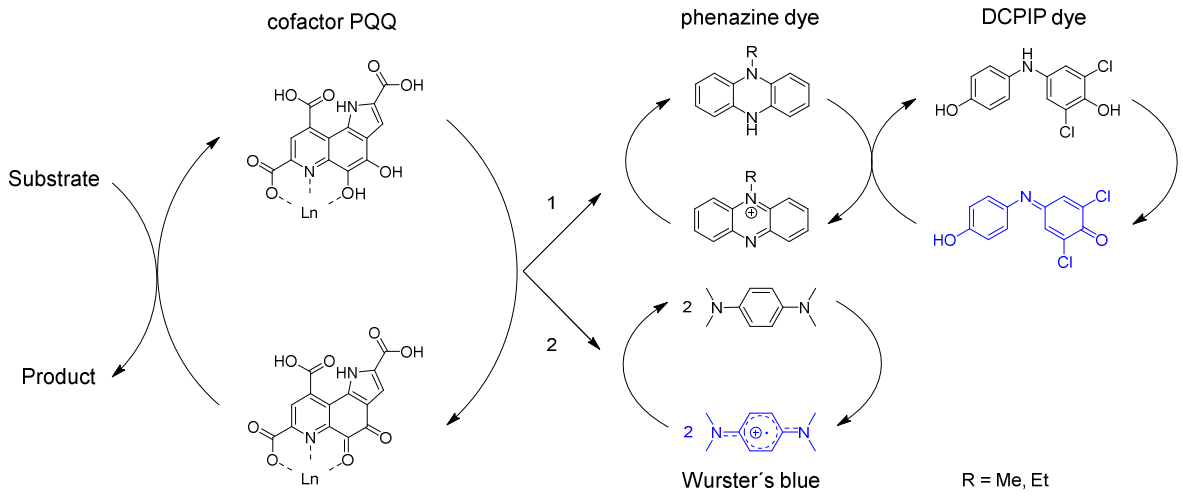

Scheme 3 Artificial MDH assays. Electron transfer proceeds from the substrate to PQQ and afterwards either via 1 (the two-electron acceptors PMS/PES and DCPIP) or 2 (via the one-electron acceptor WB). A decoloration of the dye occurs upon reduction by the uptake of transferred electrons and can be monitored at either 600 nm (DCPIP) or 610 nm (WB).

In the course of this work, both assay systems were applied for mechanistic studies of SolV MDH. The assay conditions differed slightly from those of other MDH enzymes originating from extensively studied microbes such as *M. extorquens* AM1 or *Hyphomicrobium* X. In contrast to these mesophilic model organisms, which are examined at moderate temperatures,[1] SolV is an extremophile that thrives at high temperatures of about 60 °C.[49,68] Therefore, an assay temperature of 45 °C was chosen as a compromise between the temperature optimum of the microbe and enzyme stability. Yet, during the studies, difficulties arose in reproducing results measured on different days. The assay system was therefore analyzed in more detail. In the first step, the assay components were investigated regarding their handling conditions and, in a next step, the assay was optimized for the use with SolV MDH.

2.2 Investigation of Electron Acceptors and Assay Optimization

The following section is part of the publication:

Understanding the chemistry of the artificial electron acceptors PES, PMS, DCPIP and Wurster's Blue in methanol dehydrogenase assays

Bérénice Jahn, Niko S. W. Jonasson, Hurina Hu, Helena Singer, Arjan Pol, Nathan M. Good, Huub J. M. Op den Camp, N. Cecilia Martinez-Gomez, Lena J. Daumann

Published in: *J. Biol. Inorg. Chem.* **25**, 199–212 (2020). DOI: 10.1007/s00775-020-01752-9.

2.2.1 Abstract

Methanol dehydrogenases (MDH) have recently taken the spotlight with the discovery that a large portion of these enzymes in nature utilize lanthanides in their active sites. The kinetic parameters of these enzymes are determined with a spectrophotometric assay first described by Anthony and Zatman 55 years ago. This artificial assay uses alkylated phenazines, such as phenazine ethosulfate (PES) or phenazine methosulfate (PMS), as primary electron acceptors (EAs) and the electron transfer is further coupled to a dye. However, many groups have reported problems concerning the bleaching

of the assay mixture in the absence of MDH and the reproducibility of those assays. Hence, the comparison of kinetic data among MDH enzymes of different species is often cumbersome. Using mass spectrometry, UV–vis and electron paramagnetic resonance (EPR) spectroscopy, we show that the side reactions of the assay mixture are mainly due to the degradation of assay components. Light-induced demethylation (yielding formaldehyde and phenazine in the case of PMS) or oxidation of PES or PMS as well as a reaction with assay components (ammonia, cyanide) can occur. We suggest here a protocol to avoid these side reactions. Further, we describe a modified synthesis protocol for obtaining the alternative electron acceptor, Wurster's blue (WB), which serves both as EA and dye. The investigation of two lanthanide-dependent methanol dehydrogenases from *Methylorubrum extorquens* AM1 and *Methylacidiphilum fumariolicum* SolV with WB, along with handling recommendations, is presented.

2.2.2 Introduction

Biochemical assays are powerful analytical techniques used to identify or quantify proteins, to study the binding of substrates and inhibitors, and to measure the activity of enzymes. The family of methanol dehydrogenase enzymes (MDH) has recently taken the spotlight again after it was discovered that many bacteria utilize lanthanide-dependent MDH of the XoxF family.[26,59,61,65,76,90,112] This finding has fueled an entirely new area of research – lanthanide-dependent bacterial metabolism and biochemistry. The activity of methanol dehydrogenases in vitro is routinely measured using the convenient spectrophotometric method developed by Anthony and Zatman.[53] The electron transfer from the substrate, either methanol or formaldehyde, via the redox cofactor pyrroloquinoline quinone (PQQ) in the active site is coupled to electron acceptors (EA). Because of the absence of visible light-absorbing substrates or products, a dye is required for the read-out of the assay. Usually, artificial electron acceptors, such as phenazine methosulfate (PMS), phenazine ethosulfate (PES), *N,N,N',N'*-tetramethyl-p-phenylenediamine (TMPD) derivatives like its radical cation (Wurster's blue, WB) or 2,6-dichlorophenol indophenol (DCPIP), are involved. The first two are the most widely used EA and the latter two serve as redox dyes (Chart 1).[30,53,113] The electron transfer in MDH enzymes in vivo is proposed to take place in distinct one-electron steps.[98,109] PMS, PES and WB enable the regeneration of the prosthetic group pyrroloquinoline quinone by mimicking cytochrome c_L or cytochrome c_{GJ}, the physiological electron acceptors of these enzymes.[30,70,104,114] Besides colorimetric techniques, an amperometric approach has been used to assess MDH activity. Here, methanol conversion is coupled to electron acceptors that are, in turn, linked to oxygen in an oxygen-sensitive electrode.[102,107] Studies

with the natural electron acceptor cytochrome c_L and a bovine or equine heart cytochrome as terminal electron acceptor and dye have also been reported.[69,70,102] Recently, the oxidation of methanol by Eu-MDH via cytochrome c_{GJ} driven by electrocatalytic voltammetry was also demonstrated.[104]

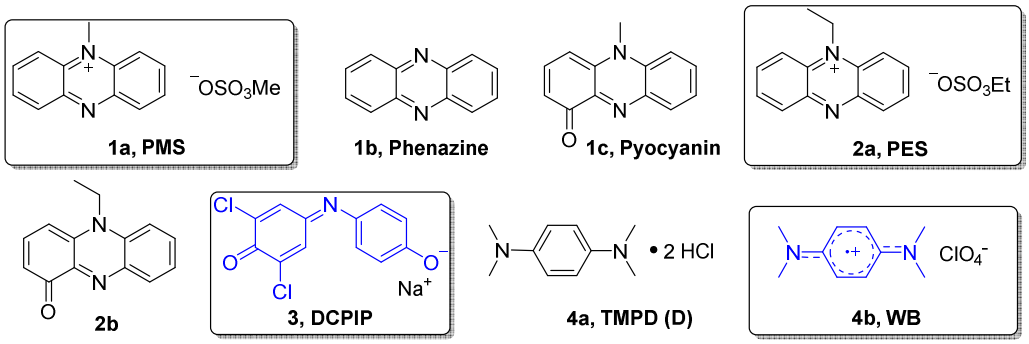

Chart 1 Electron acceptors and dyes that have been used to assess MDH activity (their degradation products are also shown): PMS (1a), phenazine (1b) and its oxidation product pyocyanin (PMS_{ox}, 1c). PES (2a) and its oxidation product (PES_{ox}, 2b). DCPIP (3), N,N,N′,N′-tetramethyl-p-phenylenediamine (TMPD) dihydrochloride (TMPDD, 4a) and N,N,N′,N′-tetramethyl-p-phenylenediamine perchlorate (Wurster's blue, WB, 4b).

While the implementation of the colorimetric assay for the analysis of MDH activity is facile, many difficulties regarding the reproducibility of assay results have been reported.[60,71] In light of the importance of MDH assays for the recently established field of lanthanide biochemistry, we revisit this assay and its components from a chemist's point of view. We provide explanations and solutions to avoid side reactions occurring in the assay mixture under different conditions. We are convinced that it is important to understand the underlying chemistry and side reactions of the artificial electron acceptors to avoid fluctuations in composition and concentration of the assay mixture, ultimately yielding more reproducible assay results.

2.2.3 Results and Discussion

2.2.3.1 A Note on MDH

MDH activity is often observed in the absence of an added substrate.[30] We stress here that the investigation of assay components PES/PMS and DCPIP does not solve the problem with this so-called endogenous substrate of MDH, but shall identify handling errors while performing colorimetric assays. It has been suggested that the endogenous substrate could stem from traces of alcohol left from the recrystallization of the buffer. An inquiry with the supplier ruled this out, as no alcohol had been used during the final purification stages of our buffer (PIPES). However, an experiment with NaCl (concentrations between 10 and 100 mM were tested) showed hardly any background reaction in the absence of the substrate compared to the PIPES buffer (10 and 100 mM tested). This background reaction from endogenous substrate can also be observed in PIPES buffer when MDH is assayed with its natural electron acceptor (e.g., cytochrome c_{GJ}). Hence, traces of other organic substances in the buffer that could act as substrates cannot be ruled out. Further, we and others have observed significant variations of MDH activity among different enzyme batches and fractions obtained after purification. Fractions exhibiting lower enzymatic activity often show a decreased PQQ absorbance (as observed around 355 nm) relative to the 280 nm feature or the complete loss of the prosthetic group (data not shown).[115] Since the proteins often have to be stored in methanol for stability, washing of MDH before conducting assays is required. Due to this procedure, a partial removal of PQQ in the active site is conceivable. Hence, full spectra (from 200 to 600 nm) should always be recorded to include the PQQ fingerprint (the absorbance spectra of the used MDH samples are presented in Figure S6) and, in addition to SDS-PAGE, 355/280 ratios should be reported to normalize for the holoenzyme content of the sample.[96,97]

2.2.3.2 The Redox Dye DCPIP

DCPIP has been used for decades as a redox dye and two-electron acceptor.[116–118] A wavelength of 600 nm is routinely used for the detection of DCPIP-coupled reactions (Scheme 4) mostly for assessing MDH activity together with PMS (1a) and PES (2a), although studies of coupling DCPIP with the natural electron acceptor cytochrome c_L have been reported.[56] The comparability of results relies often on the reported extinction coefficient ε at 600 nm. However, vastly varying values for ε_{600} have been

published even for similar conditions (Table S1). ε_{600} of DCPIP is pH dependent (Figure 6) and increases with increase in pH (this dye has a pK_a around 5.90).[108] Furthermore, a redox potential of + 217 mV has been reported.[119]

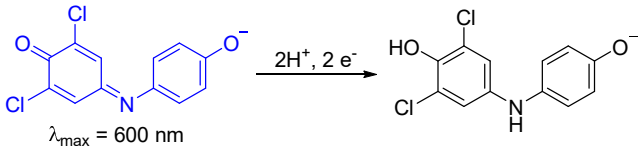

Scheme 4 Upon two electron reduction, DCPIP undergoes a distinct color change. Usually the sodium salt and neutral to alkaline pH are employed in MDH assays. Hence the deprotonated form is shown.

Variations of the reported extinction coefficient, even for similar conditions, cannot be solely attributed to different batches and purities of the DCPIP dye used (Table S1). MDH assays are run at different pH values and temperatures depending on the MDH source (extremophile, mesophile, acidophile, neutrophile, etc.). Therefore, it is important to determine the extinction coefficient of DCPIP for new assay conditions (buffer system, pH, temperature). Our measurements further showed that the solubility of DCPIP has likely been overestimated. A concentration of 10 mg DCPIP/ml water is described to be the solubility limit.

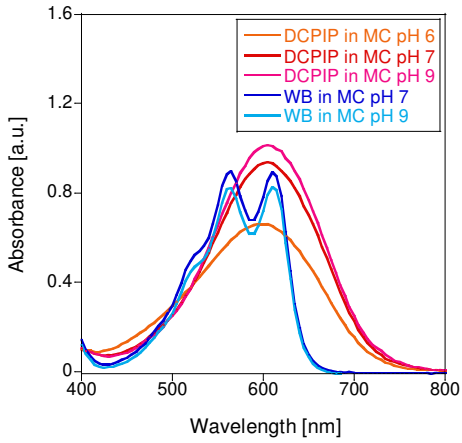

Figure 6 Absorbance spectra of 50 µM DCPIP (3) and 100 µM WB (4b) in 100 mM multicomponent buffer of pH 6 (for DCPIP), pH 7 or pH 9. Fresh samples were prepared by diluting a 2 mM stock solution of the dye with the corresponding buffer. Spectra were collected at a Cary60 UV–vis spectrophotometer at room temperature and corrected for the buffer baseline.

However, we found 2 mM of DCPIP (0.65 mg/ml) to be a good concentration in MilliQ water to give a homogeneous solution without precipitate. Whereas the powdered form of the dye is reported to be stable, DCPIP solutions should be prepared freshly every day in dark reaction tubes, as a low color stability of DCPIP in solution has been described.[120,121] Interestingly, we observed that in DCPIP-coupled

MDH assays, the enzymatic activity was higher under exclusion of oxygen compared to assays performed under aerobic conditions. This is most likely due to the slow re-oxidation of reduced DCPIP under aerobic conditions.[122] Also the bleaching of the dye in the absence of MDH was significantly decreased when oxygen was absent (data not shown). Therefore, only freshly filtered (and thus somewhat degassed) buffers should be used.

2.2.3.3 A Note on Buffers

Many bacteria that express methanol dehydrogenases grow best at elevated temperatures. Examples are the genera *Methylothermus*, *Methylococcus*, *Methylocaldum* and *Methylacidiphilum* (e.g. *M. fumariolicum* SolV or *M. infernorum* V4).[66,67] Hence, the assay of the isolated enzyme is often conducted at temperatures other than room temperature. As many buffers exhibit a change in pH upon heating, it is important to account for the concomitant change in pH as well.[123] It is thus advisable to either correct the pH at a certain temperature or to determine ε_{600} of DCPIP for the given conditions (type of buffer, pH, temperature) to ensure better comparability between assays. Furthermore, Grady, Chasteen and Harris report that 4-(2-hydroxyethyl)-1-piperazineethanesulfonic acid (HEPES) and piperazine-*N,N'*-bis(2-ethanesulfonic acid) (PIPES) and other piperazine-based buffers readily show radical formation (Chart 2).[124] This is especially troublesome when studying redox reactions. Phosphate ions are known to readily precipitate supplemented lanthanides.[100] Tris(hydroxymethyl)-aminomethane buffer (Tris) is strongly temperature dependent and can further undergo Schiff base-type condensations with aldehydes, which is problematic when investigating substrates like formaldehyde.[125,126] Additionally, the Tris buffer family shows complex formation with many metal ions as well as succinate and some members of the cyclohexylamino, acetamido and propanol family of buffers.[127] A complexation of lanthanides was further described for citrate and Good's buffers such as tricine, which will disturb metal-binding studies.[128] While there may not exist a perfect buffer system, it is important to be aware of the aforementioned potential pitfalls (Chart 2).

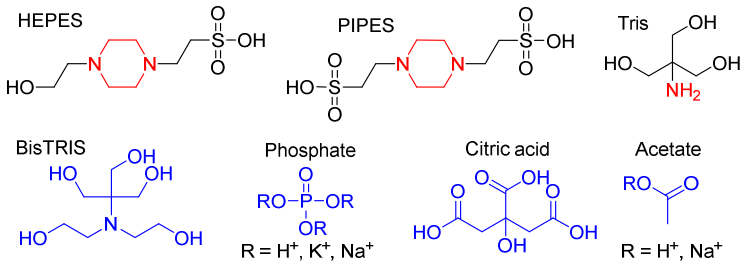

Chart 2 A selection of buffers that have been used in MDH assays. The piperazine ring in PIPES and HEPES shown in red may cause problems when investigating redox reactions. The amine of Tris can react with formaldehyde, a substrate/product of many enzymes including MDH. Buffers shown in blue are known to complex or precipitate lanthanides and may thus compete with the enzyme for the metal ion in the active site.

2.2.3.4 Artificial Electron Acceptors PES and PMS

Phenazines are applied as primary EA in DCPIP-coupled assays, replacing the physiological electron acceptor, cytochrome c_L or cytochrome c_{GJ} in artificial assays.[70,104] Although both phenazines are widely used as electron acceptors and Ghosh and Quayle reported PES as the preferred electron acceptor,[129] PMS is predominantly utilized in MDH assays.[60,72,130] In the chemistry community it is well known that PMS shows a higher tendency for radical formation, dealkylation and decomposition than PES.[129,131] However, few of these insights have made their way into the life science field. Hence, to better understand the stability and handling of these electron acceptors in a biochemistry setting and to prevent a decrease of the phenazine concentration, we investigated them more closely.

Stability of PMS and PES under storage and assay conditions

To investigate whether light-induced degradation proceeds via radical formation under certain conditions (light, pH, temperature), EPR spectroscopy was used (Figure 7 and Figure 8). First, PMS and PES were analyzed in MilliQ water and buffered aqueous solution at pH 7.2 and 9, the same conditions that we used in dye-coupled assays (100 mM multicomponent (MC) buffer, Figure 7).

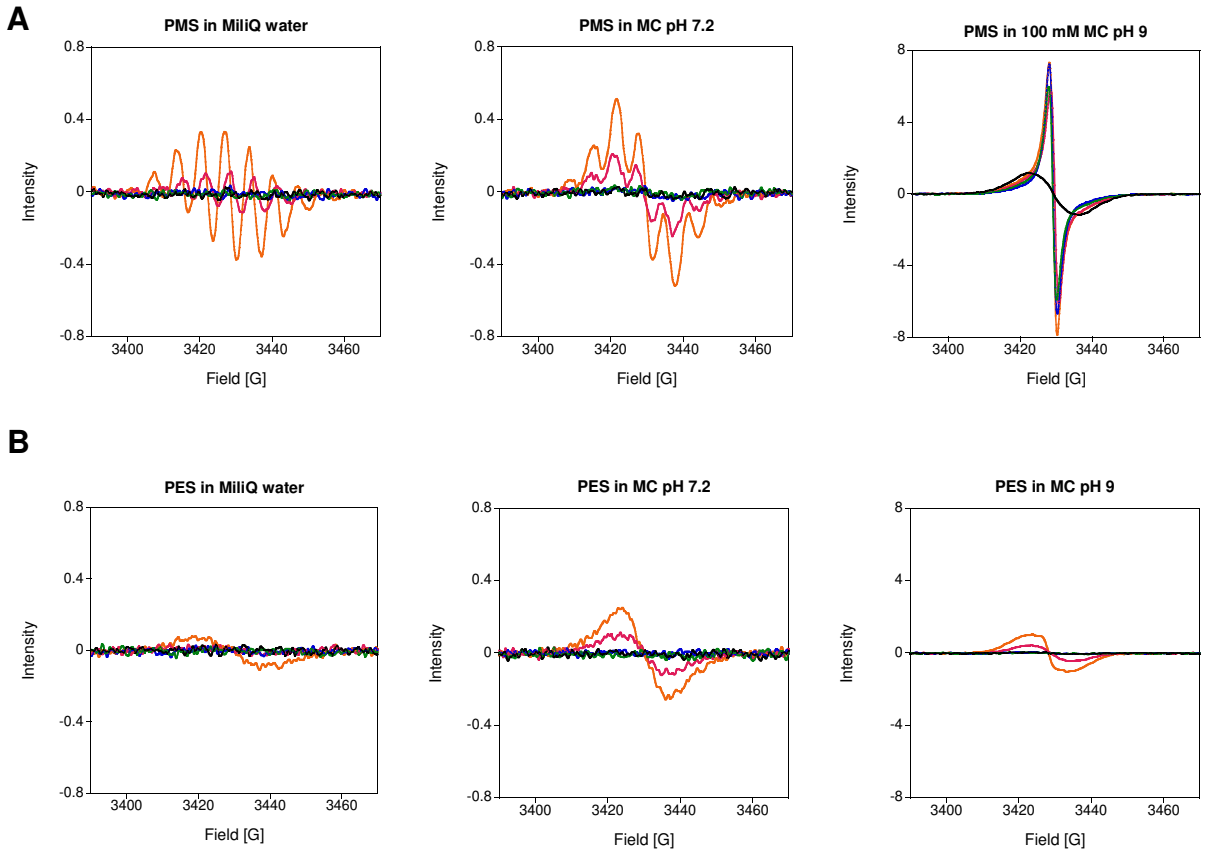

Figure 7 EPR spectra of 10 mM PMS (A) and PES (B) in MilliQ water (pH 6) or 100 mM multicomponent (MC) buffer pH 7.2 or pH 9. Solutions were prepared on a cloudy day and were either stored in an amber tube at 4 °C (black line), at RT in the dark (green line) or heated at 45 °C for 15 min in an amber tube (blue line). Additional samples were exposed to either daylight (orange line) or UV light of 254 nm (pink line) for 5 min each. Spectra were recorded at room temperature using an EMXnano EPR spectrometer.

We observed more rapid radical formation for PMS than for PES and, in both samples, the level of formed radicals was increased at alkaline pH (pH 9 resulting in a 16 × higher EPR intensity) when the samples were exposed to daylight. UV light (254 nm) led to a similar, but much smaller effect. Heating the solutions of electron acceptors prior to use, as has been recommended,[32] led to little radical formation, and neither did storage of the aqueous stock solutions at 4 °C. These results are in line with those of the literature.[129,132] Our results also indicate that radical formation is influenced not only by light exposure (sample preparation on sunny and cloudy days already showed a different radical content), but also by the pH and the buffer system (Figure 8).

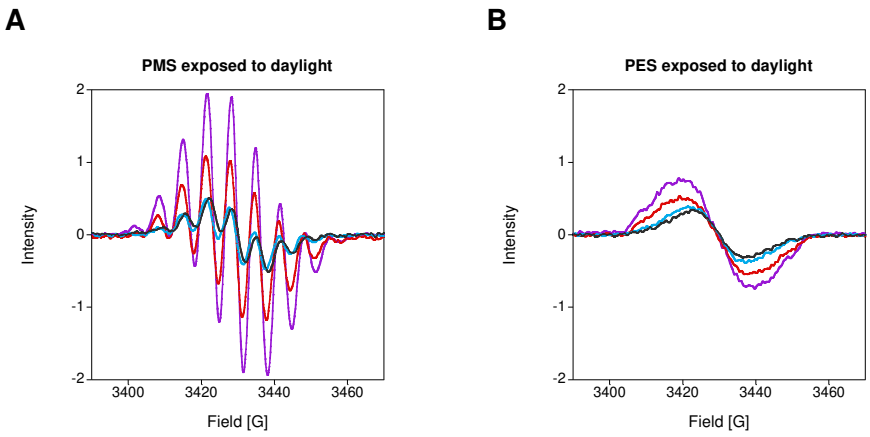

Figure 8 EPR spectra of 10 mM PMS (A) and PES (B) in MilliQ water (pH 6, purple line); 20 mM PIPES buffer of pH 6.2 (red line) and pH 7.2 (blue line); 20 mM potassium phosphate buffer of pH 7.2 (grey line). Solutions were prepared on a sunny day and were exposed to daylight for 5 min. Spectra were recorded at RT using an EMXnano EPR spectrometer.

To sum up, it is recommended using PES instead of PMS and to diligently prevent light exposure. Stock solutions of these artificial EA should be prepared fresh in MilliQ water instead of buffer and the assay mixture should be heated subsequently for at least 15 min prior to performing experiments. It is further advisable to study the absorbance of the assay mix over time in the absence of MDH upon switching to a new buffer system.

Difference between using PES or PMS and different batches of these electron acceptors in an MDH assay

During our studies, we noted differences both in the appearance and spectroscopic signatures of commercial PMS and PES samples. Table S2 shows that the elemental composition of the samples varies only within the error of the used instrument (0.30%) for both phenazine derivatives obtained from Sigma-Aldrich®, whereas the PMS sample obtained from abcr® shows a significantly lower carbon content. This sample also showed different IR and UV-vis spectra compared to the PMS samples from Sigma-Aldrich® (Figure S7; Figure S8). However, when used to determine the activity of MDH enzymes (originated from both strains AM1 and SolV), the three PMS samples yielded similar results (see Figure 9 for AM1). It was observed that PES gave higher specific activities for both AM1 and SolV MDH, and that the shelf life or Lot# of the EA did not influence the assay.

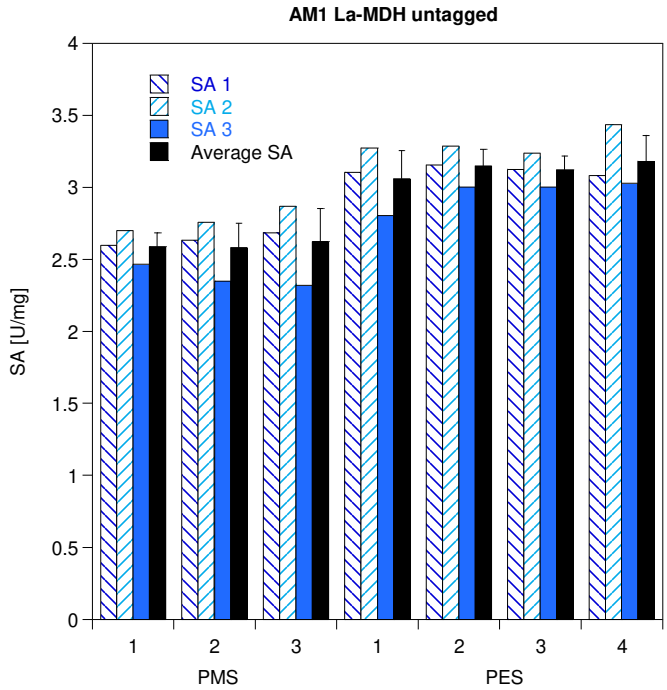

Figure 9 Specific activity (SA, in µmol min^{-1} mg^{-1}) of MDH using different PMS and PES batches of different purities and suppliers. M. extorquens AM1 La-MDH (untagged, 100 nM) in multicomponent buffer (100 mM, pH 9), 15 mM NH_4Cl at 30 °C. All samples contained 100 µM DCPIP and 50 mM MeOH, with 1 mM PES or PMS. Total volume in all wells was 200 µl. The reaction was monitored at 600 nm. SA1 and SA3 were determined by a different pair of hands than SA2 and are technical replicates.

2.2.3.5 A Combined One-Electron Acceptor and Redox Dye in One: Wurster's Blue

Besides the two-component assay system with the two-electron acceptors PMS/PES and DCPIP, the one-electron acceptor and radical cation Wurster's blue (WB, 4b in Scheme 5) can be used for the investigation of methanol dehydrogenases.[30] We refer herein to the cation radical of TMPD (4a) as WB. WB has been used for respiration studies in biochemistry and, many decades ago, also as an electron acceptor for alcohol dehydrogenases.[30,109,133,134] The absorption spectrum of a 100 µM WB solution is shown in Figure 6. From a chemical point of view, the properties of WB and its precursor, TMPD, have been extensively studied in the past,[135–140] but their characteristics and handling conditions are not commonly known in the life science field. Therefore, we synthesized WB using a modified protocol according to Michaelis and Granick from the commercially available TMPDD and analyzed WB under different storage as well as MDH assay conditions to optimize its use in biochemical assays.[141] We found that 4b is fairly stable as a solid for several weeks at room temperature under an atmosphere of nitrogen. Storage under an atmosphere of nitrogen at - 20 °C, however, is recommended for better stability.

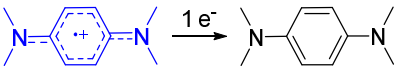

4b **4a**

Scheme 5 The radical cation Wurster's blue (4b) can undergo reduction to TMPD (4a) and can be used to monitor MDH activity.

Previously reported extinction coefficients of WB are presented in Table S3. Additionally, we determined ε_{610nm} at different pH values in a multicomponent buffer under the same conditions as we used in MDH assays. As shown in Table S3 and Figure 6, the extinction coefficient varies to a lesser extent compared to DCPIP.

Storage conditions

The decay of the radical cation can be monitored by its decoloration.[109] The blue-colored radical cation exhibits absorbance maxima around 560 nm and 610 nm and the extinction coefficient of the latter wavelength was used to calculate the specific enzymatic activity of MDH in kinetic assays.[109,142] EPR and UV-vis measurements (Figure 10) confirmed a good stability of the WB radical in MilliQ water (A) and in buffered solution of pH 7 (data not shown) as well as in samples that had been briefly stored on ice in MilliQ water and were diluted in alkaline buffer just before analysis (B). An alkaline pH led to a fast degradation of the WB radical (C). Since the radical cation has been reported stable in aqueous solutions at a pH of 3.5 – 6 but undergoes degradation outside this pH range[140] and under routinely used assay conditions (pH 9), a prolonged incubation of the dye under conditions of high pH should be avoided.

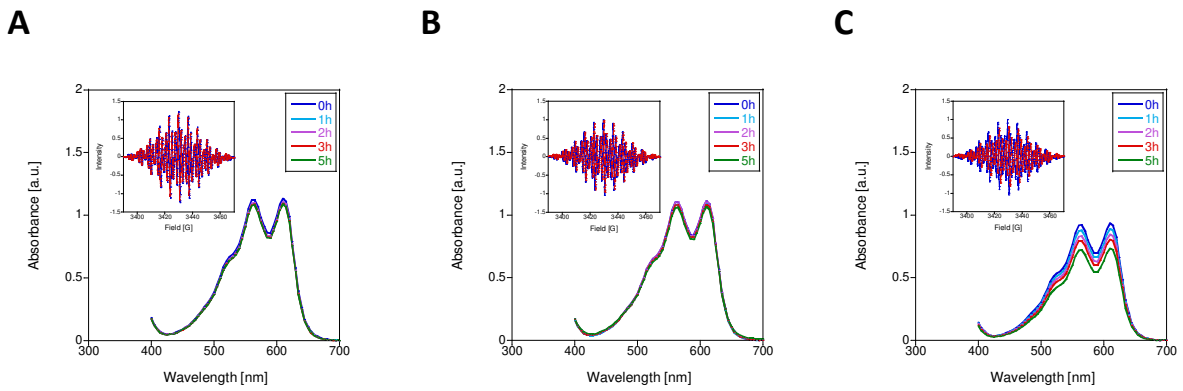

Figure 10 UV–vis and EPR spectra of 200 µM WB in solution over time. 2 mM WB samples in MilliQ water (A, B) or 100 mM multicomponent buffer pH 9 (C) were stored on ice. In the case of a WB was diluted with MilliQ water. Samples of B and C were diluted in 100 mM multicomponent buffer, pH 9. UV–Vis spectra of triplicates (A, C) and duplicates (B) were recorded at 30 °C on an Epoch2 spectrophotometer without path length correction. MilliQ water and buffer baselines were subtracted from the corresponding spectra. The standard deviation was less than 7%. EPR spectra were recorded on an EMXnano EPR spectrometer at room temperature and in the dark. Blue line: fresh sample, red line: sample that has been stored on ice for 3 h in amber tubes.

Storage temperature

Next, we analyzed WB samples that were stored under different conditions in MilliQ water and were either flash frozen in liquid nitrogen or frozen slowly before storage on ice (Figure 11). Flash freezing did not influence the radical cation concentration, whereas the storage temperature had a major effect. We found the best storage temperature to be - 80 °C, and higher temperatures of - 20 °C resulted in a decrease of the radical cation. Storage at 4 °C for 24 h nearly halved its concentration. We, thus, suggest avoiding the storage of WB solutions.

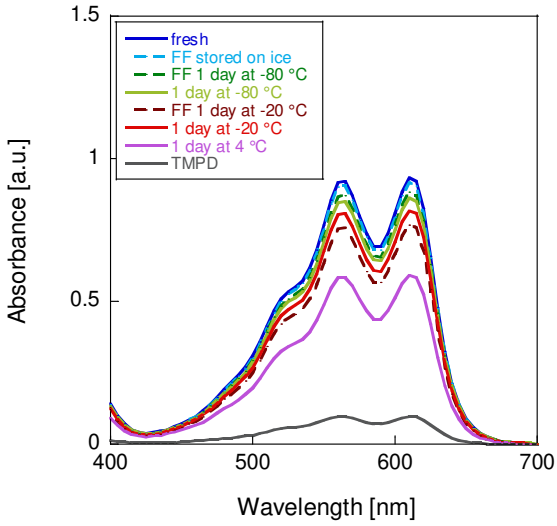

Figure 11 UV–vis spectra of differently stored WB in 100 mM multicomponent buffer pH 9. 2 mM WB samples were stored in MilliQ water and diluted with buffer to a concentration of 200 µM before measurement. Spectra of triplicates were recorded at 30 °C on an Epoch2 plate reader without path length correction. The buffer baseline was subtracted from the spectrum. The standard deviation was less than 10%. (FF, flash frozen).

Effect of pH and temperature

We further evaluated the effect of the assay condition (pH, buffer system and temperature) on WB radical cation stability. Our results (Figure 12) reveal that organic buffers with acidic and neutral pH such as MES, MOPS and MOPSO do not influence the radical cation stability negatively. Yet, PIPES buffer caused a slight decrease in absorbance over time, which was more pronounced in the inorganic potassium phosphate buffer. Further, buffers of alkaline pH such as CAPS or CHES led to a fast decomposition of the dye. Moreover, compared to a temperature of 45 °C (data not shown), the WB absorbance was more stable at 30 °C.

The negative effects of high temperature and pH on WB decomposition are also corroborated by EPR spectroscopy (Figure S9). We therefore performed the following kinetic assays at 30 °C. Interestingly, when aqueous solutions of the precursor TMPD or the dichloride salt TMPDD were heated to 45 °C, formation of the Wurster's blue radical was observed to some extent, depending on the pH of the buffer system (Figure S10 and Figure S11).

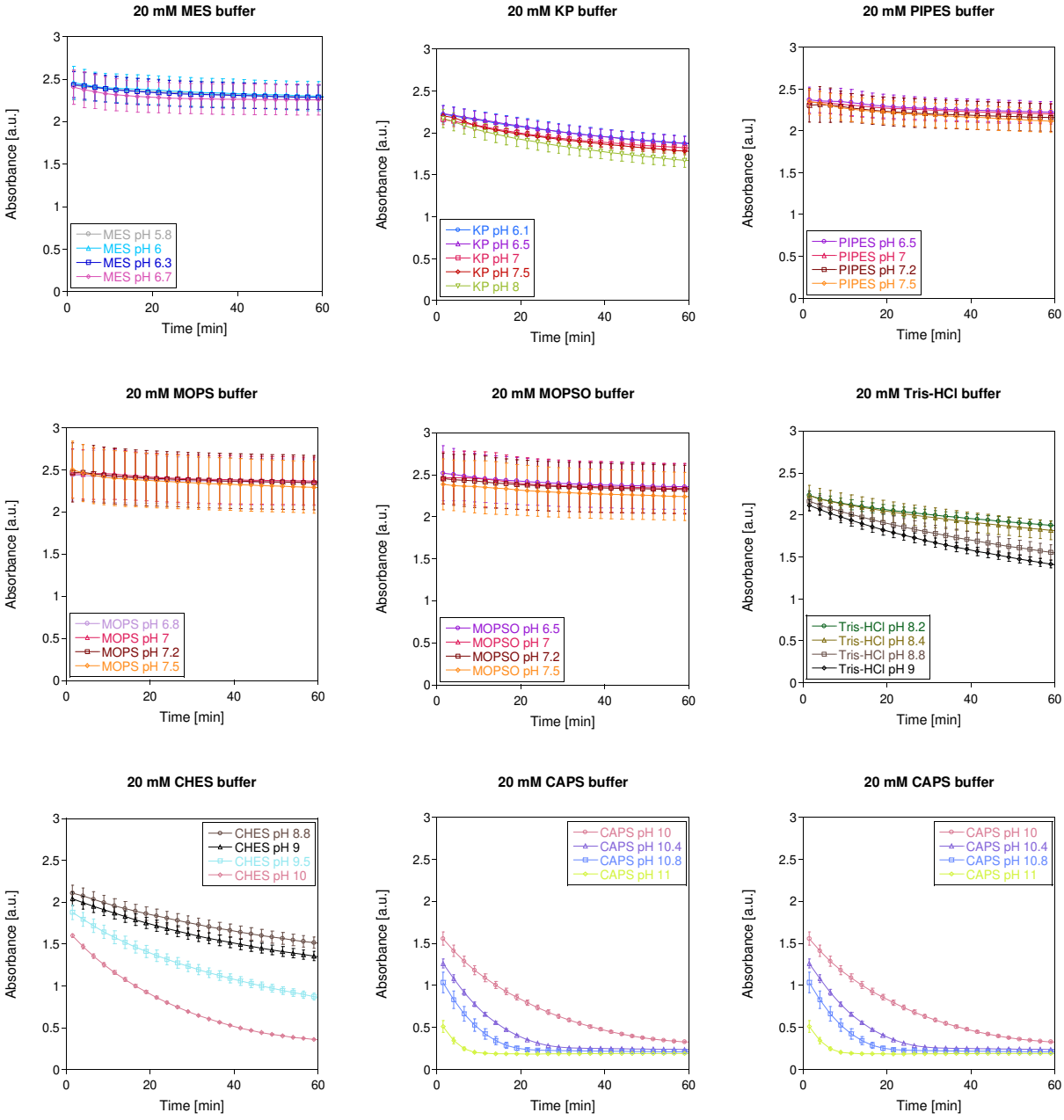

Figure 12 pH dependence of WB in different buffers. Conditions were as follows: 200 µM WB in 20 mM buffer of different pH, heated for 1 h at 30 °C. Absorbance at 610 nm was monitored with an Epoch2 plate reader. Experimental and technical (CHES and CAPS) triplicates with standard deviations are shown. Data were path length corrected to 1 cm.

WB in MDH assays

Our insights regarding the stability and handling of WB were verified using La-MDH from *M. extorquens* AM1 (Figure S12). We confirmed that flash freezing the dye in liquid nitrogen preserved the WB solution and thus did not affect MDH specific activity (SA) negatively, whereas storage of WB stocks at 4 °C led to a decreased SA even after adjustment of the WB concentration. In contrast, the MDH activity was restored by concentration adjustment in WB samples that have been stored in MilliQ water at - 20 °C and - 80 °C and shows only slight variations within the error range. Additionally, the precursor of WB, TMPD, was tested as EA for MDH. But both TMPD and a mixture of WB and TMPD led to no or decreased methanol oxidation by MDH. Next, the WB concentration dependence of both AM1 La-MDH and SolV Eu-MDH was analyzed (Figure 13). Both MDH types showed increasing SA in the range of 0 – 400 µM WB and a linear WB dependence. SolV Eu-MDH exhibited a notably lower enzymatic activity, which is likely due to the impact of Eu^{3+} on catalytic efficiency.[71] Also, a temperature of 30 °C instead of 45 °C was used, which was less than optimal for this MDH. In the case of SolV Eu-MDH, no WB inhibition occurred at 400 µM, so higher concentrations can be used.[30] For a better comparability of the two MDH types, we chose a WB concentration of 200 µM.

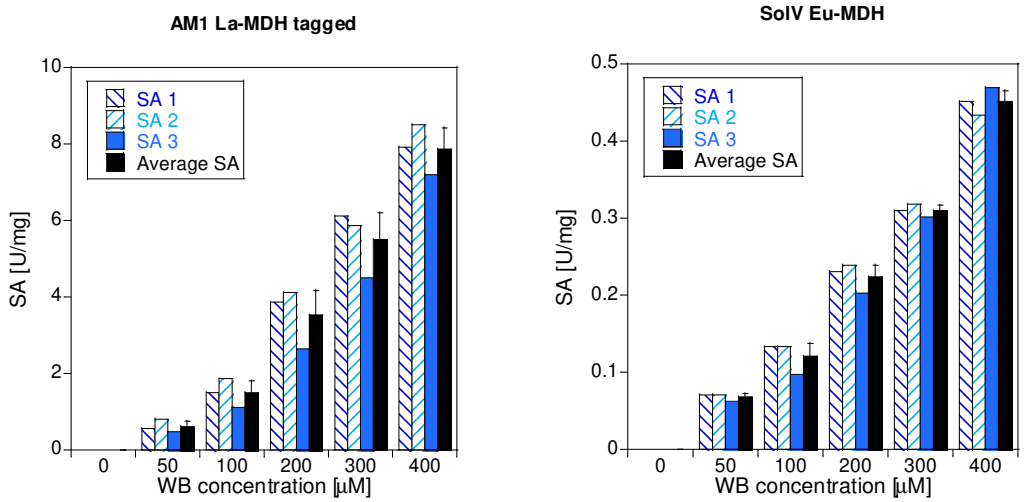

Figure 13 WB dependence of AM1 La-MDH and SolV Eu-MDH. The specific activity (SA, in µmol min^{-1} mg^{-1}) of His-tagged AM1 La-MDH (left) was determined in 100 mM multicomponent buffer, pH 9, with 15 mM NH_4Cl. SolV Eu-MDH activity (right) was measured in 100 mM multicomponent buffer, pH 7.2, with added 20 µM Eu^{3+}. The WB concentration was varied, and protein concentration was constant at 100 nM for AM1 La-MDH and 200 nM for SolV Eu-MDH. The assay was performed with 50 mM MeOH at 30 °C and 610 nm. The total volume in wells was 200 µl. All SA are technical replicates. SA1 and SA2 were determined by different pairs of hands than SA3. Data were collected at an Epoch2 plate reader.

Further, the influence of ammonia/ammonium ions on the activity of AM1 La-MDH (Figure S13) with WB was studied.[30,102] Both the free ammonia base and the ammonium ion were reported to either positively or negatively influence (as activator or inhibitor) MDH, but this mechanism is still not fully understood.[53143,144] SolV Eu-MDH shows activity without an additional activator (III.2.3 Further Assay Optimization).[49,61,71] Activity was low for both polyhistidine tagged and untagged AM1 La-MDH in the absence of NH_4Cl, while the addition of 15 mM NH_4Cl led to the highest enzymatic activity in the range studied (Figure S13). Taken together, our results show that WB can be utilized as a single reagent EA/dye for Ln-MDH assays. The step-by-step assay procedure and handling suggestions for the use of WB as electron acceptor are summarized in Table 6 below. To sum up, prolonged storage, high temperatures and pH should be avoided, if possible, as these parameters lead to rapid degradation of WB. If additives such as metal ions or ammonia are required, WB stability under the new conditions should be evaluated first without added enzyme. Using a plate reader, a concentration of 200 µM WB for routine assays presents a good starting point.

2.2.4 Conclusion

In this work, we present a thorough analysis of the buffers, electron acceptors PMS and PES and the redox dyes DCPIP and WB used in MDH assays. We provide recommendations for the handling of these compounds to minimize decomposition and unwanted side reactions in the absence of MDH. Most importantly, radical formation of the EA, leading to a non-enzymatic reduction of DCPIP in MDH assays, can be minimized through the exclusion of light. Overall, PMS is more prone to degradation than PES. Further, the one-electron acceptor and redox dye, WB, was used for the first time in assays with lanthanide-dependent MDH. This radical cation was synthesized from TMPDD using bromine and found to be best suited for a quick identification of enzymatic activity at a concentration of 200 µM. A summary of the most important handling suggestions is provided in Table 5 and Table 6.

Table 5 Handling suggestions of artificial electron acceptors for MDH assays – PES/PMS and DCPIP.

Handling suggestions for PES/PMS DCPIP assay			
Stage	Step no.	Description	Note
Stock solution preparation	1	Prepare a 100 mM PMS/PES stock solution in MilliQ water.	Exclude light, stock solution should be made fresh in amber-colored tubes and stored on ice until measurement.
	2	Prepare a 2 mM DCPIP stock solution in MilliQ water.	Exclude light, stock solution should be made fresh in amber-colored tubes and stored on ice until measurement.
	3	Prepare additives for the assay (e.g. $EuCl_3$ or NH_4Cl stock solutions).	
Determine extinction coefficient (ε_{600}) for DCPIP under chosen conditions	4	Use same buffer system (type of buffer and concentration, pH, temperature as for the assays).	Temperature can affect the pH of certain buffers significantly.
Assay mix preparation	5	Mix PMS/PES and DCPIP stock solutions in buffer to a final concentration of 100 µM DCPIP and 1 mM PMS/PES.	Assay mix should be heated for 15 min at 45 °C in the dark to reduce the background reaction, avoid radical forming buffers that will quench the electron acceptors
Spectrophotometric read-out	6	Mix assay mix with MDH/MeOH in a 96 well plate and equilibrate 2 min at assay temperature.	Minimize light exposure and monitor the background of the assay mix at 600 nm.
	7	Add MeOH/MDH to start the assay.	Minimize light exposure.

Table 6 Handling suggestions of artificial electron acceptors for MDH assays – WB.

Handling suggestions for WB assay			
Stage	Step no.	Description	Note
Stock solution preparation	1	Prepare a 1 mM WB stock solution in MilliQ water.	Low solubility limit, exclude light, stock solution should be made fresh in amber-colored tubes and used immediately.
Determine extinction coefficient (ε_{610}) for WB under chosen conditions	2	Use same buffer system (type of buffer and concentration, pH, temperature as for the assays).	Temperature can affect the pH of certain buffers significantly.
Assay mix preparation	3	Mix WB with buffer to a final concentration of 200 µM.	Acidic and neutral buffers are better, alkaline pH leads to a fast decomposition of WB, exclude light.
Spectrophotometric read-out	4	Mix WB/buffer with MDH/MeOH in a 96 well plate and equilibrate 2 min at assay temperature.	Lower temperatures are better, high temperatures cause decomposition, minimize light exposure and monitor background at 610 nm.
	5	Add MeOH/MDH to start the assay.	Minimize light exposure. Monitor background activity/decomposition of the dye prior to addition of MDH.

In summary, the PES (or PMS) and DCPIP coupled assay is the method of choice for MDH kinetic analysis and can yield reproducible results when the components are handled correctly. Parameters determined with this artificial assay (originally developed by Anthony and Zatman) such as pK_a values, pH dependence or Arrhenius activation energies from temperature-dependence measurements are similar to the ones determined from protein electrochemistry when using the natural electron acceptor cytochrome c_{GJ}.[104] The one-electron acceptor and dye WB, on the other hand, presents an easy method for routine MDH assays, for example, identifying MDH containing fractions during enzyme purification. Due to its low stability at alkaline pH, PES-DCPIP is preferable to WB as EA/dye for determining the kinetic parameters. With this study we aimed to provide information about the handling of electron acceptors used in MDH assays to promote consensus in assay measurements for better comparability of results.

2.3 Further Assay Optimization

In addition to the published investigation of electron acceptors in the context of MDH assays (above)[145], the PES-dependence of SolV MDH was analyzed and the effect of other routinely used assay components, such as cyanide and ammonia were examined to optimize the assay for studies on SolV MDH. All experiments were performed under steady-state conditions at substrate saturation using SolV MDH.

2.3.1 Phenazine Ethosulfate

The investigation of alkylated phenazines in the previous chapter showed that PES is a better electron acceptor for dye-coupled assays compared to PMS. A lower background activity was observed in the absence of MDH if PES was used concurrent with less severe bleaching of DCPIP. As described above, PMS and PES influence the specific activity of both AM1 and SolV MDH. Yet the two kinds of the phenazine dye affect the SA of both enzymes differently. At the above applied assay conditions with a phenazine concentration of 1 mM, AM1 MDH exhibits a comparatively small difference with an approximate 1.2-fold increase of the SA if PES is used (Figure 9). In contrast, PES enhances the SA of SolV MDH about twofold (Figure 14A). Although the overall enzymatic activity is about 20 times higher in the case of AM1 MDH, a stronger influence of the phenazine dye on the SA of SolV MDH is observed.

Therefore, different concentrations of the electron acceptor (ranging from 0.5 mM to 2 mM) in assays with SolV MDH were tested. The results in Figure 14A show that the effect of the primary electron acceptor is dependent on its concentration. At low concentrations, the difference in the SA is only small as a result of a concentration-dependent background reaction. At phenazine concentrations of 1 mM, however, SolV MDH was twice as active if PES was used instead of PMS. Here, the background reaction in the absence of MDH is highly increased, predominantly in the case of PMS, leading to a notably lower SA value compared to PES. At higher phenazine concentrations the difference in the SA between values measured in the presence of PMS and PES is slightly smaller. Although the background reaction increases with increasing phenazine concentrations, it has a small effect if the SA is high. This finding is consistent with the results obtained with AM1 MDH.

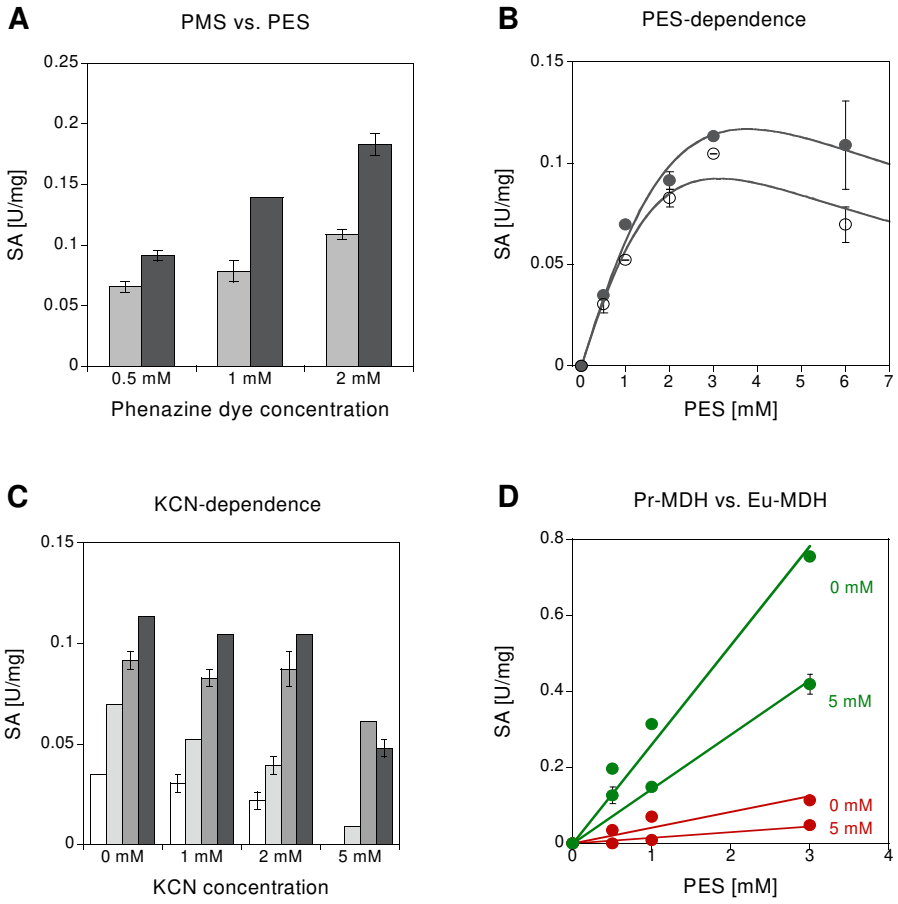

Figure 14 Influence of PMS/PES and KCN on SolV MDH activity. Conditions were as follows: 100 nM MDH, 20 mM PIPES pH 7.2, 100 µM DCPIP, 50 mM MeOH, 45 °C, n = 2. A: Comparison of PMS (light grey) and PES (dark grey). Eu-MDH 4th activity was measured in the presence of 20 µM Eu^{3+} and 1 mM KCN. B: PES-dependence of Eu-MDH 4th in the absence (closed circles) and presence (open circles) of 1 mM KCN. C: KCN-dependence of Eu-MDH 4th at PES concentrations of 0.5, 1, 2 and 3 mM (from light to dark grey). D: PES-dependence in the absence and presence of KCN (5 mM) compared: Pr-MDH (green) vs. Eu-MDH 4th (red).

In a following step, the PES-dependence of SolV MDH was studied (Figure 14B) to determine the PES optimum for the use of this electron acceptor in assays. The measured SA at different PES concentrations was fit to the equation for substrate inhibition (equation 1) to obtain the affinity constant K_m and inhibition constant K_i:[133]

$$SA = \frac{v_{max}\,[S]}{K_m + [S] \cdot (1 + \frac{[S]}{K_i})}$$

The fit of the PES-dependence (closed circles) gave an apparent maximum velocity v_{max} of 0.23 U/mg with an error in the ppm range for all calculated values. The v_{max} is significantly higher than the observed one of about 0.12 U/mg. Harris and Davidson explain this finding with MDH inhibition by PES. A saturation of the enzyme with electron acceptor is therefore not possible.[133] Further evidence for PES-dependent MDH inhibition is given by the obtained constants. The apparent affinity constant K_m (3.35 mM) is only marginally lower compared to the apparent inhibition constant K_i (4.25 mM). The PES optimum was further determined from the curve fit. A concentration of 3.5 mM PES was found to promote the highest SA of SolV Eu-MDH.

2.3.2 Potassium Cyanide

Cyanide is routinely added to many MDH assays. Since enzymatic activity has been observed in the absence of substrate, cyanide was used to suppress this so-called endogenous activity. Moreover, cyanide has been described as a protective agent and competitive inhibitor to prevent the inhibition of MDH enzymes by phenazine dyes.[30] To test if this is true for SolV MDH, KCN-dependent studies were performed to determine the optimal cyanide concentration for SolV MDH assays. The KCN concentration was varied from 0 mM to 5 mM and the enzymatic activity was measured in the presence of different PES concentrations (Figure 14C). Overall, SolV MDH activity decreases with increasing KCN concentrations in the presence and absence of added substrate. This effect is most pronounced at low PES concentrations, such as 0.5 mM and 1 mM. At higher PES concentrations (2 mM and 3 mM), the influence of cyanide on the SA is weak. When high KCN concentrations of 5 mM are applied, the SA at all tested PES concentrations is significantly decreased. Further, SolV MDH shows no enzymatic activity at low PES concentrations due to either a competitive binding of PES and cyanide at the active site[143] or inactivation of the electron acceptor by adduct formation or demethylation[145,146].

In contrast to these results, Hothi *et al.* observed only a minor effect of cyanide on MDH activity at substrate saturation.[143] Next, the PES-dependence in the presence of 1 mM KCN was examined (Figure 14B, open circles) since, at this concentration, MDH activity was least negatively affected by cyanide. Specific activities were fit to the substrate inhibition (equation 1 above). The following values were obtained with an error in ppm range: 0.2 U/mg for v_{max}, 2.9 mM for K_m and 3.35 mM for K_i. As expected, the apparent v_{max} is noticeably lower in the presence of KCN. However, the inhibition of MDH by PES is not considerably lower. Arun *et al.* found that the cyanide level in solution is dependent on the pH of the medium.[147] Alkaline pH stabilizes the cyanide concentration in solution whereas at neutral pH, vaporization of HCN is induced.[148] This effect is enhanced at high temperatures which are routinely used for MDH assays especially for that of extremophile MDH.[149] Higher KCN concentrations were also tested but resulted in strongly fluctuating SA values without a distinct PES-dependence. The PES optimum (3 mM) shifted slightly to lower concentrations in the presence of cyanide. However, this value is within the error range of the curve fit.

A comparison of Eu-MDH and Pr-MDH from SolV (Figure 14D) showed that the overall SA of Pr-MDH is significantly higher compared to Eu-MDH. However, the ratio of activity at 0 mM and 5 mM KCN and various PES concentrations is similar for both enzyme derivatives. Therefore, PES and KCN influence SolV MDH in a lanthanide-independent fashion.

2.3.3 Ammonia

Ammonia is widely used as a MDH activator. While it is not necessary for MDH activity when assayed with its natural electron acceptor cytochrome c_L, ammonia activation was found to be crucial in artificial assays at high pH.[61,92,102,150] Yet the effect of this activator has not before been studied in WB-assays of Ln^{3+}-dependent MDH enzymes. Therefore, this work has analyzed both AM1 and SolV MDH with respect to their ammonia dependence under their respective optimal assay conditions. Three different buffer systems were used: PIPES (routinely used assay buffer for SolV MDH in this work), Tris (routinely used AM1 assay buffer) and multicomponent buffer. The latter was utilized since it allows the comparison of both MDH enzymes due to its broad pH range. As described above, AM1 La-MDH is dependent on ammonia activation if measured in artificial assays (Figure S13).[145] The investigation of SolV Eu-MDH in the presence and absence of 15 mM NH_4Cl, however, showed that the activity varies only within the error range and no clear enhancement of SolV Eu-MDH activity by ammonia is observed in WB assays (Figure 15). Both of the used buffer systems are redox active, yet

the multicomponent buffer presents a stronger redox activity compared to PIPES, resulting in an about twofold higher SA.[124] The ammonia independence of SolV Eu-MDH in the WB-assay is in line with Pol *et al.*, who reported that SolV MDH (cultivated with the early lanthanides La^{3+}, Ce^{3+}, Pr^{3+} and Nd^{3+} and assayed with the PES/DCPIP-assay) does not require ammonia.[49]

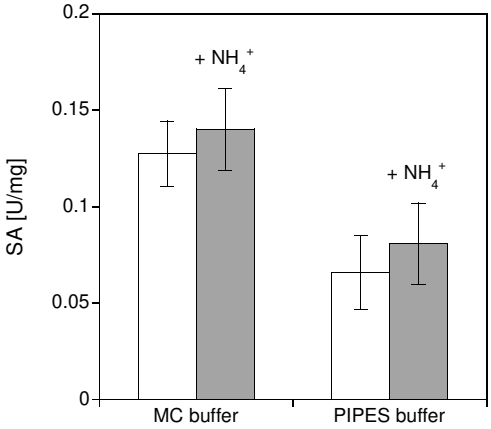

Figure 15 Influence of ammonia on SolV Eu-MDH activity. MDH was assayed in the presence (grey) and absence (white) of ammonium chloride (15 mM). Conditions were as follows: 200 nM Eu-MDH 4th, 100 mM multicomponent (MC) buffer or 20 mM PIPES, pH 7.2, respectively; 200 µM WB, 50 mM MeOH, 45 °C, n = 2.

2.3.4 Conclusion

The investigation of MDH enzymes is carried out using assays that are artificial in every way. Therefore, possible side reactions such as enzyme inhibition or inactivation have to be considered and conditions have to be optimized to obtain comparable in vitro results. Since a possible binding of PES and KCN close to the active site cavity has been described for other MDH enzymes,[97] the influence of these assay components on the enzymatic activity was analyzed in more detail to exclude a falsification of results. SolV MDH exhibits a strong PES- and KCN-dependence. A comparison of PMS and PES confirmed that PES is the better electron acceptor at various concentrations. A PES concentration of about 3.5 mM was found to promote the highest SA if SolV MDH is assayed at a concentration of 100 nM. Yet, MDH inhibition by PES was observed. The addition of cyanide had no effect on the latter inhibition but itself decreased the activity of SolV MDH at high concentrations. A comparison of different SolV MDH derivatives showed that the effect of PES and cyanide is similar in the presence of different central metal ions. Further, the ammonia independence of SolV MDH was also confirmed for WB assays. Based on these findings and the previously published results[145], an assay system was

designed for the kinetic investigation of SolV MDH. PES was chosen over PMS to avoid a falsification of assay results caused by strong background reactions leading to a non-enzymatic bleaching of the DCPIP dye. Due to MDH inhibition by phenazine dyes, a low PES concentration of 1 mM was chosen for further assays as a compromise between MDH inhibition and the limitation of substrate oxidation rates. Further, cyanide was excluded from measurements since it did not significantly influence the PES-dependent MDH inhibition.

3 The Impact of Metals

3.1 Introduction

Metalloenzymes such as methanol dehydrogenases are key players in the methanol metabolism of methylo- and methanotrophs.[26,49,53] Hibi *et al.* reported the first Ln^{3+}-dependent MDH enzyme, presenting the biological role of rare earth elements.[31] Further studies showed that lanthanides not only promote MDH activity but also control the expression levels of different MDH-types, the Ca^{2+}-dependent MxaF and the Ln^{3+}-dependent XoxF enzyme, based on the availability of metal ions.[32,33] Growth studies with several Ln^{3+}-dependent methylotrophs showed that early lanthanides strongly promote growth.[32,60] In good accordance, *M. fumariolicum* SolV that has been cultivated in the presence of a single lanthanide, exhibits differential growth rates dependent on the supplied metal ion. The growth rate decreases with the lanthanide series from left to right. Early lanthanides like La^{3+} support fast growth, whereas a late lanthanide like Yb^{3+} promotes hardly any growth. The growth rate in the presence of Eu^{3+} lays between that of La^{3+} and Yb^{3+} and was less than half of that observed with La^{3+}.[71] How lanthanide-dependent bacteria deplete REE from the environment and how the exact uptake mechanism functions, is yet not know and is subject to further research. However, the investigation of MDH activity and its comparison to SolV growth will give further insights into the function of lanthanides in these bacteria. Therefore, the role of the central metal ion and how MDH activity changes if different lanthanides are used, was investigated and affinity constants were determined.

La-MDH and Eu-MDH were applied for the investigation of the lanthanide ion´s impact on SolV MDH activity. All the used MDH samples were partial-apo enzymes in regard to the central metal ion. A higher degree of unoccupied active sites was observed if the cell growth was slow. La-MDH exhibit a La^{3+} metalation state of 80%, whereas Eu-MDH possesses a europium occupation of only 70%. The partial-apo nature of SolV MDH allows to study the impact of certain metal ions on MDH activity. Titration experiments were performed using either the dye-coupled assay, Eu^{3+} luminescence or isothermal titration calorimetry. The activity was measured in the presence of a certain metal ion and the amount of added metal ions necessary to obtain the highest enzymatic activity in assays was determined. The kinetic parameters obtained by various techniques were compared.

3.2 Impact of Metals on SolV Eu-MDH Activity in Dye-Coupled Assays

The previously purified Eu^{3+}-containing SolV MDH derivative (Eu-MDH 4^{th}) with an europium occupation of about 70% was used for the following studies.

The following section is part of the publication:

Similar but not the same: First Kinetic and Structural Analyses of a Methanol Dehydrogenase Containing a Europium Ion in the Active Site

Bérénice Jahn, Arjan Pol, Henning Lumpe, Thomas R. M. Barends, Andreas Dietl, Carmen Hogendoorn, Huub J. M. Op den Camp and Lena J. Daumann

Published in: *ChemBioChem* **19**, 1147-1153 (2018). DOI: 10.1002/cbic.201800130.

3.2.1 Abstract

Since the discovery of the biological relevance of rare earth elements (REEs) for numerous different bacteria, questions concerning the advantages of REEs in the active sites of methanol dehydrogenases (MDHs) over calcium(II) and of why bacteria prefer light REEs have been a subject of debate. Here we report the cultivation and purification of the strictly REE-dependent methanotrophic bacterium *Methylacidiphilum fumariolicum* SolV with europium(III), as well as structural and kinetic analyses of the first methanol dehydrogenase incorporating Eu in the active site. Crystal structure determination of the Eu-MDH demonstrated that overall no major structural changes were induced by conversion to this REE. Circular dichroism (CD) measurements were used to determine optimal conditions for kinetic assays, whereas inductively coupled plasma mass spectrometry (ICP-MS) showed 70 % incorporation of Eu in the enzyme. Our studies explain why bacterial growth of SolV in the presence of Eu^{3+} is significantly slower than in the presence of La^{3+}/Ce^{3+}/Pr^{3+}: Eu-MDH possesses a decreased catalytic efficiency. Although REEs have similar properties, the differences in ionic radii and coordination numbers across the series significantly impact MDH efficiency.

3.2.2 Titration Experiments

Eu-MDH titration experiments were conducted to determine the additional amount of Eu^{3+} that is necessary to achieve full occupancy of all active sites. Although there is debate about whether this approach can be used to determine association constants, it is well-suited for comparison of the affinities of similar metals (i.e., REEs) or for determination of saturation for further kinetics investigations.[151–153] Different concentrations of $EuCl_3$ were added to the partial-apo Eu-MDH (≈70 % of active sites occupied by Eu). Results are presented in Figure 17A and demonstrate that enzymatic activity follows typical Michaelis–Menten behavior. The metal association constant was determined to be (2.6 ± 0.6) µM. We were also interested in how different REEs influence the activity of the MDH, because they were shown to impact growth rates of strain SolV. Klebensberger and co-workers have shown that the specific activities of a PQQ-dependent ethanol dehydrogenase were dependent on the REE in question, with Pr^{3+} yielding a specific activity more than twice as high as that of the La^{3+} derivative.[151] Our findings shown in Figure 16 support this observation and might provide an explanation for why strain SolV grows more slowly in the presence of Eu^{3+}.

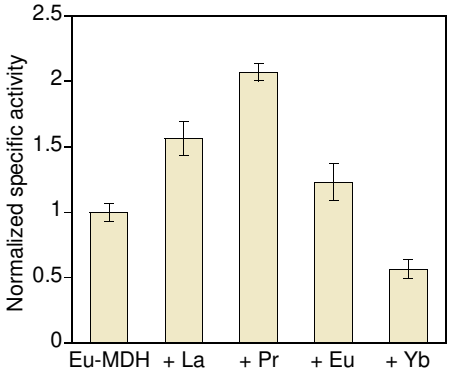

Figure 16 Titration of different REEs (20 µM) against the Eu-MDH (200 nM). Conditions: 20 mM PIPES pH 7.2, 1 mM PES, 1 mM KCN, 100 µM DCPIP, 45 °C. Normalized specific enzymatic activity with standard error of the mean (SEM, n = 4) is shown.

Addition of 20 µM La^{3+} and Pr^{3+} to 0.2 µM partial-apo Eu-MDH increased the specific activity by factors of 1.5 and 2, respectively. As already shown in Eu titration experiments (Figure 17A), the MDH activity also increases with the addition of Eu^{3+}, albeit not as dramatically as with La^{3+} and Pr^{3+}. The observed low activity in the presence of Yb^{3+} is surprising and might suggest that there is a dynamic exchange with the metal ion already bound to the active site (here Eu), because binding of Yb^{3+} in 30 % of the apo-enzyme should lead either to no (additional) activity or to a catalytically competent active site. Future investigation into this matter could exploit the luminescent properties of Eu^{3+}.[154] It is reasonable

to assume that Yb^{3+} can bind to the active site, but that a catalytically competent active site is not formed with this REE. The absence of catalytic activity in the presence of Yb^{3+} was also observed by Klebensberger *et al.* with a REE-dependent alcohol dehydrogenase (PedH) isolated from *P. putida* KT2440.[151] Further, Masuda *et al.* recently reported that heavy REEs, such as Ho^{3+} and Lu^{3+}, did not support growth of *Methylobacterium aquaticum*.[155]

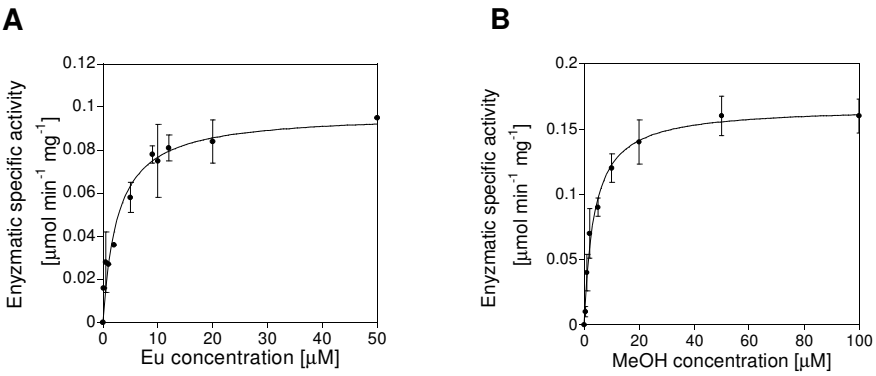

Figure 17 Experiments with SolV Eu-MDH. A: Europium(III) titration into 100 nM of the Eu-MDH. Conditions: 20 mM PIPES pH 7.2, 1 mM PES, 1 mM KCN, 80 µM DCPIP, 45 °C. The graph was fitted according to the Michaelis-Menten equation. The activity without added europium was set to zero and was subtracted from the values obtained with added europium. Average of specific enzymatic activity with SEM (n = 3) is shown. B: Specific enzymatic activity of 100 nM Eu-MDH supplemented with 20 µM $EuCl_3$ with SEM (n = 3). Conditions: 20 mM PIPES pH 7.2, 1 mM PES and KCN, 80 µM DCPIP, 45 °C.

Figure 17B shows the Michaelis–Menten kinetics of 100 nM Eu-MDH. The maximum turnover rate from the best curve fit was (189 ± 6) nmol min^{-1} mg^{-1}. The corresponding Michaelis–Menten constant K_m was determined to be (3.62 ± 0.44) µM. Additionally, k_{cat} was determined to be 0.20 s^{-1} and the catalytic efficiency (k_{cat}/K_m) was 55.24 mM^{-1} s^{-1}. Remarkably, the affinity of the Eu-MDH in our experiments, with an affinity constant (K_m) of (3.62 ± 0.44) µM, was 4.5 times lower than that of the mixed REE-MDH (La, Ce, Pr) from strain SolV reported in the literature (obtained under slightly different assay conditions), with a K_m of 0.80 µM.[49] Furthermore, the catalytic efficiency with Eu^{3+} instead of the earlier REEs was decreased more than 200-fold. This could provide a plausible explanation for the slow growth of the strain SolV in the presence of that metal ion. However, to confirm this, La-MDH and the other derivatives would have to be isolated and purified from SolV (and other bacteria) and their kinetic parameters would have to be determined under the same conditions as used here, because the assay conditions are known to have a significant impact on these parameters.[49,143] We are interested in whether or not these differences in activity are a direct result of the lanthanide contraction and concomitant change in coordination number or whether Lewis acidities and changes in PQQ activation must also be considered. The last two factors might provide an

explanation for the differences in activity of La- or Pr-dependent MDH compared to Eu-MDH (Figure 16).

3.2.3 Conclusion

The coordination chemistry of REEs is known to show a high degree of structural diversity, and the absence of strong ligand field effects can make predictions of the coordination numbers and geometry difficult.[156] In REE dependent methanol dehydrogenases almost all ligands and the coordination geometry are determined by the protein environment and result in a coordination number of nine. Addition of the substrate as a tenth ligand might depend on the nature and characteristics of the REE ion in the active site. As Cotton and Raithby so appropriately describe it: "discontinuities can arise at any point in the lanthanide series, so where possible each of the elements should be examined in any particular study."[95] To conclude, we present the first structural and kinetic study of a methanol dehydrogenase with a europium ion in the active site and isolated from a strictly REE-dependent bacterium. Our results show that, although rare earth elements have similar properties, the differences in ionic radii and coordination numbers across the series impact the catalytic efficiency of this MDH, which might explain why bacteria depend on the larger, more abundant REEs for growth.

3.3 Further Investigation of the Impact of Metals on SolV Eu-MDH Activity in Dye-Coupled Assays

Further metal binding studies involved additional metal ions, such as Ca^{2+} and Ba^{2+}, to answer the question of whether the XoxF-type MDH from SolV is exclusively made for lanthanide ions. The homologue of XoxF-type MDH enzymes, MxaF, carries a calcium ion in its active site.[72] Ca^{2+} has a similar ionic radius to La^{3+}, whereas the Lewis acidity is lower.[42,157] However, an essential Asp has been reported recently in *M. extorquens* AM1 that is crucial for lanthanide coordination and therefore for in vivo catalytic function and in vitro activity of purified XoxF-type MDH. A replacement of this Asp residue by Ala, as found in the MxaF-type MDH, did not promote MDH activity in the absence of La^{3+} and presence of Ca^{2+}, suggesting that the *M. extorquens* XoxF MDH active site is exclusively designed for lanthanide ions.[73] The active site of SolV MDH also presents this additional Asp residue, Asp^{301}.[49] It

was therefore investigated, if this MDH does not function with Ca^{2+} too. Ba^{2+} was also tested, since a replacement of Ca^{2+} by Ba^{2+} or Sr^{2+} in the MxaF-type MDH has been reported.[93,158]
To examine the effect of Ca^{2+} and Ba^{2+} on XoxF-type SolV MDH activity, assays were performed using the 70% occupied Eu-MDH. The addition of Ca^{2+} and Ba^{2+} ions alone, as well as mixtures of La^{3+} with either these metals or Eu^{3+}, were tested (Figure 18).

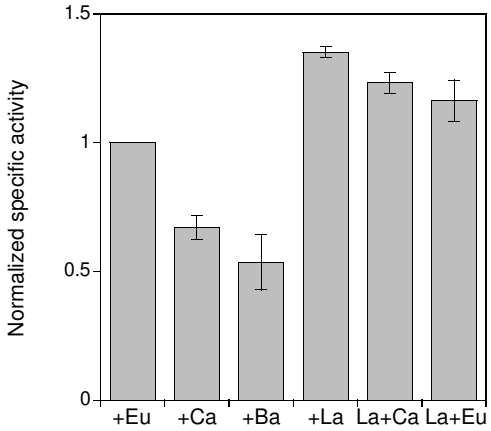

Figure 18 Metal binding studies of SolV MDH with different metals. SA of Eu-MDH in the presence of 100 µM metal. Data were normalized to the activity with added Eu. Conditions: 200 nM MDH, 20 mM PIPES pH 7.2, 1 mM PES, 1 mM KCN, 100 µM DCPIP, 45 °C, n = 2.

The activities in the presence of the respective metal ion were compared to the activity of fully occupied Eu-MDH (after the addition of $EuCl_3$ to the assay). The SA decreases significantly with Ca^{2+} (70% of SA) and is approximately halved after Ba^{2+} addition. Besides the fact that the growth of SolV was unsuccessful in the presence of normal cultivation medium, which contains high amounts of calcium, this result presents further evidence for the strict Ln^{3+}-dependent nature of SolV XoxF-type MDH, because both Ca^{2+} and Ba^{2+} ions are known to promote catalytic activity in MDH enzymes.[49,76,93,159] As observed above, La^{3+} addition enhances MDH activity. The SA is approximately 1.5-fold higher compared to fully Eu^{3+}-metalated MDH. When La^{3+} is mixed with either Ca^{2+} or Eu^{3+} in a 1:1 ratio (50 µM La, 50 µM of the other metal ion), the activity decreases slightly, showing a higher preference of SolV for La^{3+} than for Ca^{2+} or Eu^{3+}. The values of the latter two SA are similar within the error range, further proving the preference of SolV MDH for early lanthanides such as La^{3+}.[49] In contrast to reported results on MxaF MDH from *M. extorquens*, Ba^{2+} ions notably decrease the activity of SolV MDH.[93]

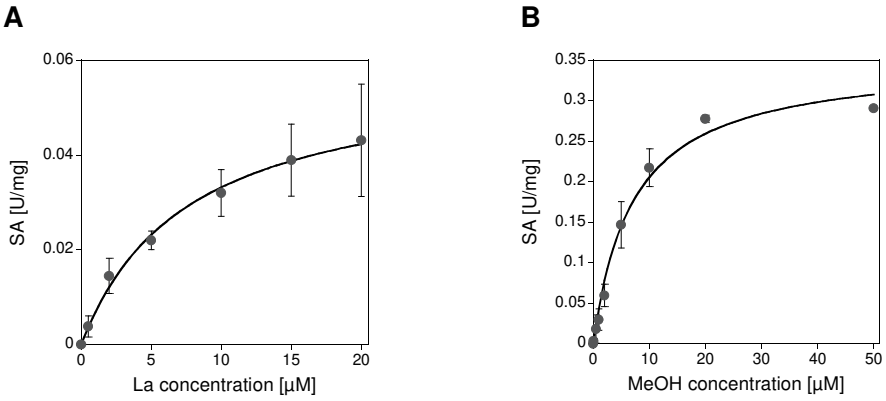

Figure 19 Experiments with La-MDH. A: La^{3+} titration to 100 nM SolV La-MDH. Conditions: 20 mM PIPES pH 7.2, 1 mM PES, 1 mM KCN, 80 µM DCPIP, 45 °C. The activity without added lanthanum was set to zero and was subtracted from the values obtained with added lanthanum, n = 3. B: Specific enzymatic activity of 100 nM SolV La-MDH supplemented with 20 µM $LaCl_3$. Conditions: 20 mM PIPES pH 7.2, 1 mM PES and KCN, 80 µM DCPIP, 50 mM MeOH,45 °C, n = 3. Graphs were fit according to the Michaelis-Menten equation.

In addition to the above investigation of Eu-MDH, titration experiments were conducted with the La-MDH derivative from SolV (Figure 19A). The metal association constant was calculated from the curve fit according to Michaelis and Menten. The SA in the absence of $LaCl_3$ was set to zero and subtracted from the SA obtained at different La^{3+} concentrations. The metal binding constant K_d was determined as (7.6 ± 1.1) µM. The obtained value is comparatively high, suggesting a threefold-better affinity of Eu-MDH for Eu (K_d = 2.6 µM). Yet the change in enzymatic activity is approximately 20-fold smaller for the La^{3+} titration. Hence, this technique is unsuitable for making a comparison of the affinity constants between the MDH derivatives. Also, Eu-MDH and La-MDH present different percentages of metalation and PQQ content. Therefore, the titration experiments were used to determine the amount of the respective lanthanide necessary for full enzymatic activity. In the same method as for Eu-MDH, a concentration of 20 µM metal was chosen for further kinetic investigations (Figure 19B). Kinetic parameters were determined at substrate methanol concentrations of 0 – 50 µM. A maximum turnover rate v_{max} of (351 ± 18) nmol min^{-1} mg^{-1} was calculated from the best curve fit, with the corresponding Michaelis-Menten constant K_m of (7.08 ± 1.11) µM. The latter is in the same order as the K_m value determined for Eu-MDH with the same substrate. The v_{max} value, however, is nearly doubled. A comparison of the MDH derivatives is difficult due to the indirect dye-coupled assay method. As discussed above (III.2 Assay Optimization), the used assay is error-prone, which impedes reproducibility. A comparison of two or more derivatives of an enzyme is only possible if performed simultaneously. Therefore, further kinetic investigations of SolV MDH (III.4 Substrate Kinetics) involved only the Eu-MDH derivative and the substrate methanol was used as control to correct for MDH activity over the experimental period.

3.4 Impact of Metals on SolV Eu-MDH Activity Analyzed by Luminescence and Calorimetry

SolV MDH activity has been analyzed regarding the effect of different metal ions (above). Kinetic parameters, such as the dissociation constant, were determined for both Eu^{3+} binding to Eu-MDH and La^{3+} binding to La-MDH. However, the dye-coupled assay is an indirect method to measure the activity of enzymes and the accurate determination of parameters and constants is challenging.[153] Therefore, to further study the role of lanthanides in SolV MDH, direct and more sensitive techniques were applied. Eu^{3+}-luminescence and isothermal titration calorimetry were used to further characterize the metal binding to SolV MDH and to obtain reliable affinity constants.

3.4.1 Investigation of Eu-MDH with TRLFS

Time-resolved laser-induced fluorescence spectroscopy (TRLFS) is a powerful tool to study fluorescent metal ions in their chemical environment.[160,161] Actinides such as Cm^{3+} or U^{6+} and their non-radioactive trivalent lanthanide analogues like Eu^{3+} are widely used due to their f-electron structure.[160,162–164] UV irradiation of Eu^{3+} results in red photoluminescence with a sharp emission spectrum caused by the $^5D_0 \rightarrow {}^7F_J$ transitions with J = 0 – 6.[165] Based on this, the measured emission spectra of Eu^{3+} in solution (Figure 20) typically exhibit five transition peaks $^7F_0$ to $^7F_4$, whereas $^7F_5$ and $^7F_6$ are either forbidden or rarely observed.[165] The relative peak intensity changes depending on the coordination environment.[162] While $^7F_1$ is largely independent on the environment, the hypersensitive transition to $^7F_2$ is strongly influenced by changes in the first coordination sphere of the Eu^{3+} ion.[162,165]

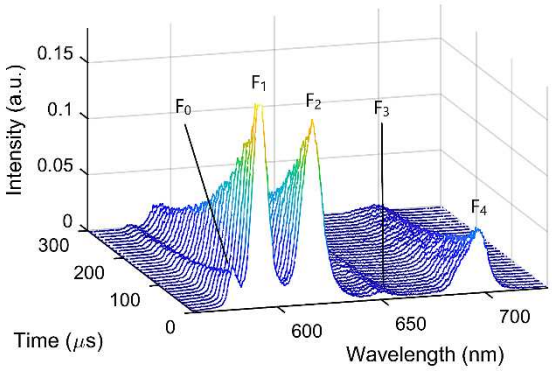

Figure 20 Time-resolved emission spectrum of Eu^{3+} in PIPES buffer. $^5D_0 \rightarrow {}^7F_J$ transitions are denoted as F_0 to F_4. The figure was kindly provided by Dr. B. Drobot and modified.

The direct exaltation of Eu^{3+} with time-resolved emission spectroscopy not only allows the study of the spectral signature but also a temporal analysis. The obtained decay lifetimes give environmental information, such as ligand or water coordination to the Eu^{3+} ion.[162,164,166]

Luminescence spectroscopy has been widely used for the study of metal binding to enzyme sites.[154,166] Due to the similarities between Ca^{2+} and Ln^{3+}, Eu^{3+} and Tb^{3+} have been applied as fluorescent probes in Ca^{2+}- and Mg^{2+}-containing enzymes.[167–170] Besides the direct irradiation of the lanthanide ion, indirect excitation techniques utilizing the antenna effect through an organic molecule have been used.[171] However, the Ln^{3+} binding to methanol dehydrogenases has not been studied by luminescence spectroscopy. Therefore, time-resolved laser-induced fluorescence spectroscopy has been applied, making use of the interesting photophysical properties of Eu^{3+}, to obtain reliable parameters for the lanthanide binding to the active site of SolV MDH. The Eu^{3+} in the sample was excited at 394 nm using a Nd:YAG laser to determine the chemical environment in the first coordination sphere of Eu^{3+} and the lifetimes of the Eu^{3+} species.

The investigation of Eu-MDH with TRLFS proceeded in two steps. First, preliminary experiments were conducted since titration experiments in solution showed that Eu^{3+} is only partially present as free aquo ion in pure water samples and forms complexes with the routinely used assay buffer PIPES. Therefore, the influences of Chelex®-treatment and PIPES buffer were analyzed. A sodium chloride solution was tested for use in metal titration experiments as an alternative medium to ensure ionic strength. In a second step, Eu^{3+} and La^{3+} titrations were performed under optimized conditions.

3.4.1.1 Investigation of Eu^{3+} Complexation in the Buffer System

For the purpose of metal titrations, the medium is routinely treated with Chelex resin® in order to remove unwanted divalent transition metals from the medium. The chelating agent carries an iminodiacetic acid as matrix active group by which ions are bound and removed from the medium. To study the effect of solution treatment with the chelating agent on Eu^{3+} complexation, two samples were analyzed with the help of TRLFS: Eu^{3+} in untreated and Chelex®-treated ultrapure water. The pH was adjusted to 5 in order to prevent the formation of Eu carbonate species from disturbing the detection of the aquo ion.[172] The Chelex®-treated Eu^{3+} solution showed two Eu^{3+} species (Figure 21), whereas the Eu^{3+} sample in untreated MilliQ water exhibited only the Eu^{3+} aquo ion which is coordinated by nine water molecules and has a lifetime of 110 µs.[164] The second Eu^{3+} species in the Chelex®-treated sample shows a clear complexation of Eu^{3+} by ligands that might have been released during the chelexing process. It has a lifetime of approximately 230 µs and carries four remaining water molecules in the first coordination sphere. The content of the complexed species has been estimated to < 5%. Thus, 95 % of Eu^{3+} should be present as aquo ion. Nevertheless, Chelex® resin was excluded from further experiments due to its Eu^{3+}-binding properties. Further, sulfuric acid that has been used to adjust the pH of PIPES assay buffer showed a weak Eu^{3+} complexation.

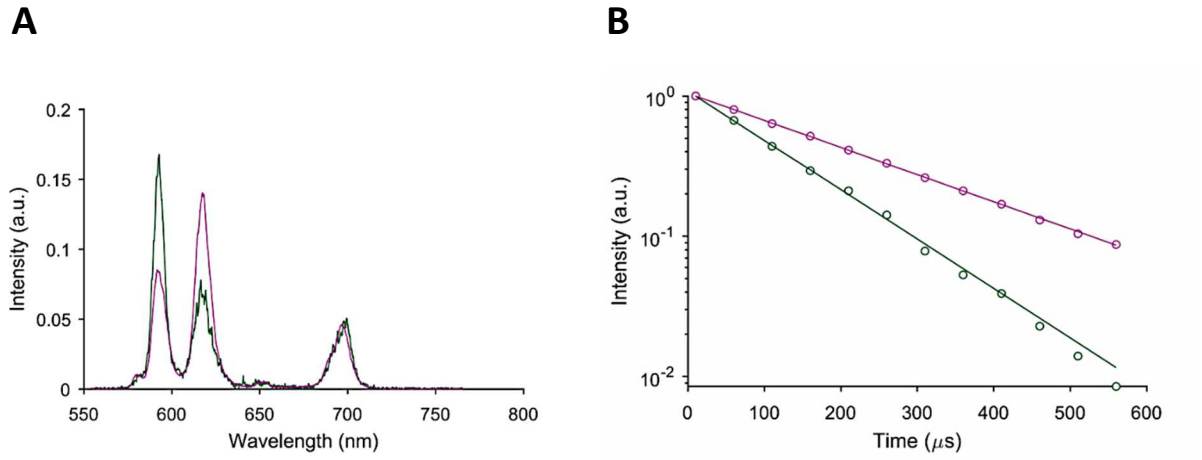

Figure 21 Distribution and lifetimes of Eu^{3+} species in Chelex®-treated ultrapure water. Emission spectra (A) and lifetimes (B) of the Eu^{3+} species: aquo ion (green) and bound Eu species (purple). Conditions: 20 µM $EuCl_3$ in Chelex®-treated MilliQ water, 4 °C, extinction wavelength: 394 nm. Data were recorded with a pulsed Nd:YAG OPO Panther laser system. The figures were kindly provided by Dr. B. Drobot.

In a second step, PIPES titrations were performed. Two Eu^{3+} solutions, one in MilliQ water and one in 20 mM PIPES buffer, were prepared and the latter was titrated stepwise to the Eu-MilliQ water sample. To simulate assay conditions, measurements were conducted at pH 7 and 20 µM $EuCl_3$. In the course

of titration, three Eu^{3+} species are formed (Figure 22). Under MilliQ water only conditions, a sole free Eu^{3+} aquo ion is observed with a lifetime of 110 µs. Yet, the addition of even low amounts of PIPES buffer (up to a concentration of approx. 500 µM) nearly halves the amount of free Eu^{3+} in solution and leads to the formation of a 1:1 Eu-PIPES complex. This asymmetric Eu^{3+} species is indicated by the appearance of the symmetry forbidden F_0 transition peak.[165] It has a longer lifetime of 165 µs due to a reduced water molecule content of six remaining waters in the first coordination sphere.[31,32] The 1:1 Eu-PIPES complex emerges concomitantly with the addition of PIPES and its concentration is highest at approx. 2 mM. Further addition of PIPES buffer decreases the F_0 transition peak again, showing that the asymmetric complex is transformed into a symmetric 1:2 Eu-PIPES species which is already observable after the addition of 200 µM PIPES buffer. The latter species is coordinated by only three remaining water molecules and exhibits a lifetime of 275 µs. It emerges at a PIPES concentration of 200 µM and increases with further PIPES addition. The concentration of the free Eu^{3+} species decreases dramatically during the course of titration and no aquo ion is detectable after the addition of already 10 mM PIPES buffer.

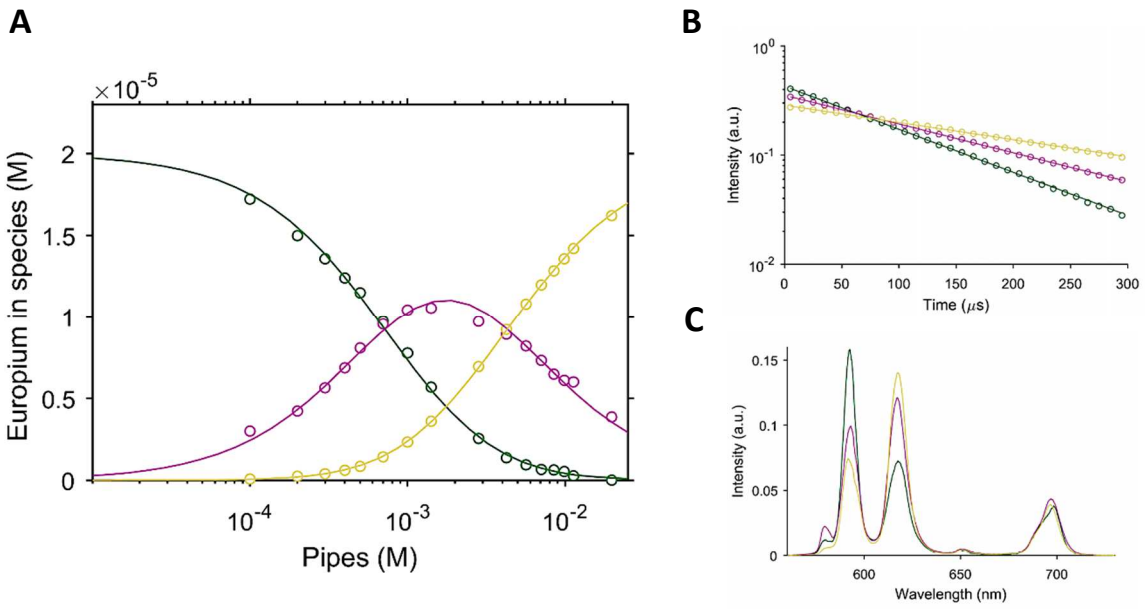

Figure 22 PIPES titration in the presence of 20 µM Eu^{3+}. Species distribution during the titration (A), decay lifetimes (B) and emission spectra (C) of the formed Eu^{3+} species: Eu^{3+} aquo ion in green, 1:1 Eu-PIPES complex in magenta, 1:2 Eu-PIPES complex in yellow. Conditions: 20 mM PIPES buffer (pH 7) was titrated stepwise to MilliQ water (pH 7) at 4 °C, excitation wavelength: 394 nm. Both solutions contained 20 µM $EuCl_3$. Data were recorded with a pulsed Nd:YAG OPO Panther laser system. The figures were kindly provided by Dr. B. Drobot.

Metal binding properties have been described for buffers like phosphate and citrate.[100,175] This process is problematic as metalloenzymes that need metals for activity will be inhibited in the presence of complexing buffers.[176] Further, the release of protons by the buffer upon metal binding leads to a lowering of the solution's pH.[177] Good's buffers like 1,4-piperazinediethanesulfonic acid (PIPES) have been proposed as alternatives[101] but there is no consensus in the literature whether they complex metal ions.[127] PIPES titrations performed with the help of TRLFS showed that this buffer, which is routinely used for the kinetic investigation of SolV MDH in the dye-coupled assay, indeed efficiently binds Eu^{3+} already at low concentrations. This result gives an explanation why a 100-fold excess of metal (20 µM Ln^{3+} if 200 nM MDH are used) is required in the artificial assays although the enzyme is in a 70% metalation state.

3.4.1.2 Probing NaCl for Replacement of PIPES Buffer in Luminescence Studies of SolV MDH

As described above, PIPES showed a comparatively strong Eu^{3+} complexation. To avoid metal binding by the assay buffer, PIPES was replaced by sodium chloride to give ionic strength. Different NaCl solutions were tested and a concentration of 100 mM was found to give best stability of SolV Eu-MDH. Enzymatic activity, as well as folding and the PQQ fingerprint of SolV Eu-MDH, were studied in pH-adjusted NaCl solution (Figure 23). Eu-MDH 2nd was either washed twice in 20 mM PIPES buffer pH 7.2 or re-buffered in 100 mM NaCl pH 7 using a spinfilter. CD and UV-visible absorption spectra (Figure 23B and C, respectively) of both Eu-MDH samples exhibit proper integrity and stability of the enzyme in NaCl solution. Moreover, no loss of the cofactor PQQ was observed. Interestingly, Eu-MDH in 100 mM NaCl pH 7 showed a strongly decreased enzymatic activity at the beginning (initial rate of the first minutes) compared to the four times more active PIPES sample, whereas the NaCl sample adapted a similar, but still slightly lower turnover velocity after approx. 15 minutes. As described by Grady and co-workers, piperazine-based buffers like PIPES can form radicals and therefore show redox activity.[124] Further, a possible substrate, which might be present in organic buffers owing to their purification, was discussed.[53,98,110] An inquiry at the supplier, however, did not confirm the use of methanol in buffer recrystallization and NMR analysis of the PIPES batch did not show any alcohol contaminations.

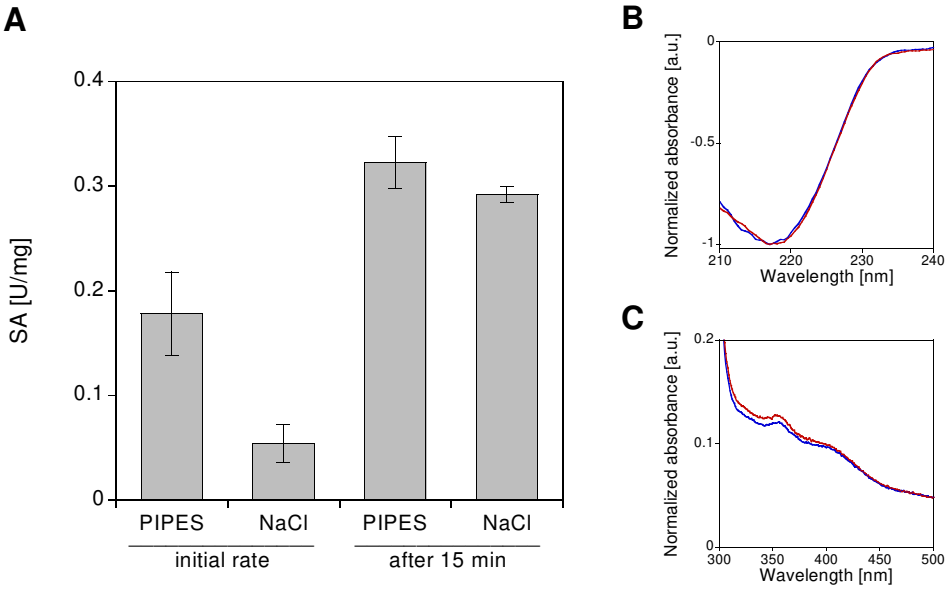

Figure 23 Analysis of SolV Eu-MDH washed in 20 mM PIPES pH 7.2 (blue) vs. re-buffered in 100 mM NaCl pH 7 (red). A: MDH activity assay. Conditions: 200 nM Eu-MDH 2nd, 20 µM Eu^{3+}, 1 mM PES, 100 µM DCPIP, 50 mM MeOH, 45 °C, n = 3. SA was determined for the first minute (initial rate) and after 15 min. B: Normalized CD spectra (Jasco J-810). C: Normalized UV-visible spectra (Cary60). Conditions were as follows: 1 mm CD cuvette, room temperature.

From the assay results, a strong influence of the buffer's redox behavior is visible at low enzymatic activities, whereas if MDH is highly active, the effect of the buffer is negligible. Further, the weak metal complexation in NaCl solution, resulting in higher amounts of available Eu^{3+}, may play an additional role. Previous experiments showed that high REE concentrations do not promote further enzymatic activity but rather lead to a decreased SA. Therefore, in a next step, metal titrations were performed in both media to determine the optimal Eu^{3+} concentration in NaCl-based MDH assays. Different concentrations were chosen that give best MDH stability: 20mM PIPES pH 7.2 and 100 mM NaCl pH 7. The enzymatic activity of a two-fold washed Eu-MDH in the respective medium at different Eu^{3+} concentrations (Figure 24) was measured using the DCPIP/PES-assay system with assay mix prepared in the respective medium (PIPES or NaCl). A possible influence of the Lewis acidity was excluded by adjusting the pH of the $EuCl_3$ solution. Since a different purification batch of Eu-MDH has been used for the investigation of the metal effect above and additionally cyanide was excluded from the assay mix, the metal binding constant K_d differed slightly and was determined as 3.8 µM for the PIPES measurement. In the case of the NaCl assay, a curve fit was not applicable. Yet, a faster saturation of the active site with Eu^{3+} is observed if NaCl is utilized. Also, the maximum turnover velocity is higher at metal saturation. Further, the highest SA is obtained at about 5 µM of added Eu^{3+}. Although this value is four times lower compared to the titration experiment in PIPES buffer (20 µM), a 25-fold excess of

Eu^{3+} is still needed to fully metalate all active sites when using the dye-coupled assay method. The enzymatic activity decreases slightly if higher Eu^{3+} concentrations of approx. 20 µM are added and even more dramatically at 50 µM of added metal.

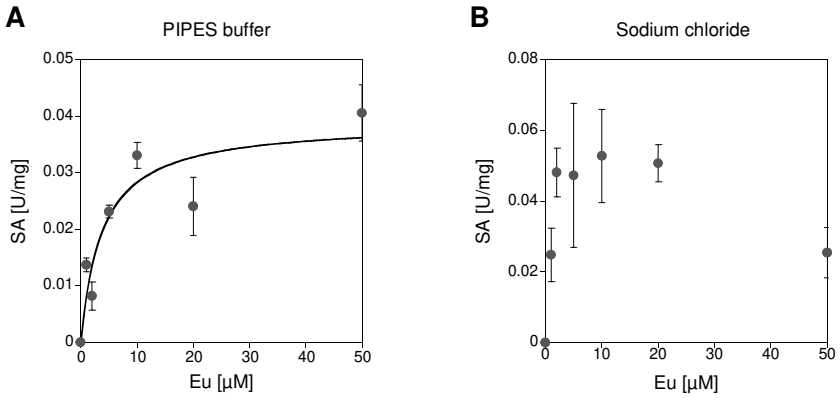

Figure 24 Eu^{3+} titration to Eu-MDH in PIPES vs. NaCl. Conditions: 200 nM Eu-MDH 2nd, 20 mM PIPES pH 7.2 (A) or 100 mM NaCl pH 7 (B), 1 mM PES, 100 µM DCPIP, 50 mM MeOH, varied concentrations of $EuCl_3$, 45 °C. The activity without added Eu^{3+} was set to zero and was subtracted from the values obtained with added Eu^{3+}, n = 3. Graph A was fit according to the Michaelis-Menten equation.

Based on these results, all further TRLFS and ITC experiments were performed in 100 mM NaCl solution.

3.4.1.3 Titration Experiments Using TRLFS

Metal binding studies using luminescence techniques have been applied to several enzymes like *Escherichia coli* methionine aminopeptidase or human factor Xa protease by replacing their physiological metal ions, such as Ca^{2+} or Co^{2+}, with lanthanides.[154,170] Lanthanides with luminescent properties, such as Eu^{3+} or Tb^{3+}, were used to characterize metal binding to enzymatic sites and to obtain binding constants.[168,169,178] The discovery of Ln^{3+}-dependent enzymes made it possible to study the interesting photophysical properties of these metals in their natural environment. Since the growth of SolV was poor in the presence of late lanthanides,[71] Eu^{3+} and not Tb^{3+} luminescence was used for the examination of metal binding to SolV MDH by TRLFS.

Eu-MDH was re-buffered in 100 mM NaCl pH 6.5 with added 1 mM methanol for protein stability. A slightly more acidic pH was applied compared to that used in activity assays to ensure the presence of the Eu^{3+} aquo ion. Both Eu^{3+} and La^{3+} titrations were conducted at room temperature with a pulsed

Nd:YAG optical parametric oscillator (OPO) laser system. A low laser power was adjusted since a destruction of the cofactor PQQ has been observed at high energy levels (Figure S14). Eu^{3+} was excited directly at 394 nm. For the La^{3+} titration, the 70% metalated Eu-MDH was first saturated with Eu^{3+} before La^{3+} was added. Parallel factor (PARAFAC) analysis of both series revealed a three species model.

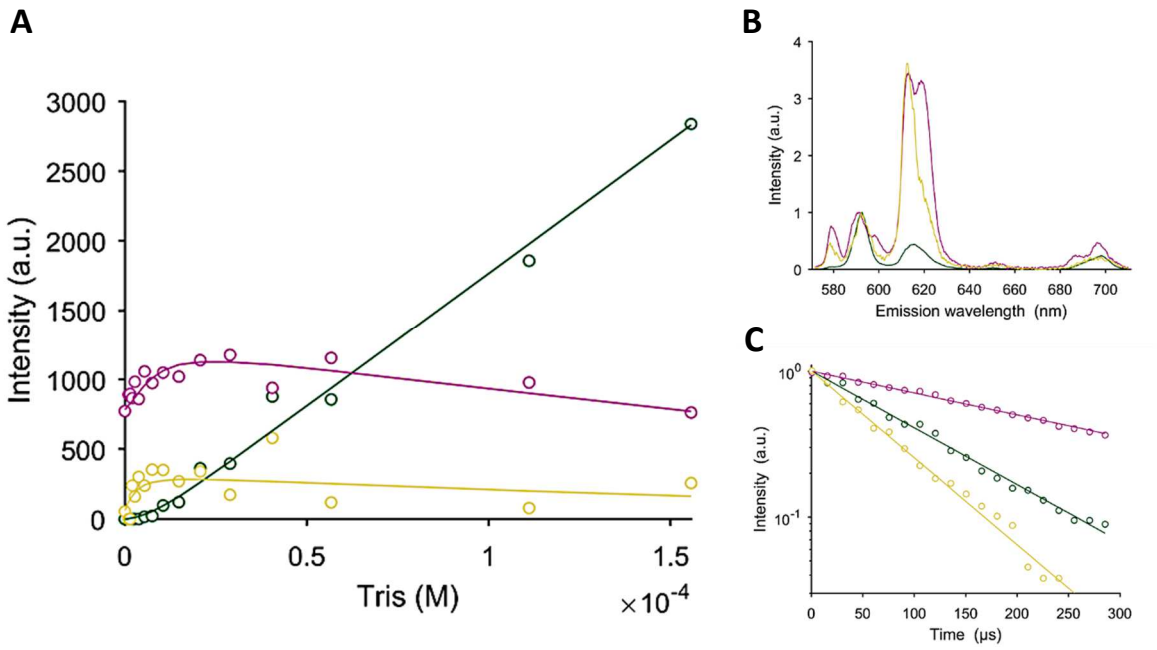

Figure 25 Eu titration to Eu-MDH. The titration of 10 µM re-buffered Eu-MDH 2nd with $EuCl_3$ was followed using Eu^{3+} luminescence. Both solutions contained 100 mM NaCl pH 6.5 with added 1 mM methanol. TRLFS measurements were performed at room temperature with a pulsed Nd:YAG OPO laser system at an excitation wavelength of 394 nm. Eu^{3+} species distribution during the titration process (A), emission spectra (B) and lifetimes (C) are shown. Green: Eu^{3+} aquo ion. Magenta: MDH-bound Eu^{3+}. Yellow: unspecifically bound Eu^{3+} species. The figures were kindly provided by Dr. B. Drobot.

The titration of Eu^{3+} to 10 µM Eu-MDH (Figure 25) shows a saturation of the partial apo-enzyme at approx. 3 – 4 µM of added Eu^{3+}. This value is consistent with the 70% metalation state of the enzyme. Further addition of the lanthanide leads to a strong emergence of the Eu^{3+} aquo ion with a lifetime of 111 µs and nine coordinating water molecules[164], indicating no further binding of the metal to the active site of MDH. Concurrent to the saturation of the enzyme, two other Eu^{3+} species significantly increase. The MDH-bound Eu^{3+} species is visible from the beginning of the titration and has a longer lifetime of 290 µs, with only three water molecules in the first coordination sphere. This species shows a maximum at approx. 20 µM of added metal, whereas a further addition of Eu^{3+} decreases the intensity again. This finding can be explained by the dilution effect as the volume in the cuvette increases during the titration process. A similar behaviour is observed for a third Eu^{3+} species. Although

it is not visible from the beginning, it forms with Eu^{3+} addition. The lifetime of this species is 75 µs, indicating a further quenching of the Eu^{3+} ion. Whether SolV MDH has further metal binding sites apart from the active center is not known. Therefore, this third species could not be assigned. Further, an estimation of the number of water molecules in the coordination sphere of this Eu species according to the Horrocks equation was not possible.[166] Dissociation constants were determined from this measurement. A value of $6.3 \cdot 10^{-7}$ was calculated for the unspecific binding, whereas the value for the active site bound Eu^{3+} species showed a slightly weaker binding with a value of $3.2 \cdot 10^{-6}$. This K_d value is in good agreement with the previously determined value of 3.8 µM. Surprisingly, the latter was obtained from the indirect dye-coupled assay method in the presence of PIPES buffer. It is unclear whether the enhanced redox behavior of the buffer system or a stronger affinity of the enzyme than of the buffer for the Eu^{3+} ion is responsible for the similar K_d values and this must be further evaluated. The possibility of a direct comparability of affinity constants obtained by different methods remains under debate.[153]

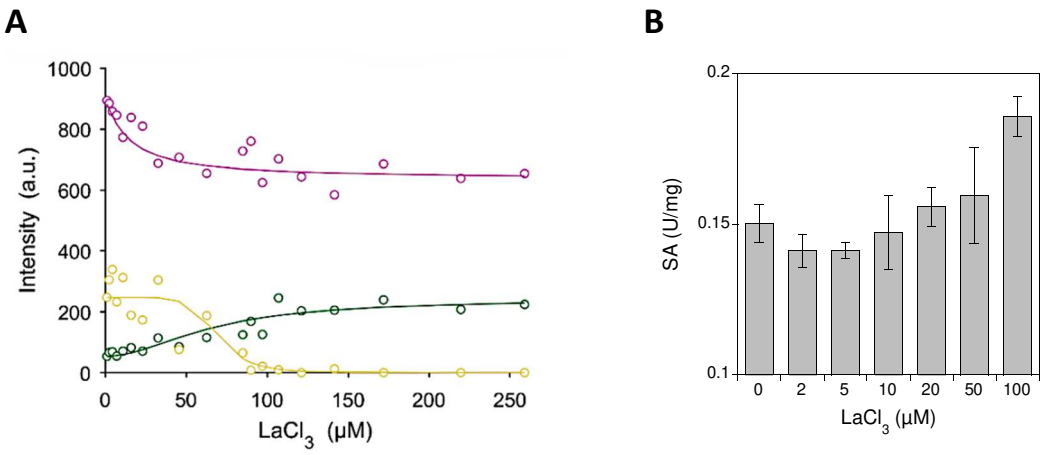

Figure 26 La^{3+} titration to saturated Eu-MDH. A: TRLFS experiment. 10 µM Eu-MDH 2nd re-buffered in 100 mM NaCl pH 6.5 with added 1 mM methanol were saturated with an excess of $EuCl_3$ (15 µM) and $LaCl_3$ was subsequently titrated. TRLFS measurements were performed at room temperature with a pulsed Nd:YAG OPO laser system at an excitation wavelength of 394 nm. Green: Eu^{3+} aquo ion. Magenta: MDH-bound Eu^{3+}. Yellow: unspecifically bound Eu^{3+} species. The figure was kindly provided by Dr. B. Drobot. B: MDH assay. Conditions: 200 nM Eu-MDH 2nd, 100 mM NaCl pH 7, 1 mM PES, 100 µM DCPIP, 50 mM MeOH, 45 °C. MDH was saturated with 20 µM Eu^{3+}; La^{3+} concentrations were varied.

The La^{3+} titration was performed in a second step (Figure 26A). To do so, a 10 µM Eu-MDH sample was saturated with an excess of $EuCl_3$ (15 µM) and La^{3+} was then titrated stepwise to the enzyme mixture. Small concentrations of La^{3+} caused a slight increase of free Eu^{3+}. Yet, the addition of approx. 100 µM La^{3+} was required to reduce the MDH-bound Eu^{3+} species to 75%. Further addition of La^{3+} caused no additional displacement. Concurrent with the reduction of the MDH-bound Eu^{3+}, the unspecifically bound Eu^{3+} species decreased highly and almost disappeared at a concentration of approx. 100 µM

added La^{3+}. The results were verified using the dye-coupled MDH assay with NaCl as buffer substitute (Figure 26B). Eu-MDH was first saturated with Eu^{3+} and the SA was measured at different La^{3+} concentrations. Low concentrations of La^{3+} did not promote additional activity, only higher amounts of about 100 µM slightly increased the SA.

These results show that La^{3+} and likely other early lanthanides, which are naturally utilized by rare earth element-dependent microbes, are preferentially incorporated into the active site of MDH.[32,47,60] However, a replacement of all active site bound metal ions cannot be achieved. Interestingly, nearly the same amount of Eu^{3+} that has been added to saturate the enzyme has been displaced. Therefore, a weaker binding of afterwards supplemented lanthanide ions compared to already incorporated ones, is likely or the magenta MDH-bound species may consist of two Eu^{3+} species that differentially bind to the enzyme. Additionally, since an unusual disulphide bridge, built by adjacent cysteines, is located close to the PQQ cofactor and metal ion in the active site of MDH enzymes,[73,179] this residue could also influence the strength of the metal binding. Thus, further research on this matter is required.

3.4.1.4 Titration Experiments Using ITC

Isothermal titration calorimetry (ITC) allows the analysis of titration experiments under constant temperatures. Binding events such as the binding of drugs, inhibitors or metal ions to biomolecules can be studied regarding their thermodynamics. The heat capacity of the binding event (endothermic or exothermic reaction) is measured against a reference cell in an adiabatic system.[180,181] Many bacterial metalloenzymes have been subject to ITC analysis.[182,183] The discovery of the biological role of rare earth elements prompted the use of ITC to study the interaction of chalcophores like methanobactin or the calcium-binding messenger protein calmodulin with lanthanides, as well as the thermodynamic analysis of lanthanide-binding proteins like lanmodulin.[33,81,184] The binding of lanthanides to MDH enzymes, which has not been studied by ITC yet, will provide affinity constants for different lanthanides, helping to further investigate the lanthanide binding properties to the active site of XoxF MDH.

ITC experiments were conducted by titrating the same 70% metalated Eu-MDH purification fraction as used for TRLFS, with three different lanthanides: the early rare earth elements lanthanum and europium and the late lutetium. Both solutions (30 µM re-buffered Eu-MDH and 3 mM lanthanide solution) contained 100 mM NaCl pH 7 with added 1 mM methanol. Since the pH is not crucial for the measurement technique, optimum conditions for SolV MDH were used. The ITC thermograms (Figure

S15) were fit to a two-species model with a MDH-bound lanthanide and a second species that could not be assigned. The latter has only a minor influence in the La^{3+} and Lu^{3+} titration to Eu-MDH, whereas the Eu^{3+} titration shows a strong presence of the second species. For which reasons only the Eu^{3+} titration exhibits a distinct formation of the second species is unclear, but this finding could possibly result from buffer contaminations or a stripping of the hydration sphere. The stoichiometry, affinity constants and enthalpies were determined for all three titrations (Table 7). The ITC analysis shows that 0.2 mol of Eu^{3+} and La^{3+} respectively bind to 1 mol of Eu-MDH; for Lu^{3+} a value of 0.4 mol was obtained. These values are in good agreement with the estimated Eu^{3+} occupation of the used SolV Eu-MDH of approx. 70%. The determined affinity constant K_d exhibits the best binding to the active site for La^{3+}, whereas Lu^{3+} shows the weakest binding. Based on the lanthanide contraction, the Lu^{3+} ion has the smallest radius and thus cannot fill the active site of SolV MDH.[35] Computational chemistry calculations showed that the coordination to the central metal ion changes upon going from a lighter lanthanide to a heavier one. The Glu residue in the active site switched from a bidentate to a unidentate binding and the coordination of PQQ to the lanthanide changed from chelate binding to a unidentate mode.[99] This may explain why Lu^{3+} binding to the active site of SolV MDH is weak. Although Lu^{3+} has the highest Lewis acidity of the three studied lanthanides, a sufficient polarization of the cofactor PQQ and substrate should not be possible. Reported competition studies are in good accordance with the ITC results, showing that the addition of Lu^{3+} led to a decreased MDH activity if a mixture of a lanthanide and Lu^{3+} or solely Lu^{3+} have been added to the assay.[185] Metal titrations with La^{3+}, Eu^{3+} and Lu^{3+} using the dye-coupled assay were performed to obtain affinity constants and a similar behaviour was observed. The enthalpies, however, show the opposite trend (with an enthalpy of 24 kJ/mol determined for both La^{3+} and Eu^{3+} and an enthalpy of 68 kJ/mol for the Lu^{3+} binding), but are in good agreement with the stoichiometry. This is most probably a result of differential contributions of forces to the binding enthalpy (van der Waals interactions and hydrogen bonds) and the binding entropy (hydrophobicity).[186]

Table 7 Stoichiometry, affinity and enthalpy that have been determined from the integrated thermograms of the Eu^{3+}, La^{3+} and Lu^{3+} titrations to 30 µM Eu-MDH. The MDH-bound Ln^{3+} species is denoted as 1, the second species as 2.

Ln	**Stoichiometry (n)**		**Affinity constants (K_d) [M]**		**Enthalpy ΔH [kJ/mol]**	
	n_1	**n_2**	**K_{d1}**	**K_{d2}**	**ΔH_1**	**ΔH_2**
La^{3+}	0.2	8.3	$1.6 \cdot 10^{-5}$	$7.9 \cdot 10^{-2}$	24	11
Eu^{3+}	0.2	6.8	$5.0 \cdot 10^{-5}$	$1.3 \cdot 10^{-3}$	24	6.4
Lu^{3+}	0.4	6.8	$4.0 \cdot 10^{-4}$	$1.3 \cdot 10^{-2}$	68	0.8

3.4.2 Conclusion

Preliminary experiments showed that Chelex® treatment, the choice of medium (buffer or ionic strength only) and the applied acids for pH adjustment can impact the number of Eu species in solution. Both Chelex® treatment of the medium and PIPES buffer showed Eu^{3+} complexation. Thus, the buffer was consequently replaced by sodium chloride. CD and UV-visible absorption spectroscopy showed that a pH adjusted 100 mM sodium chloride solution did not affect protein integrity.[187,188] The enzymatic activity in NaCl solution was similar to that in the PIPES buffered assay mix if 20 µM Eu^{3+} were supplied; lower concentrations enhanced the activity even further. Therefore, it was shown that NaCl can be successfully used for metal titrations of SolV MDH. TRLFS and ITC experiments gave further insights into metal binding to the active site of XoxF MDH and allowed the determination of affinity constants. TRLFS measurements have been performed for both Eu^{3+} and La^{3+} titration to 70% metalated Eu-MDH. A concentration of 3 – 4 µM Eu^{3+} was sufficient to saturate all active sites. La^{3+} replaced Eu^{3+} to some extent, but an approximate 75% occupation with Eu^{3+} persisted, indicating that there must be a differential binding of the lanthanide ion if it is supplied to a partial apo-enzyme. ITC experiments gave further evidence for a stronger affinity of La^{3+} for the active site compared to later lanthanides such as Eu^{3+} and Lu^{3+}, which is in accordance with SolV growth studies and supports the important role of MDH enzymes for lanthanide-dependent bacteria.

4 Substrate Kinetics

4.1 Introduction

Methanol dehydrogenases catalyze the oxidation of methanol in methano- and methylotrophic bacteria,[1,30,106] which proceeds via a two-electron mechanism.[61] While methanol is the preferred substrate, other primary alcohols are also converted by MDH enzymes.[30,61,90] The catalytic reaction of MDH generates formaldehyde, which in turn is transformed to formic acid by methanopterin- or folate-dependent enzymes.[106,189,190] Formate dehydrogenases further convert the toxic formic acid to generate carbon dioxide.[191] This mechanism of periplasmic methanol conversion involving several enzymes is found in the well-studied model organism *M. extorquens* AM1.[192] In contrast, a direct conversion of methanol to formate was observed in other quinoprotein-carrying bacteria. Both MxaF and XoxF MDH were found to be capable of converting methanol directly to formic acid in a four-electron oxidation and without the need of another enzyme.[61,193] While the formaldehyde conversion rate is slow for Ca^{2+}-dependent MxaF enzymes, the Ln^{3+}-dependent XoxF MDH from *M. fumariolicum* SolV shows a high affinity for formaldehyde and is capable of catalyzing the two oxidation steps: methanol to formaldehyde and further to formate (Scheme 6).[49,61] The same was observed for MDH enzymes purified from *inter alia Methylosinus* and *Methylocystis* species.[194,195]

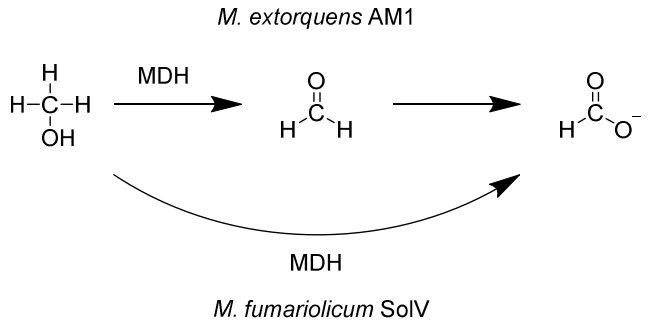

Scheme 6 Methanol conversion by XoxF in M. extorquens AM1 and M. fumariolicum SolV compared. In AM1 MDH catalyzes the oxidation of methanol to formaldehyde. SolV MDH, however, is able to perform both oxidation steps: methanol to formaldehyde and formaldehyde to formate.

Kinetics of methanol dehydrogenases have been extensively studied in the past, yet there is still debate about the exact mechanism of substrate oxidation. The discovery of Ln-dependent bacteria encouraged the investigation of XoxF-type MDH enzymes. In 2014, Pol *et al.* characterized a mixed REE

XoxF from SolV that has been cultivated in the presence of the early lanthanides La^{3+}, Ce^{3+}, Pr^{3+} and Nd^{3+}, and that exhibits a higher activity than the known Ca^{2+}-dependent MDH enzymes. This finding was explained by the higher Lewis acidity of REE compared to Ca^{2+}.[49] To understand in what way the properties of the central metal ion (Lewis acidity, ionic radius) influence substrate oxidation, a MDH enzyme was examined in this work that contains a single lanthanide element. The Eu^{3+}-derivative was chosen as this REE not only possesses interesting spectroscopic properties, but also exhibits a higher Lewis acidity than the early lanthanides as well as a smaller radius. Interestingly, it was observed that Eu^{3+} leads to a slower growth of SolV compared to La^{3+} or Pr^{3+}. To investigate if the differential growth of SolV is dependent on MDH activity, as about 15% of the bacterial biomass consist of MDH,[30,196] substrate kinetic studies were conducted. The obtained parameters were compared to the mixed REE-MDH from SolV to get further insights into the role of the central metal ion in the catalytic mechanism since this will allow to easily tune MDH activity for industrial application.

4.2 Alcohols as Substrates

Purified Eu-MDH has been examined using the previously optimized PES/DCPIP-assay. MDH was washed and allowed to consume residual methanol before the substrate was added. The initial rates were measured and fit according to Michaelis and Menten. From the analyzed alcohols only methanol, ethanol and n-propanol showed Michaelis-Menten behavior with substrate saturation (Figure 27). Higher alcohols were also tested, but either the enzymatic activities deviated strongly (butanol to heptanol) or the substrate was hardly converted by MDH as in the case of isopropanol. The latter observation is consistent with the mixed REE-MDH enzyme.[49] Secondary alcohols might either be too bulky to fit into the active site or cannot be sufficiently polarized by the active site base of the Asp^{301} residue, thereby preventing its conversion.[30,185]

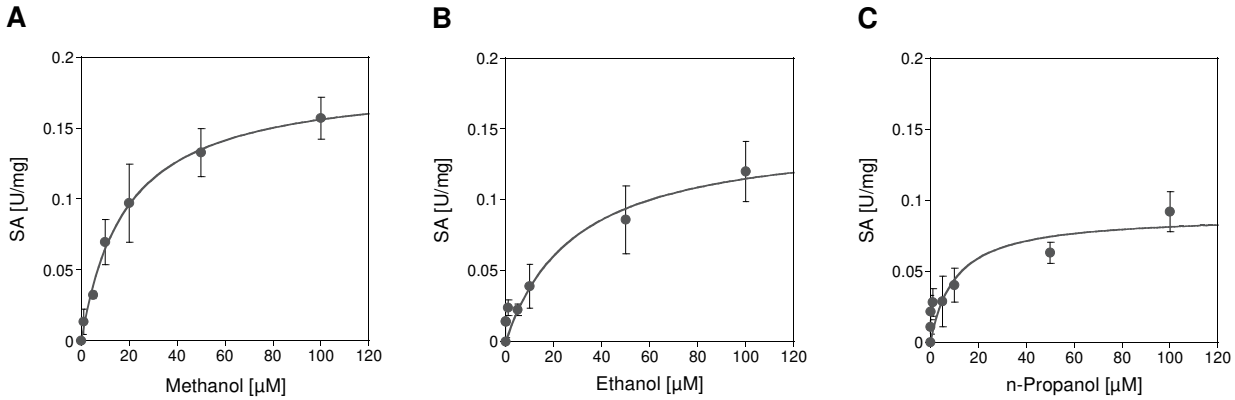

Figure 27 Kinetics of SolV Eu-MDH in the presence of different alcohols: methanol (A), ethanol (B) and n-propanol (C). Data were fit according to the Michaelis-Menten equation. Conditions: 200 nM Eu-MDH 1st, 20 mM PIPES pH 7.2, 1 mM PES, 100 µM DCPIP, 45 °C, n = 2.

Kinetic parameters (Table 8) were determined from the best curve fit (Figure 27). Eu-MDH exhibits the highest maximum velocity with methanol (0.172 U/mg), which is slightly decreased if ethanol is used (0.148 U/mg). With n-propanol the v_{max} value is almost halved (0.09 U/mg). The turnover number, k_{cat}, is in good accordance with this trend. The Michaelis-Menten constant K_m, however, shows a stronger affinity of Eu-MDH for n-propanol (10.23 ± 6.59 µM) than for ethanol (14.68 ± 6.86 µM). This finding is contrary to the values obtained by Pol *et al.* with a mixed REE-MDH, showing that the affinity decreases with the chain length of the alcohol.[49] Yet, the K_m values calculated for the Eu-MDH enzyme exhibit a comparatively high error and are therefore similar within the error range. The k_{cat}/K_m ratio, a measure for the catalytic efficiency of an enzyme, is consistent with the assumption that the alcohols are converted by Eu-MDH in the following order: methanol > ethanol > n-propanol.

Table 8 Kinetic parameters determined from the best curve fit according to Michaelis and Menten for SolV Eu-MDH in the presence of different alcohols (Figure 27).

Substrate	v_{max} [U/mg]	K_m [µM]	k_{cat} [s^{-1}]	k_{cat}/K_m [$mM^{-1}·s^{-1}$]
Methanol	0.172 ± 0.027	8.09 ± 4.86	0.182 ± 0.029	22.50
Ethanol	0.148 ± 0.027	14.68 ± 6.86	0.157 ± 0.029	10.69
n-Propanol	0.090 ± 0.016	10.23 ± 6.59	0.095 ± 0.017	9.29

A comparison of the K_m values for methanol obtained in the presence (Figure 17B) and absence (Figure 27A) of cyanide shows that the affinity is similar within the error range: 3.62 ± 0.44 µM in the presence of KCN and 8.09 ± 4.86 µM in the absence of KCN. Only the catalytic efficiency is highly increased if

cyanide is used in assays (55.24 $mM^{-1} \cdot s^{-1}$). This finding indicates that cyanide influences the turnover of the substrate or the re-oxidation of PQQ but not the binding event.

The cyclic alcohol cyclopropanol was further tested since it was shown to act as a suicide substrate on MDH enzymes.[197,198] Increasing concentrations of cyclopropanol were added to Eu-MDH in the presence of residual methanol and the enzymatic activity was measured with the PES/DCPIP-assay (Figure 28). Already low concentrations of this inhibitor led to a decrease of the SA and the addition of 1 mM cyclopropanol halved the activity of Eu-MDH. Surprisingly, an excess of the suicide substrate (50 mM) did not cause a total activity loss of Eu-MDH, although a complete inactivation of MDH has been described by Duine and co-workers.[197] A participation of residual methanol and therefore a competitive binding of both substrates is reasonable since cyclopropanol was added from the beginning of the measurement when residual methanol is still present. Further, Duine and co-workers reported that cyclopropanol binds to PQQ and that only the oxidized cofactor, not the semiquinone form (PQQH), is inactivated.[197,199] Therefore, a rescue of Eu-MDH by the primary electron acceptor PES in the assay mix is also likely.

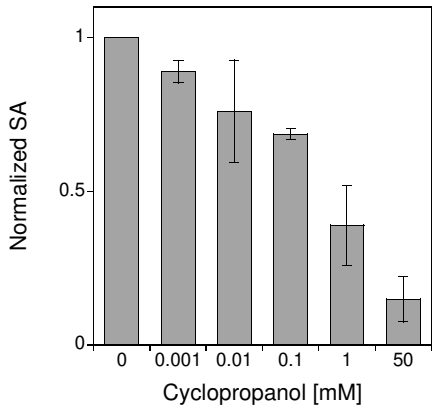

Figure 28 Inhibition study with the suicide substrate cyclopropanol. The cyclopropanol concentration was varied in the presence of residual MeOH. Conditions: 200 nM Eu-MDH 1st, 20 mM PIPES pH 7.2, 100 µM DCPIP, 1 mM PES, 20 µM $EuCl_3$, 45 °C, n = 2.

4.3 Aldehydes as Substrates

The kinetics of purified Eu-MDH with aldehydes were measured in the same way as with primary alcohols. Formaldehyde and acetaldehyde showed Michaelis-Menten behavior (Figure 29) whereas higher aldehydes like propionaldehyde and butyraldehyde were hardly converted by the enzyme.

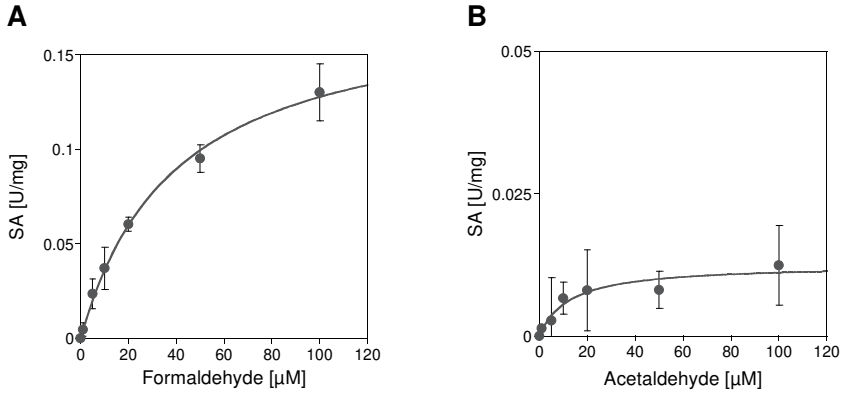

Figure 29 Kinetics of SolV Eu-MDH in the presence of different aldehydes: formaldehyde (A) and acetaldehyde (B). Data were fit according to Michaelis and Menten. Conditions: 200 nM Eu-MDH 1st, 20 mM PIPES pH 7.2, 1 mM PES, 100 µM DCPIP, 45 °C, n = 2.

The kinetic parameters (Table 9) extracted from the best curve fit show an approx. 14-fold higher maximum velocity v_{max} and turnover number k_{cat} if formaldehyde is supplied compared to acetaldehyde. The affinity constant, however, suggests a higher affinity of Eu-MDH for acetaldehyde with a value of 17.16 ± 3.88 µM for formaldehyde and a slightly decreased K_m of 12.48 ± 4.87 µM for acetaldehyde. However, the error is again comparatively high and the difference between the K_m values is therefore small. Furthermore, data obtained from the acetaldehyde measurement series exhibit a high standard deviation. A comparison of the catalytic efficiency nevertheless shows a clear preference of Eu-MDH for formaldehyde, which is in line with the results on the mixed REE-MDH. Yet, in contrast to the obtained results with Eu-MDH, Pol *et al.* reported that the mixed REE-enzyme did not oxidize acetaldehyde in the dye-coupled assay.[49]

Table 9 Kinetic parameters determined from the best curve fit according to Michaelis and Menten of SolV Eu-MDH in the presence of different aldehydes (Figure 29).

Substrate	v_{max} [U/mg]	K_m [µM]	k_{cat} [s^{-1}]	k_{cat}/K_m [s^{-1}·mM^{-1}]
Formaldehyde	0.178 ± 0.008	17.16 ± 3.88	0.189 ± 0.008	11.01
Acetaldehyde	0.013 ± 0.002	12.48 ± 4.87	0.014 ± 0.002	1.12

The hydrated form of the aldehyde, the geminal diol, has been proposed to be the actual substrate for MDH enzymes.[106] The rate of hydration of the analyzed aldehydes in water was therefore determined via NMR spectroscopy (Figure S16) and compared to the literature values.[200] While formaldehyde is present as 100% geminal diol under assay conditions, acetaldehyde presents only about 80% of the hydrate form. In higher aldehydes the hydration state is further reduced. High temperatures, as applied in SolV MDH assays, further reduce the geminal diol content.[201] This might explain why Eu-MDH only sufficiently converts formaldehyde and partially converts acetaldehyde but not higher aldehydes. Also, Itoh *et al.* reported that the substrate specificity depends on the size of the active site.[202]

4.4 Glycine Ethyl Ester as Alternative Substrate

Glycine ethyl ester (GEE) has been proposed as an MDH activator[97] and was therefore tested in the PES/DCPIP-assay of SolV MDH. The investigation of the GEE-dependence of Eu-MDH, however, resulted in Michaelis-Menten behavior (Figure 30), suggesting a conversion of this compound by the enzyme. In the presence of excess methanol (50 mM), GEE leads to a maximum velocity of 0.185 ± 0.006 U/mg and an affinity constant K_m of 1.12 ± 0.20 µM. The replacement of methanol by an excess of deuterated substrate (50 mM MeOD) showed a similar behavior with a notably twice as high increase in the SA at saturating GEE concentrations. The v_{max} value was calculated as 0.361 ± 0.007 U/mg with an approx. seven times lower affinity (K_m = 7.46 ± 0.51 µM). This finding indicates a possible kinetic isotope effect of SolV MDH.

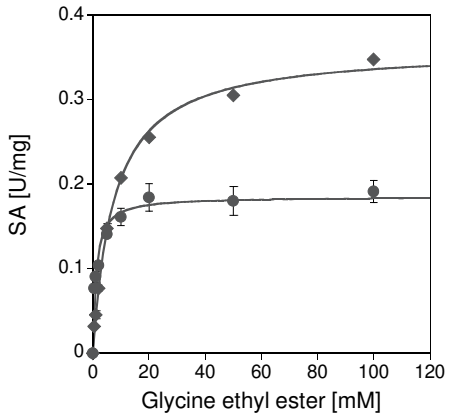

Figure 30 Kinetics of SolV Eu-MDH with glycine ethyl ester as substrate in the presence of either 50 mM MeOH (circles) or 50 mM MeOD (rhombuses). Data were fit according to Michaelis and Menten. Conditions: 200 nM Eu-MDH 1st, 20 mM PIPES pH 7.2, 1 mM PES, 100 µM DCPIP, 45 °C, n = 2.

Because of the surprising Michaelis-Menten behavior, GEE was examined under assay conditions (pH 7.2, 45 °C). NMR analysis (Figure S17) revealed that GEE decomposes at pH values > 7 by producing the MDH substrate ethanol (Scheme 7).

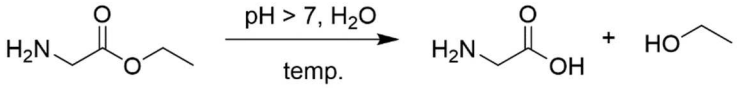

Scheme 7 Elimination of ethanol during GEE incubation at pH > 7 as observed by ^{1}H-NMR spectroscopy.

This effect is even more pronounced at alkaline pH, which is routinely applied in MDH assays. A use of this compound in MDH assays to obtain accurate kinetic parameters is therefore inadvisable.

4.5 Conclusion

The kinetics of purified Eu^{3+}-dependent SolV MDH have been studied using different alcohols and aldehydes. Eu-MDH shows a similar behavior to its mixed REE-derivative, although the affinity constants are approx. 10 times higher. This finding correlated with the slower growth rate of SolV in the presence of Eu^{3+}. In contrast to the mixed REE-MDH with a broad affinity for primary alcohols, Eu-MDH was found to only catalyze the oxidation of methanol, ethanol and propanol efficiently. Yet, acetaldehyde, which was excluded as a substrate for the mixed REE-MDH, is consumed at low rates by the Eu-MDH derivative. These variations in substrate specificity give further evidence that the properties of the central metal ion play a crucial role in the catalytic process of MDH. A tuning of MDH activity for e.g. industrial applications by changing the lanthanide ion is thus possible. The kinetic analysis further showed that formaldehyde is converted at a maximum velocity similar to methanol, as described for a variety of MDH enzymes, supporting the hypothesis that also the Eu^{3+}-dependent MDH is able to efficiently convert methanol into formate. GEE was tested as an activator and found to be a substrate itself due to its weak stability under assay conditions.

5 Kinetic Isotope Effect Studies

5.1 Introduction

The analysis of kinetic isotope effects (KIE) is applied to gain mechanistic knowledge of enzymatic reactions (e.g. the investigation of the rate-limiting step) or to provide deeper insights into the function of nuclear quantum tunneling, dynamic motion or electrostatics during enzyme catalysis.[203–209] The analysis of deuterium KIE is often applied by reason of the relatively high mass difference between hydrogen, deuterium and tritium that leads to a clearly observable KIE.[210] The KIE is the ratio of rate constants of a reaction involving a light (k_H) and a heavy (k_D) isotope.[204] KIE can be divided into primary and secondary isotope effects depending on their chemical step: if the bond to the isotope is cleaved or formed a primary KIE is present, whereas if the isotopically labeled atom is on another position than the bond that is being broken or formed, it is referred to as a secondary KIE. Generally, primary KIE are larger than secondary effects. KIE can be defined as normal if the lighter isotope reacts faster ($k_H/k_D > 1$) or inverse if the reaction with the heavy isotope proceeds quicker ($k_H/k_D < 1$).[204,211] In enzymology, steady-state assays or stopped-flow techniques are combined with MS or NMR analysis as well as computational methods to assess the KIE.[212–214] It has been reported that ADHs from various organisms exhibit KIE.[215,216] Studies on the hydride transfer in ADH by Klinman and co-workers revealed that hydrogen tunneling occurs during catalysis.[217,218] In contrast, the KIE of PQQ-dependent methanol dehydrogenases has been examined with regard to ligand binding. Hothi *et al.* reported an unusual KIE that has been assigned to different affinities for protiated and deuterated substrate at the active site, which is influenced by differential binding of ammonium, PES or GEE at stimulatory and inhibitory sites.[97,143] Yet, the postulated MDH activator GEE was found to be a MDH substrate itself (III.4.4 Glycine Ethyl Ester As Alterative Substrate). Therefore, the reported results obtained in KIE studies are questionable.

To investigate if a KIE is true for SolV MDH, preliminary studies were conducted. As MDH inactivation by phosphate buffer impeded NMR analysis, steady-state kinetics at substrate saturation were chosen as the analytical method. Fully labelled (CD_3OD) substrate was used to investigate whether a deuterium isotope effect exists for SolV MDH as it does for other PQQ-dependent MDH enzymes. Since its catalytic mechanism is still not fully understood, the analysis of the KIE can help to shed light into this matter. The influence of deuterated solvent and substrate, temperature and pH on the overall catalytic activity of Eu-MDH were examined, as was the influence of the interaction of the electron

acceptor PES and the alternative activator GEE with Eu-MDH in the presence of protiated and deuterated methanol.

5.2 Influence of Deuterated Buffer and Substrate

To investigate the deuterium isotope effect, SolV Eu-MDH was assayed with the PES/DCPIP-assay. MDH was analyzed in buffer that was either prepared in MilliQ water (H_2O-PIPES, pH 7.2) or in D_2O (D_2O-PIPES, pD 7.2) and in the presence of either protiated (MeOH) or deuterated substrate (d^3-MeOD). Since the path length correction was unsuccessful in the case of D_2O, raw data (initial slope) is shown instead of the enzymatic specific activity wherever experiments were performed in deuterated buffer (Figure 31A and B). At excess substrate concentrations (50 mM) both D_2O-buffer and MeOD slow the catalytic activity (Figure 31A) and the latter is consumed at a similar rate in both deuterated and non-deuterated buffer. Also, although the buffer seems to highly influence the enzymatic activity, deuterated substrate has a significant negative effect, resulting in an overall higher conversion of protiated MeOH than of MeOD by SolV Eu-MDH.

To investigate if the KIE is influenced by the solvent isotope effect, a mixture of H_2O-PIPES and D_2O-PIPES was applied (Figure 31B). Since this effect results from the exchange of catalytically active protons in some positions of enzyme and substrate, it will lead, if present, to altered kinetic and equilibrium constants and falsify the outcome of the KIE.[219,220] The buffer ratio was varied from 100% H_2O-PIPES to 100% D_2O-PIPES and the enzymatic activity was measured in the presence of protiated methanol. The addition of increasing D_2O-PIPES concentrations caused a slowing of substrate turnover, which is evidence of a clear solvent isotope effect that should be considered in further KIE studies. The non-linear progression suggests a proton inventory of more than one proton being involved in the reaction.[220,221] The substrate deuterium isotope effect was studied by the variation of the MeOH to MeOD ratio (Figure 31C) in H_2O-PIPES and showed a similar behavior. The highest SA of 0.179 U/mg is reached at 100% MeOH, which is in good agreement with the overall activity of this purification fraction (III.1 SolV MDH Derivatives). With increasing MeOD concentrations, the catalytic activity significantly slows to a value of 0.005 U/mg at 100% deuterated methanol. This trend is best illustrated in Figure 31D, which shows the correlation of the rate constants with mixed substrate dependent on the deuterium atom fraction in the substrate. The calculation of the rate constant k_{cat} at 100% of each substrate gave a value of 0.189 ± 0.004 s^{-1} for k_H (MeOH) and 0.005 ± 0.003 s^{-1} for k_D (MeOD), revealing an unusually large KIE (k_H/k_D) on k_{cat} of 36. Since MDH was measured in H_2O-PIPES and the proton at the oxygen atom is exchangeable, an influence of the solvent through hydrogen exchange is

conceivable. Hydrogen exchange in MeOH makes the determination of the KIE's nature (primary or secondary) difficult, so the nature was therefore not analyzed in this study.[222] Additionally, an effect of the itself redox-active PIPES buffer on the outcome of the KIE should be considered.[16]

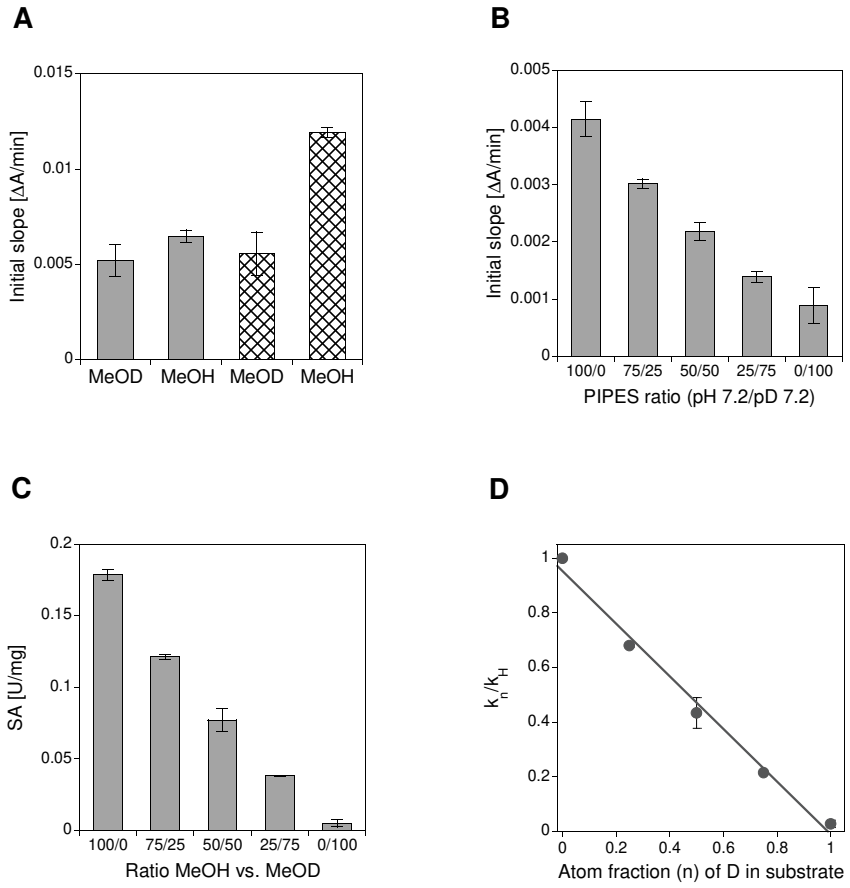

Figure 31 Steady-state DCPIP/PES-assay on the solvent and substrate KIE. Conditions: SolV Eu-MDH, 20 µM Eu^{3+}, 1 mM PES, 100 µM DCPIP, 50 mM substrate, 45 °C, n = 3 unless stated otherwise. A: Activity (initial slope) of 200 nM Eu-MDH in 20 mM D_2O-PIPES pD 7.2 (filled columns) vs. 20 mM H_2O-PIPES pH 7.2 (crosshatched columns) in the presence of MeOH or d^3-MeOD. B: Activity (initial slope) of 30 nM MDH at different ratios of 20 mM H_2O-PIPES pH 7.2 and 20 mM D_2O-PIPES pD 7.2 in the presence of MeOH. C: SA of 200 nM MDH at different ratios of MeOH and MeOD in 20 mM H_2O-PIPES pH 7.2, n = 2. D: Ratios of k_{cat} calculated from C with mixed isotopic substrate (k_n) over MeOH only (k_H) plotted against the atom fraction of deuterium in the substrate (n).

A simultaneous analysis of the KIE with Pr-MDH was unsuccessful due to the high enzymatic activity of this derivative and a too rapid consumption of the dye DCPIP. To further study the KIE using Pr-MDH, the assay must first be optimized.

5.3 Influence of the pH Value on the KIE

A pH-dependent deuterium isotope effect is known for the Zn-dependent NADH alcohol dehydrogenase from yeast as well as other enzyme groups, but has not been reported for MDH enzymes.[214,223,224] Since the determination of pK_a values is crucial for the study of acid-base reactions at the active site of enzymes, the pH-dependency of SolV MDH was investigated in the presence of deuterated substrate. SolV Eu-MDH was assayed across a pH range of 5.8 to 8.5 and the obtained rate constants k_{cat} at different pH were fit with equation 2:

$$k_{cat}(pH) = \frac{k_{cat,max}}{1 + 10^{(pH-pK_{a1})} + 10^{(pK_{a2}-pH)}}$$

The fit results in a bell curve (Figure 32A) that shows a deactivation of the enzyme under acidic as well as basic conditions. As observed before, the overall turnover of substrate at optimum conditions is four times higher if MeOH is supplied. The pH optimum of Eu-MDH lies in the neutral region with both substrates and shifts only slightly from pH 7.4 (MeOH) to pH 7 (MeOD). The first value is in the range of reported data.[104]

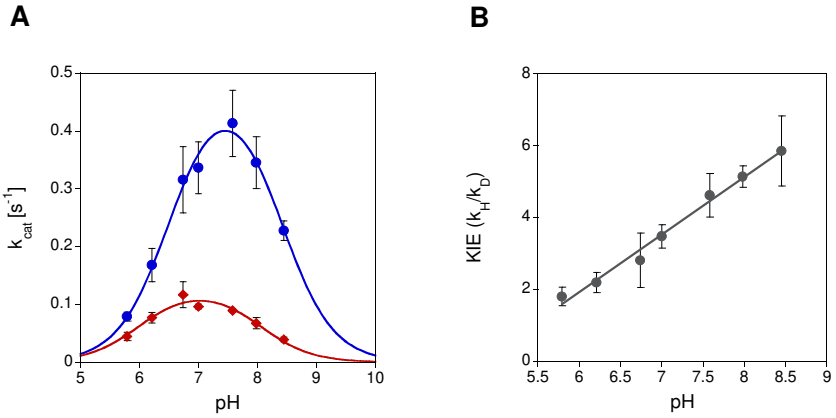

Figure 32 Dependence of Eu-MDH on solution pH (A) in the presence of the substrate MeOH (blue circles) or d^3-MeOD (red rhombuses) and (B) the corresponding kinetic isotope effect calculated from k_{cat} of MeOH (k_H) divided by k_{cat} of MeOD (k_D). Conditions: 200 nM SolV Eu-MDH, 10 mM multicomponent buffer (citric acid, Bis-Tris, Tris and CHES, 2.5 mM each) of different pH, 20 µM Eu^{3+}, 1 mM PES, 100 µM DCPIP, 50 mM substrate (MeOH or d^3-MeOD), 45 °C, n = 3. The plotted pH is the value at assay temperature.

The pK_a values were calculated from the curve fit and show a single basic group in the acidic limb (pK_{a1}), as well as a single acidic group in the basic limb (pK_{a2}). These pK_a values may correspond to the two charged amino acids in the active site of SolV MDH, Asp and Glu.[49,71] If MeOH is supplied, a pK_{a1} of

6.51 ± 0.81 and a pK_{a2} of 8.4 ± 0.74 are obtained. The latter value is in good agreement with previously published data on SolV MDH, whereas the pK_a in the acidic limb is somewhat higher.[104] In the presence of MeOD, a similar behavior that is slightly shifted to smaller pK_a values of 6 ± 0.48 (pK_{a1}) and 8.04 ± 0.51 (pK_{a2}) is observed. The shifts of both the pH optimum and pK_a values to the more acidic region indicate a deprotonation of functional groups in the active site of SolV MDH upon MeOD addition. Asp is described as actively participating in substrate conversion in the two proposed mechanism, addition elimination and hydride transfer (Scheme 8).[30] Although the latter mechanism, which suggests a double involvement of Asp as catalyst, is favored by many researchers, it is still under debate.[75,225] Yet, Good *et al.* reported that the aspartate in the active site is essential for lanthanide coordination and is therefore needed for the catalytic function of XoxF in vivo and the activity of purified enzyme in vitro.[73] Conversely, a participation of Glu instead of Asp was proposed by Zhang and co-workers.[226] While the alteration of pK_a values and enzymatic activity due to MeOD addition do not prove a certain mechanism, the rate-limiting step must be dependent on protonation of functional groups (most likely Asp) in the active site of SolV MDH.

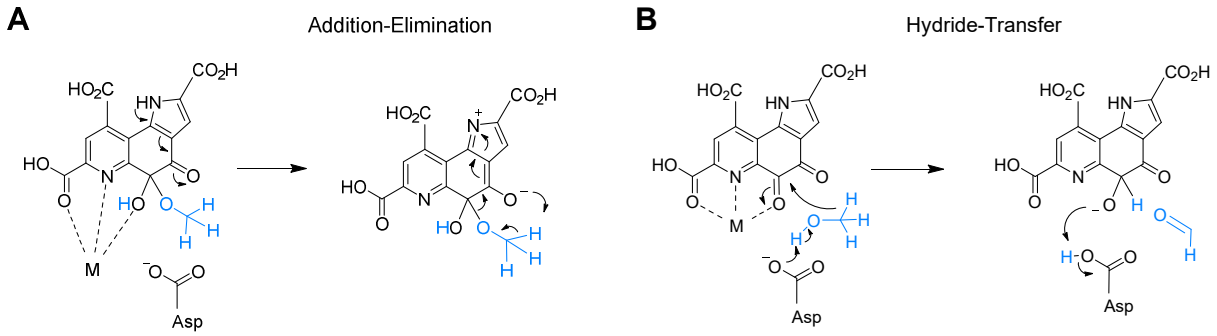

Scheme 8 Possible mechanisms for methanol oxidation by MDH enzymes. A: Addition-elimination mechanism via a hemiketal. B: Hydride-transfer. The substrate methanol is shown in blue. M stands for the central metal ion.

The KIE on k_{cat} was calculated for the pH-dependence of SolV MDH (Figure 32B). Its size increases with increasing pH from 1.8 ± 0.3 (pH 5.8) to 5.6 ± 1 (pH 8.5), showing a normal and not inverse deuterium isotope effect. Further experiments on the pH-dependence with substrate labeled at a specific position, as performed for other ADH, are needed to give a better understanding of the catalytic mechanism.[227,228] The KIE at assay conditions (pH 7, 45 °C) was calculated as 3.5 ± 0.3. Interestingly, the KIE is 10 magnitudes smaller in multicomponent buffer at pH 7 compared to the KIE in PIPES buffer at pH 7.2 (determined from Figure 31C), which might be explained by the redox behavior of the multicomponent buffer influencing the outcome of the dye-coupled assay[124,145] as well as by different activity levels of the used MDH samples.

Experiments on the pD-dependence were not successful in 96-well plates due to incorrect path length correction. Additionally, the raw data fluctuated strongly with an expected strong shift to the more basic pH region.[219] Further, the extinction coefficient of the dye DCPIP decreased unusually strongly at slightly acidic pD, indicating a reaction of the dye with D_2O. Therefore, the pH-dependence of the solvent isotope effect was not further analyzed.

5.4 Influence of the Temperature on the KIE

The temperature-dependence of the KIE has been analyzed for various enzymes. A correlation of the KIE with the distance of the acceptor and donor in the active site as well as hydrogen tunneling have been discussed.[204,216,229] Hothi *et al.* found that the KIE of PQQ-dependent MDH from *M. methylotrophus* is temperature-independent.[97,143] To study the impact of the temperature on the KIE of SolV Eu-MDH, experiments were conducted in the presence of MeOH and d^3-MeOD using the artificial DCPIP/PES-assays at different temperatures in H_2O-buffer (Figure 33). Activation energies as well as the KIE were calculated.

Figure 33A shows an exponential dependence of the rate constant k_{cat} with increasing temperature that is slightly more pronounced in the case of MeOH. This results in a temperature-dependence of the KIE (Figure 33B), which is higher at 25 °C (2.8 ± 0.1) and decreases with temperature to 1.8 ± 0.1 at 45 °C. A high KIE at room temperature is assigned to tunneling effects of hydrogen that contribute to enzymatic reactions, whereas the tunneling probability decreases with increasing temperature.[230] Nevertheless, it has been reported that some thermophilic ADH are capable of modulating the reaction barrier for tunneling at higher temperatures.[218] Whether this mechanism is true for SolV MDH cannot be determined with the data presently obtained on the temperature-dependence. Further studies on the primary and secondary KIE are necessary to answer this question.[204] The observed KIE is normal and has a value of 2 ± 0.2 for assay conditions (45 °C, pH 7.2). It is thus somewhat smaller compared to the KIE determined from the pH-dependence measurement. Since different concentrations of Eu-MDH were used in each experiment (200 nM for pH and 150 nM for temperature studies) while the concentrations of assay components and substrate were kept constant, a change in the KIE due to the modified assay parameters is conceivable.

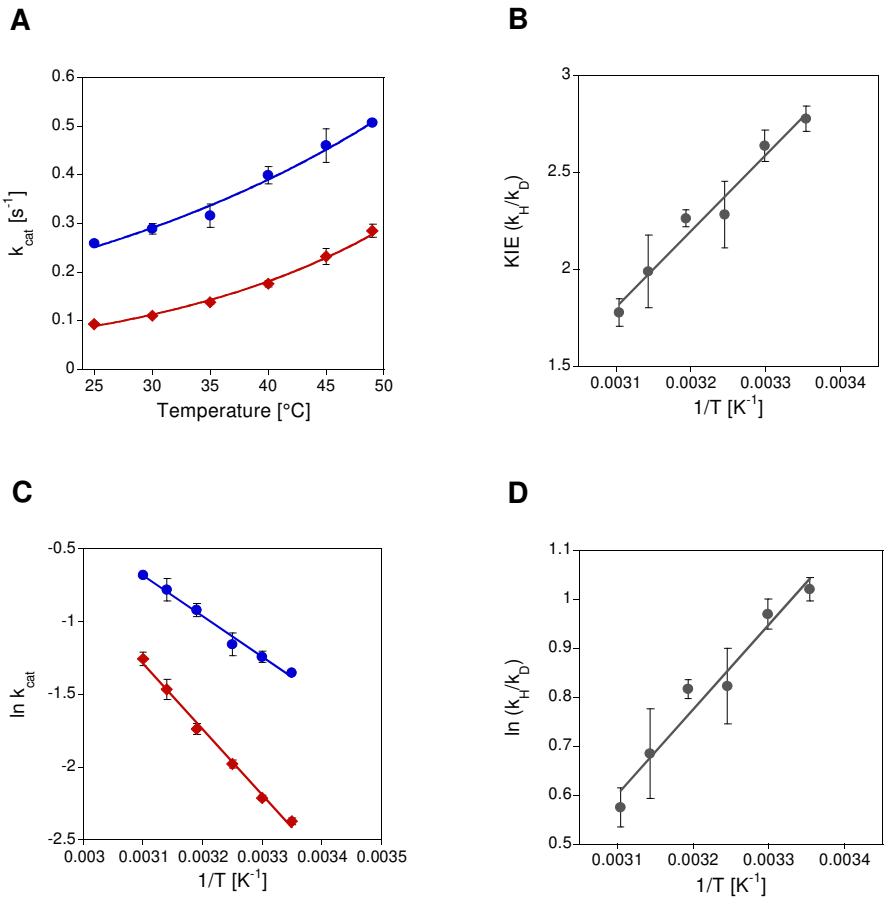

Figure 33 Temperature dependence of Eu-MDH in the presence of MeOH or MeOD. Conditions: 150 nM SolV Eu-MDH, 10 mM multicomponent buffer (citric acid, Bis-Tris, Tris and CHES, 2.5 mM each) pH 7.2, 20 µM Eu, 1 mM PES, 100 µM DCPIP, 50 mM MeOH (blue circles) or d^3-MeOD (red rhombuses), temperature was varied from 25 – 45 °C, n = 3. A: Rate constant k_{cat} at different temperatures and in the presence of different substrate. B: KIE on k_{cat}. C: Arrhenius plots in the presence of different substrates. D: Arrhenius plot of the KIE on k_{cat}.

To determine activation energies, Arrhenius plots (Figure 33C and D) were used and the natural logarithm of k_{cat} or of the KIE were fit with the Arrhenius equation (equation 3), where R is the gas constant (8.314 J K^{-1} mol^{-1})[104]:

$$\ln(k_{cat}) = \frac{-E_a}{R}\left(\frac{1}{T}\right) + \ln(A)$$

Activation energies were calculated from the best curve fit in the range of 25 – 45 °C. An E_a of 23.1 kJ mol^{-1} was determined in the presence of MeOH. This value is similar to those of other MDH enzymes, such as Ca-MDH (27.8 kJ mol^{-1}) and Sr-MDH (27.9 kJ mol^{-1}) from *M. extorquens*.[93] However, the notable deviation from the literature value of 30.4 kJ mol^{-1} for SolV MDH indicates distinct differences between purification fractions.[104] The E_a in the presence of MeOD is approx. two-fold

higher (37.4 kJ mol^{-1}). Further, the KIE on the Arrhenius pre-exponential factor (A_H/A_D), which is used as a measure for the tunneling probability of hydrogen, was analyzed using Figure 33D.[204] A value of 0.008 was obtained which is approx. 200-fold smaller compared to the KIE on k_{cat}. The values of both the E_a and the KIE on A and the KIE on k_{cat} strongly support a temperature-dependence of the deuterium isotope effect for SolV MDH. This finding is the opposite of that of Hothi *et al.* for *M. methylotrophus* MDH.[97,143]

5.5 Influence of PES on the KIE

In contrast to other ADH enzymes, the KIE of PQQ-dependent MDH has only been analyzed with regard to ligand binding. Studies with *Hyphomicrobium* X, *M. extorquens* AM1 and *M. methylotrophus* revealed that the KIE is dependent on ammonia concentration and that PES and cyanide compete for binding at the catalytic site, which is further affected by GEE-binding.[92,97,109,143] Since ammonia activation is not necessary for SolV MDH activity (III.2.3 Further Assay Optimization) this activator was omitted from the study.[49] Furthermore, cyanide was excluded based on the general decision to conduct assays in the absence of this compound (III.2.3 Further Assay Optimization).

To investigate the effect of artificial electron acceptor binding on SolV MDH, the enzymatic activity was assayed at different PES concentrations in the presence of MeOH or d^3-MeOD (Figure 34), with the substrate added after the consumption of residual MeOH. The obtained initial velocity was fit to the equation for substrate inhibition (equation 1) because of the decrease in enzymatic activity at high PES concentrations.[133] The apparent PES optimum was determined from the best curve fit (Figure 34A). Overall the SA increases strongly until the optimal PES concentration is reached and then decreases slowly, indicating MDH inhibition by PES as described by Anthony.[30] MDH inhibition occurs fastest if MeOD is supplied and a PES optimum of 1.4 mM is observed with the deuterated substrate. By contrast, an approx. 2.5-fold higher PES concentration of 3.3 mM is necessary for obtaining the highest activity if MeOH is added. Further, the maximum initial velocity differs between the substrates and correlates with the degree of MDH inhibition by PES. The lowest v_{max} of 0.1 U/mg is observed if Eu-MDH uses MeOD as substrate. MeOH, however, leads to a significantly higher v_{max} of 0.39 U/mg. As observed before in pH-dependence experiments under the same conditions as for PES-dependence, the enzymatic activity is lowered to one quarter in the presence of deuterated substrate. A similar effect was observed for *M. methylotrophus* MDH in the presence of small ammonia concentrations.[143] Steady-state kinetic parameters were obtained using equation 1 and are presented in Table 10. For

both substrates, the calculated values for the maximum initial velocity are significantly higher compared to the observed values (0.29 U/mg for MeOD and 0.61 U/mg for MeOH). The same behavior was also observed for *P. dentrificans* MDH in the presence of MeOH. Harris and Davidson explained this finding with the inhibition of MDH by PES, which in turn prevents the saturation of the enzyme with an excess of electron acceptor.[133] The Michaelis-Menten constant K_m and inhibition constant K_i were calculated for both substrates using equation 1. If MeOH was present as substrate, the apparent K_m value of 2.19 mM was slightly lower compared to the K_i value of 4.89 mM for PES. In the case of MeOD as substrate, the difference between the two values was quite small with 1.44 mM for K_m and 1.28 mM for K_i. In contrast to the above mentioned MDH from *P. dentrificans*, substrate inhibition by PES is only minor if MeOH is supplied but has a considerable effect in the presence of MeOD. Therefore, a possible interaction of substrate and PES at the same enzymatic site is conceivable.[133]

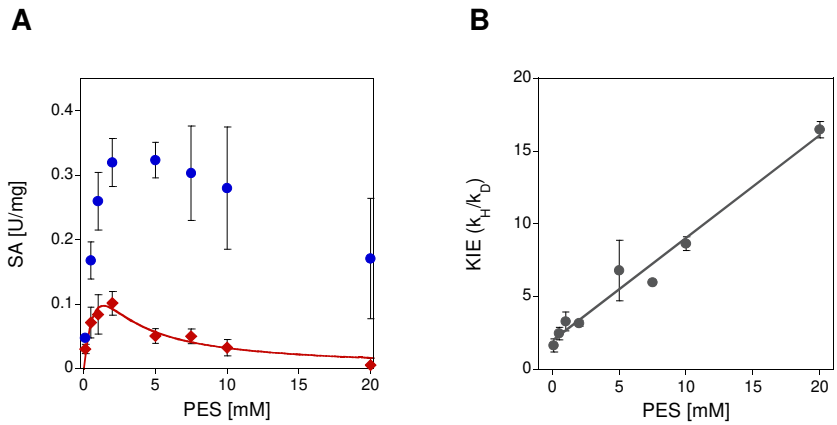

Figure 34 PES-dependence of Eu-MDH. A: SA in the presence of substrate MeOH (blue circles) or MeOD (red rhombuses). Conditions: 200 nM SolV Eu-MDH, 20 mM PIPES pH 7.2, 20 µM Eu, 100 µM DCPIP, 50 mM substrate (MeOH or d³-MeOD), PES concentration varied, 45 °C, n = 2. B: KIE of the PES-dependence.

The results presented in (Figure 34B) show a strong PES-dependence of the deuterium isotope effect on k_{cat} which can be classified as normal and increases highly from 1.7 ± 0.4 (0.1 mM PES) to 16.5 ± 0.6 (20 mM PES). For assay conditions (1 mM PES) a KIE of 3.3 ± 0.7 was obtained, which is in good agreement with the KIE determined in pH-dependence studies.

Table 10 Steady-state kinetic parameters determined from the the curve fit (Figure 34) and calculated with equation 1 for the reaction of PES with protiated and deuterated methanol.

Substrate	PES [mM]	$V_{max,obs}$ [U/mg]	V_{max} [U/mg]	K_m [mM]	K_i [mM]
MeOH	3.3	0.39	0.61	2.19	4.89
MeOD	1.4	0.10	0.29	1.44	1.28

5.6 Conclusion

A great variety of enzymes have been analyzed regarding a kinetic isotope effect. Alcohol dehydrogenases are among the classical models for enzymology and a KIE has been widely studied; however, data about a KIE of PQQ-dependent MDH are sparse.[204,211] In this study, SolV Eu-MDH was analyzed in the presence of deuterated substrate in order to investigate if a deuterium isotope effect exists for this enzyme. Experiments in D_2O-buffer revealed a solvent isotope effect which must be considered in KIE experiments. Since 5% of the assay mixture is made up of substrate, a possible exchange of deuterium for some protons during the measurement must also be considered. Measurements on the substrate isotope effect showed that MeOD dramatically decreases SolV MDH activity. However, kinetic complexity cannot be ruled out since a possible intrinsic isotope effect was not analyzed. Further, due to easily exchangeable protons on the oxygen of methanol, the analysis of primary and secondary KIE was impossible with this substrate. Further experiments should include alternative substrates that can be stably labeled. SolV MDH exhibits a small pH- and temperature-dependent KIE with values ranging from 2 to 3. This KIE deviates highly from the one determined in substrate isotope effect experiments, most probably due to the redox-active buffer and differential activity levels of the used MDH samples. The pH-dependent KIE suggests that more than one isotope sensitive step is present during MeOH conversion. The temperature-dependence shows a clear difference in activation energies and further supports a KIE for SolV MDH. A possible tunneling of the hydrogen atom can be probed with further experiments on the primary and secondary isotope effect. Experiments should include alternative substrates, as well as the use of tritium as isotope together with the Swain-Schaad relationship.[204] To elucidate the precise mechanism of SolV MDH catalysis, *in silico* methods could also be helpful. The investigation of the interaction of ligands with deuterated substrate showed a stronger inhibition of SolV MDH with deuterated substrate, indicating a competitive binding of PES and substrate at the same site. Overall, a small normal deuterium isotope effect of 2 to 3 was found for SolV MDH, but further analysis of the KIE is required.

Methods

IV. Methods

1 SolV MDH Purification

M. fumariolicum SolV MDH was purified from frozen cell pellets at the Radboud University Nijmegen, Netherlands, together with H. Singer under the supervision of Dr. A. Pol.

1.1 Cell Disruption

Frozen cell pellets were thawed in warm water or overnight on ice. DNAse I (30 µg/ml) was added and cells were diluted in 10 mM PIPES pH 7.2 with 1 mM MeOH on ice. The cells were cracked using a French press with a pre-cooled cell at room temperature, applying a chamber pressure of 20,000 psi. The cell disruption process was repeated twice. The cell walls and organelles were removed by two centrifugation steps: 10,000 rpm for 15 min and 15,000 rpm for 2 h 15 min at 4 °C, respectively.

1.2 Fast Protein Liquid Chromatography (FPLC)

SolV Eu-MDH and Pr-MDH were purified as a dimer consisting of 63 kDa monomers each over a pre-cooled 20% SP-sepharose column with accessory UV-visible detector and sample collector (Äkta purifier, GE Healthcare, Chicago, IL, USA). All FPLC steps were carried out under ice cooling (4 °C). The supernatant was loaded using an external pump with a flow-rate of 13 ml/min. The column was washed with 10 column volumes (2 l) of 10 mM PIPES pH 7.2 with added 1 mM MeOH (flow-rate: 50 ml/min) for about 2.5 h. The column-bound protein was eluted using a NaCl gradient (supplemented with 1 mM MeOH) at a salt concentration of 20 – 30%. Fractions were collected in 5 ml portions in an ice water-cooled collector. Purified MDH was either aliquoted subsequently or re-purified under the same conditions. MDH samples were flash frozen in liquid nitrogen and stored at - 80 °C.

1.3 Sodium Dodecyl Sulfate Polyacrylamide Gel Electrophoresis (SDS-PAGE)

Purified MDH was separated in terms of molecular weight using discontinuous SDS polyacrylamide gel electrophoresis as described by Laemmli.[231] Gels were prepared in commercially available casting chambers. The casting chamber was assembled and checked for tightness. Both, the resolving and stacking gel were mixed according to Table 11. TEMED and APS were added to the gel for polymerization. The resolving gel was poured between the two plates and overlayed with 70% EtOH. The stacking gel was added on top after the resolving gel was polymerized.

Table 11 Reagents and volumes for the preparation of a 10% SDS-PAGE gel.

Gel type	MilliQ water	40% PAA (37.1:1)	1.5 M Tris pH 8.8	0.5 M Tris pH 6.8	10% SDS	10% APS	TEMED
10% resolving gel	4.9 ml	2.5 ml	2.5 ml	-	0.1 ml	50 µl	10 µl
4% stacking gel	3.2 ml	0.5 ml	-	1.25 ml	0.05 ml	25 µl	7.5 µl

MDH was diluted with 4x sample buffer and heated up to 95 °C for 5 min. 30 µl purified MDH/lane (7.5 µg) were loaded onto the gel. The gel was run at 50 mA for 20 min and afterwards at 100 mA for 30 min. The resolving gel was stained with Coomassie brilliant blue stain solution for 1 h, shaking, and subsequently destained in destain solution containing MeOH/acetate for 2 h.

2 Preparation of MDH Samples

Frozen MDH aliquots were thawed on ice, washed or re-buffered twice in the desired buffer system and the protein concentration was adjusted.

2.1 Washing Procedure

The washing procedure was applied for re-buffering and removal of substrate, product or degraded protein. The MDH sample was diluted in the respective buffer in a 1:10 ratio and centrifuged at 4,500 rpm and 4 °C until the initial volume was reached using a centrifugation filter unit with a 30 kDa molecular weight cut-off. The washing step was repeated twice.

2.2 Determination of Protein Concentration

The protein concentration was determined via the Edelhoch method[232] in a Cary60 UV-visible spectrophotometer (Agilent Technologies, Santa Clara, CA, USA) using either a 1 cm-path length quartz cuvette or a TrayCell equipped with a 10x cap. A buffer baseline was subtracted from the spectrum and the absorbance at 280 nm was used for the calculation of protein concentration according to the Lambert-Beer Law (equation 4) with A being the absorbance at 280 nm, c being the concentration of the protein, d being the path length of the cell and ε being the molar extinction coefficient for SolV MDH (158 $cm^{-1} \cdot mM^{-1}$).[49]

$$A_{280\text{nm}} = \varepsilon \cdot c \cdot d$$

In the case of the measurements with the Traycell a previously determined MDH specific factor was utilized for calculating the protein concentration. The following sample specific factors (SSF) were applied: 1.46 for AM1 La-MDH and 2.56 for SolV MDH. The protein concentration was calculated according to equation 5, that derives from the Lambert-Beer Law:

$$\text{concentration (mg/ml)} = \frac{1}{\text{SSF}} \cdot A_{280\text{ nm}} \cdot \text{dilution factor}$$

3 UV-Visible Spectra

UV-visible spectra of MDH samples, PQQ or the electron acceptors were recorded at either a Cary60 UV-visible spectrophotometer equipped with a Peltier element (Agilent Technologies, Santa Clara, CA, USA) in a 1 cm- or 1 mm-path length quartz cuvette or in 96 well plates using an Epoch2 or Synergy HTX microplate reader (BioTek Instruments, Winooski, VT, USA) with path length correction to 1 cm by the Gen5 software (BioTek Instruments, Winooski, VT, USA). Full spectra (200 – 800 nm) were recorded with a step size of 1 nm.

3.1 Absorbance Spectra of the Electron Acceptors and Dyes

Absorbance spectra of PMS, PES, DCPIP and WB were recorded at the respective temperature and in the respective buffer in 1 cm-path length quartz cuvettes or 96 well plates. The buffer baseline was subtracted from the spectrum unless stated otherwise.

3.1.1 Absorbance Spectra of DCPIP and WB

2 mM stock solutions of both dyes were prepared in MilliQ water in amber-colored tubes. WB was shaken for 1 h at room temperature and afterwards put into an ultrasonic bath for 5 min. The time to dissolve WB varied between experiments and was dependent on the particle size of the dye. Subsequently after preparation, stock solutions were diluted in the respective buffer to a concentration of 50 µM (DCPIP) or 100 µM (WB) and the absorbance was recorded in triplicates.

3.1.2 WB Storage Experiments

2 mM WB stock solutions were prepared as described above. The samples were either analyzed just after preparation or were stored on ice, flash frozen in liquid nitrogen for about 20 s and allowed to thaw on ice immediately in the case of the “FF on ice sample” or stored at - 20 °C or - 80 °C or were slowly frozen at - 20 °C or - 80 °C. Samples that were stored on ice were either diluted with MilliQ

water or 100 mM multicomponent buffer pH 9. Samples were thawed on ice before analysis if frozen and diluted to a concentration of 200 µM in either MilliQ water, 100 mM multicomponent buffer pH 7.2 or pH 9. Spectra were collected at 30 °C.

3.1.3 Absorbance Spectra of PMS and PES

10 mM stock solutions were prepared in MilliQ water and were subsequently diluted to a concentration of 125 µM in MilliQ water. Spectra were recorded after sample preparation at room temperature. Afterwards samples were exposed to daylight for 1 day and spectra were recorded again under the same conditions.

3.2 Determination of Molar Extinction Coefficients

Absorbance spectra of 100 µM solutions of DCPIP or WB in the respective buffer at the respective temperature were recorded as at least triplicates using the Epoch2 or Synergy HTX microplate reader with path length correction to 1 cm. The molar extinction coefficients ε at different conditions (pH, temperature, buffer system) were calculated from the absorbance at 600 nm (DCPIP) or 610 nm (WB) using equation 4 above.

3.3 PQQ Fingerprint of MDH Samples

PQQ spectra of MDH samples were recorded in CD cuvettes with 1 mm path length (total volume: 200 – 300 µl) at the respective temperature and buffer using the Cary60 UV-visible spectrophotometer. MDH was washed or re-buffered twice before the measurement unless stated otherwise. The protein concentrations ranged between 0.5 – 1 mg/ml.

3.4 PQQ Spectra

PQQ spectra were recorded at the Helmholtz Zentrum Dresden Rossendorf, Germany. Two stock solutions were prepared: 1.7 mM PQQ in 100 mM NaCl pH 6.5 with added 1 mM MeOH and one drop of 1 M NaOH, and 3 mM $EuCl_3$ in 100 mM NaCl pH 6.5 with added 1 mM MeOH. The stock solutions were mixed in 100 mM NaCl pH 6.5 with added 1 mM MeOH to obtain a solution consisting of 10 µM PQQ and 10 µM Eu^{3+}. UV-visible absorption spectra were collected at room temperature using a Lambda 750 spectrophotometer (PerkinElmer, Waltham, MA, USA) in the range of 200 – 800 nm with a step size of 0.1 nm. The PQQ solution was either measured subsequently after preparation or after exposure to a high energy or low energy Nd:YAG OPO laser with a wavelength of 394 nm.

3.5 Analysis of TMPD, TMPDD and WB in Time-Dependent Experiments

2.5 mM stock solutions of *N,N,N´,N´*-tetramethyl-p-phenylenediamine (TMPD) and *N,N,N´,N´*-tetramethyl-p-phenylenediamine dihydrochloride (TMPDD) and a 2 mM stock solution of WB were prepared as described above. The stock solutions were diluted with different 20 mM buffers (MES, potassium phosphate (KP), PIPES, MOPSO, MOPS, Tris-HCl, CHES, CAPS) of different pH or MilliQ water to a concentration of 200 µM. The measurements were carried out at the Epoch2 microplate reader at 610 nm and either 30 °C or 45 °C for 1 h.

4 Electron Paramagnetic Resonance (EPR) Spectroscopy

The analysis of radical formation in aqueous PES, PMS and WB samples was performed using a EMXnano benchtop EPR spectrometer (Bruker, Billerica, MA, USA). Samples were analyzed subsequently after preparation. The samples were picked up using a capillary that was sealed with wax afterwards. EPR spectra were recorded at room temperature and in the dark.

PMS/PES: Stock solutions of 100 mM PES and PMS were prepared in MilliQ water in amber-colored tubes. Stock solutions were diluted to a concentration of 10 mM in MilliQ water, 100 mM multicomponent buffer of pH 7.2 or 9, 20 mM PIPES buffer pH 6.2 or pH 7.2 or 20 mM KP buffer pH 7.2. Samples were treated differently before measurement: storage in the dark at room temperature or at 4 °C for 30 min, heating at 45 °C for 15 min in amber-colored tubes, exposure to daylight or UV light of 254 nm for 5 min. The PMS and PES samples were prepared and analyzed on both a sunny and a cloudy day.

WB: A 2 mM WB stock solution in MilliQ water was prepared as described above and was diluted in 100 mM multicomponent buffer of pH 7.2 or pH 9 to a concentration of 200 µM. WB samples were analyzed on a sunny day only.

5 Circular Dichroism (CD) Spectroscopy

CD spectra were collected at a J-810 CD and ORD spectropolarimeter (Jasco, Tokyo, Japan) equipped with a thermostatted cell holder. Measurements were performed in a 1 mm-path length CD quartz cuvette at either 4 °C, room temperature (MDH derivatives, MDH stability, NaCl experiment) or 45 °C. MDH was washed/re-buffered twice in either 20 mM PIPES pH 7.2, 20 mM KP pH 7 or 100 mM NaCl pH 7 and either measured subsequently after preparation or after different incubation periods at various temperatures. Data were collected in the range of 190 – 260 nm with a data pitch of 0.5 nm, standard sensitivity, a band width of 1 nm, a scan speed of 200 nm/min, three accumulations and a D.I.T. of 0.5 sec. A buffer baseline was recorded separately and was subtracted manually from the measured spectrum. CD spectra were processed with the Spectra Manager II software version 2.06.00 (Jasco, Tokyo, Japan).

6 Activity Assays

The activity of MDH was determined using the DCPIP/PES or WB assay. Measurements were conducted on an Epoch2 or Synergy HTX microplate reader with path length correction to 1 cm (Gen5 software) or at the Cary60 UV-visible spectrophotometer equipped with a Peltier element. A temperature of 30 °C or 45 °C was adjusted and the instrument was left to equilibrate to the set temperature for at least one hour prior to the measurements.

6.1 Determination of Kinetic Parameters

The specific enzymatic activity (SA) was calculated from the initial rate of substrate conversion (slope of the first few minutes) using equation 6 with ε being the extinction coefficient of the used dye (Table S1, Table S3 and Table S4):

$$\text{enzyme unit U } [\mu\text{mol} \cdot \text{min}^{-1}] = \frac{\text{inverted slope (initial rate)}}{\varepsilon\ [\text{cm}^{-1} \cdot \text{M}^{-1}] \cdot \text{path length [cm]}} \cdot 10^6 \cdot \text{assay volume [l]}$$

and equation 7:

$$\text{SA } [\mu\text{mol } \cdot \text{min}^{-1} \cdot \text{mg}^{-1}] = \frac{\text{enzyme unit U } [\mu\text{mol} \cdot \text{min}^{-1}]}{\text{amount of enzyme [mg]}}$$

For the analysis of substrate kinetics and metal titrations, the SA values were fit according to Michaelis and Menten by applying equation 8:

$$v_0 = \frac{v_{max} \cdot [S]}{K_m + [S]}$$

with v_0 being the initial velocity, v_{max} the maximum turnover speed, [S] the substrate concentration, and K_m the Michaelis-Menten constant. v_{max} [µmol · min^{-1} · mg^{-1}] and K_m [mM] were read from the best curve fit. In the case of metal titrations K_m denotes K_{assoc}, the metal association constant.

The turnover number k_{cat} was determined using equation 9 with $[E_0]$ being the total enzyme concentration:

$$k_{cat}\,[s^{-1}] = \frac{\frac{v_{max}\,[\mu mol\ \cdot min^{-1} \cdot mg^{-1}]}{[E_0][mol]}}{60\ s} = \frac{\frac{v_{max}\,[\mu mol\ \cdot min^{-1} \cdot mg^{-1}]}{\left(\frac{1}{MW\,[g/mol]}\right) \cdot 1000}}{60\ s}$$

And the catalytic efficiency was calculated using equation 10:

$$\text{catalytic efficiency}\,[s^{-1} \cdot mM^{-1}] = \frac{k_{cat}\,[s^{-1}]}{K_m\,[mM]}$$

6.2 DCPIP/PES Assay

All of the used stock solutions were prepared in MilliQ water and stored on ice: 100 mM PMS, 100 mM PES, 2 mM DCPIP, all in amber-colored tubes, 100 mM KCN, 1 M substrate (alcohols or aldehydes), 500 mM NH_4, 20 mM metal. The general procedure involved the following steps: PMS/PES and DCPIP stock solutions were mixed with the respective buffer to obtain the assay mix and were heated for 15 min at 45 °C in the dark. For assays performed at 30 °C, the heating step was omitted. Meanwhile MDH was washed, diluted in the respective buffer and stored on ice. Assay mix, MDH, metal and assay additives were mixed. The reaction was monitored in the dark at 45 °C (unless stated otherwise) and 600 nm. The measurement was started with the addition of substrate. All assay steps were conducted under the exclusion of light.

6.2.1 SolV MDH Assays in the Cary60 Spectrophotometer

All of the measurements were acquired on the Cary60 UV-visible spectrophotometer at 45 °C in a stirred 1 cm-path length quartz cuvette and a total volume of 1 ml. The assay mix containing 20 mM PIPES pH 7.2, PES, DCPIP and KCN, was heated for 15 min at 45 °C to alleviate background reactions of the assay mix in the absence of enzyme. Initial rates (the first 1.5 min of the slope) were used for the calculation of specific enzymatic activities.

6.2.1.1 Metal Titrations

The final assay mix was comprised of 1 mM PES, 1 mM KCN, 80 µM DCPIP, 4 mM methanol and different concentrations of metals (for Eu^{3+} and La^{3+}: 0 – 50 µM). Measurements were performed by monitoring the background reaction for one min at 600 nm before the addition of 100 nM MDH.

6.2.1.2 Substrate Kinetics

The final assay mix was comprised of 1 mM PES, 1 mM KCN, 80 µM DCPIP and 20 µM Eu^{3+} (Eu-MDH) or 20 µM La^{3+} (La-MDH). The background was monitored for one minute at 600 nm. 100 nM MDH were added to start the measurement. Different concentrations of methanol (0 – 100 µM) were added after the residual methanol in the MDH sample has been used up by the enzyme. Additionally, excess methanol (1 M) was added after another three min to correct for fluctuations in the activity during the day.

6.2.2 SolV MDH Assays in the Microplate Reader

All of the measurements were acquired on either the Epoch2 or Synergy HTX microplate reader at 45 °C or 30 °C in 96 well plates with a total volume of 200 µl and path length correction to 1 cm. The assay mix (100 µl/well) contained 2 mM PMS or 2 mM PES, 200 µM DCPIP and the respective buffer and was heated for 15 min at 45 °C in amber-colored tubes unless stated otherwise, to alleviate background reactions of the assay mix in the absence of enzyme.

6.2.2.1 Stability of MDH

The heated assay mix contained 20 mM PIPES pH 7.2, PES and DCPIP. Depending on the type of experiment, MDH was incubated in either 20 mM PIPES buffer pH 7.2 or in pre-heated assay mix for different time spans at either 4 °C, room temperature or 45 °C. 100 µl assay mix and 90 µl MDH in PIPES or 190 µl of a mixture of assay mix and MDH were added to the 96 well plate and were incubated

for 2 min at 45 °C in the dark. 10 µl 1 M methanol were added to start the reaction. The final concentrations in the well were: 200 nM MDH, 1 mM PES, 100 µM DCPIP, 50 mM methanol. Initial rates (first 3 min of the slope) were used to calculate specific activities.

6.2.2.2 Studies with Electron Acceptors for Assay Optimization

Two types of experiments were performed. For the analysis of the specific activity of MDH at 30 °C 100 mM multicomponent buffer pH 7.2 (consisting of 25 mM citric acid, 25 mM Bis-Tris, 25 mM Tris-HCl and 25 mM CHES) was utilized whereas for the experiment at 45 °C chelexed 20 mM PIPES buffer pH 7.2 was used. A 1 mM solution of DCPIP was mixed with either 10 mM PMS or 10 mM PES. When the normal assay conditions were applied (45 °C), the mixture of DCPIP and PMS or DCPIP and PES was additionally incubated in a dry block heater for 15 min at 45 °C and 1 mM KCN was included in the assay. The electron acceptors, 1 M methanol (10 µl) and the corresponding buffer were added into a 96 well plate. The plate was incubated for 2 min at 30 °C or 45 °C in an Epoch2 microplate reader. Washed SolV MDH was mixed with buffer and 2 mM $EuCl_3$ (2 µl) and was added into the plate. The decrease in absorbance was followed at 600 nm for 20 min. The total volume of 200 µl/well consisted of 100 nM Eu-MDH, 20 µM $EuCl_3$, 50 mM MeOH, 100 µM DCPIP and 1 mM PMS or PES. For the background control the absorbance at 600 nm was monitored as described above except that no MDH was added. For calculating initial rates, the first 5 min of the slope were used.

6.2.2.3 PES- and KCN-Dependence

Data were collected using the Epoch2 microplate reader. DCPIP was mixed with either different concentrations of PES or KCN in 20 mM PIPES pH 7.2 and was heated for 15 min at 45 °C in amber-colored tubes. PES was added to the DCPIP/KCN mixture, while KCN was added to the DCPIP/PES mixture. 100 µl of each assay mix and 90 µl MDH in PIPES buffer were added to a well of the 96 well plate each. The plate was subsequently incubated for 2 min at 45 °C in the microplate reader (darkness). Afterwards, 10 µl methanol were added to start the measurement. The reaction was followed at 600 nm and 45 °C for 30 min. The final assay mixture contained: 100 nM MDH, 100 µM DCPIP, 50 mM methanol and either 0 – 6 mM PES and 1 mM KCN or 0 – 5 mM KCN and 1 mM PES. The

background was monitored under the same condition in assay mixtures without MDH. Initial rates were used to calculate specific activities.

6.2.2.4 Metal Binding Studies

Metal binding experiments were performed on the Epoch2 microplate reader in 20 mM PIPES pH 7.2. All metal solutions (chloride salts of REE, Ca or Ba) were prepared in MilliQ water. Assay mix containing PES, DCPIP and KCN was prepared as described above. 100 µl of assay mix were added to a 96 well plate and were incubated at 45 °C for 5 min in the dark. 80 µl MDH in PIPES and 10 µl of the metal solution or MilliQ water were added and the plate was incubated for another 2 min at 45 °C. The reaction was started by adding 10 µl of 1 M methanol. The final concentrations per well (200 µl) were: 200 nM MDH, 1 mM PES, 100 µM DCPIP, 1 mM KCN, 50 mM MeOH and 20 µM or 100 µM metals, depending on the type of experiment. On average four measurements were used to calculate specific activities from initial rates.

6.2.2.5 Activity of MDH in NaCl

Stock solutions of DCPIP and PES were mixed with 100 mM NaCl pH 7 and heated at 45 °C for 15 min in amber-colored tubes. 100 µl assay mix, 80 µl NaCl re-buffered MDH and 10 µl 400 µM $EuCl_3$ were added to a 96 well plate. In the case of metal titrations, different concentrations of the REE (0 – 50 µM) were added. The mixture was incubated for 2 min at 45 °C in the dark. The measurement was started by adding 10 µl of 1 M methanol. The final assay contained: 200 nM MDH, 100 mM NaCl pH 7, 1 mM PES, 100 µM DCPIP, 20 µM or other concentrations of Eu^{3+} and 50 mM methanol. The specific enzymatic activity was calculated from initial rates (first min of the slope) and after 15 min. Activities were compared to those obtained from the same assay with PIPES buffer.

6.2.2.6 Substrate Kinetics

Alcohols, aldehydes and GEE were analyzed as MDH substrate. 1 M solutions of alcohols and aldehydes and a 2 M GEE solution all in MilliQ water were prepared and stored at 4 °C until use. The substrate was diluted to different concentrations in MilliQ water. The assay mix was prepared as described above: 2 mM PES and 200 µM DCPIP in 20 mM PIPES pH 7.2 heated for 15 min at 45 °C in the dark. 100 µl assay mix, 10 µl $EuCl_3$ and 80 µl MDH in PIPES buffer were added to a 96 well plate. The plate was incubated for 2 min at 45 °C in the dark. The reaction was followed for 10 min before 10 µl of different substrate concentrations (0 – 100 µM for alcohols and aldehydes and 0 – 100 mM for GEE) were added. Initial rates (first one to five min) were used for the calculation of the specific activity.

6.2.2.7 Inhibition Studies

Measurements were performed in 20 mM PIPES pH 7.2 on the Synergy HTX microplate reader. Cyclopropanol was diluted in MilliQ water to obtain a 1 M stock solution. The stock solution was further diluted to different concentrations in MilliQ water. The assay mix was prepared as described above. MDH was washed once in PIPES buffer. 100 µl of assay mix, 10 µl of $EuCl_3$ and 80 µl of MDH in PIPES were mixed in a 96 well plate. The plate was incubated for 2 min at 45 °C. 10 µl of different cyclopropanol concentrations were added regardless of the presence of residual methanol. Initial rates (first 5 min of the slope) at varied inhibitor concentrations (0 – 50 mM) were used to calculate the specific enzymatic activity.

6.2.2.8 Deuterium Isotope Effect

The activity of MDH in the presence of protiated and deuterated methanol was analyzed using assay mix and solutions that have been prepared in MilliQ water as described above. For experiments with deuterated buffer, the assay mix and all solutions were prepared in D_2O and MDH was washed in D_2O-buffer. The substrate was either diluted in MilliQ water (MeOH) or D_2O (d^3-MeOD) to a 1 M concentration. Measurements were conducted on an Epoch2 or Synergy HTX microplate reader with path length correction to 1 cm at 45 °C and in the dark and a total volume of 200 µl. The path length

correction was not successful in the case of deuterated medium due to the absence of absorption at 975 nm that is usually used for the path length correction in microplate readers.

Analysis of the Solvent and Substrate Isotope Effect

Two types of assay mix were prepared: one in 20 mM PIPES pH 7.2 and one in 20 mM D_2O-PIPES pD 7.2. MDH was washed in either H_2O-PIPES or D_2O-PIPES. 100 µl assay mix, 10 µl $EuCl_3$ and 80 µl MDH in the respective PIPES buffer were added to the 96 well plate. The plate was incubated for 5 min at 45 °C before the measurement was started by adding 10 µl of 1 M substrate. The final concentrations in the well were: 200 nM MDH (unless stated otherwise), 1 mM PES, 100 µM DCPIP, 20 µM $EuCl_3$ and 50 mM substrate.

For the H_2O vs. D_2O-PIPES experiment, assay mix, $EuCl_3$ and MDH in MilliQ water were mixed in one half of the wells while assay mix, $EuCl_3$ and MDH in D_2O were added to the other half of the wells. MeOH and d^3-MeOD were added to H_2O as well as to D_2O wells to start the measurement.

The solvent deuterium isotope effect was analyzed by mixing different ratios of H_2O-PIPES and D_2O-PIPES from 0% to 100% deuterated buffer. The stock solution as well as the washed MDH had the same ratio of protiated to deuterated solvent. Protiated MeOH was used as substrate. 30 nM MDH were measured instead of 200 nM.

The substrate deuterium isotope effect was measured in H_2O-PIPES (assay mix, MDH) while different ratios of MeOH to d^3-MeOD (pre-mixed in safe lock tubes) were used to start the assay.

Analysis of the pH-Dependence of the KIE

Experiments were performed in 10 mM MC buffer (2.5 mM citric acid, 2.5 mM Bis-Tris, 2.5 mM Tris, 2.5 mM CHES) of different pH (ranging from pH 5.8 to 8.5). One assay mix was prepared for each pH value as described above. The MDH sample was washed in 10 mM MC pH 7.2. 100 µl assay mix, 10 µl $EuCl_3$ and 80 µl MDH in the respective MC buffer were added to the 96 well plate. The plate was incubated for 5 min at 45 °C before the measurement was started by adding 10 µl of 1 M MeOH or d^3-MeOD. The final concentrations in the well were: 200 nM MDH, 1 mM PES, 100 µM DCPIP, 20 µM $EuCl_3$ and 50 mM substrate.

Analysis of the Temperature-Dependence of the KIE

Experiments were performed in 10 mM MC buffer pH 7.2 (2.5 mM citric acid, 2.5 mM Bis-Tris, 2.5 mM Tris, 2.5 mM CHES). The assay mix was prepared in H_2O-buffer as described above and the MDH sample was washed in 10 mM MC pH 7.2. 100 µl assay mix, 10 µl $EuCl_3$, 50 µl MC buffer and 10 µl MeOH or d^3-MeOD were added to the 96 well plate. The plate was incubated for 2 min at the same temperature as the assay was performed at, ranging from 25 – 49 °C. The measurement was started by adding 30 µl of MDH in MC buffer. The final concentrations in the well were: 150 nM MDH, 1 mM PES, 100 µM DCPIP, 20 µM $EuCl_3$ and 50 mM substrate. The molar extinction coefficient of DCPIP in 10 mM MC pH 7.2 was determined at each temperature (Table S4) and used to calculate the SA.

Analysis of the PES-Dependence of the KIE

Experiments were performed in 20 mM PIPES pH 7.2 at 45 °C. One assay mix was prepared for each PES concentration (0.5 – 20 mM) and heated as described above. The MDH sample was washed in 20 mM PIPES pH 7.2. 100 µl of the respective assay mix, 10 µl $EuCl_3$ and 80 µl MDH in PIPES buffer were added to the 96 well plate. The plate was incubated for 5 min at 45 °C before the measurement was started by adding 10 µl of 1 M MeOH or d^3-MeOD. The final concentrations in the well were: 200 nM MDH, 100 µM DCPIP, 20 µM $EuCl_3$, 50 mM substrate and varied concentrations of PES.

Titration of GEE

Experiments were performed in 20 mM PIPES pH 7.2. The GEE stock solution was diluted in MilliQ water to different concentrations ranging from 0 – 100 mM. The assay mix was prepared as described above. 100 µl assay mix, 10 µl $EuCl_3$, 10 µl GEE and 70 µl MDH in PIPES buffer were added to the 96 well plate. The plate was incubated for 2 min at 45 °C before the measurement was started by adding 10 µl of 1 M MeOH or d^3-MeOD. The final concentrations in the well were: 200 nM MDH, 1 mM PES, 100 µM DCPIP, 20 µM $EuCl_3$, 50 mM substrate and varying concentrations of GEE.

6.2.3 AM1 MDH Assay – PMS vs. PES

AM1 MDH was kindly provided by the Group of Dr. N. C. Martinez-Gomez from the Michigan State University, East Lansing, MI, USA. MDH was both tested with and without polyhistidine-tag and this is indicated by U (untagged) or T (tagged), respectively. Measurements were performed at 30 °C in an Epoch2 microplate reader. 20 µl of 1 mM DCPIP, 20 µl of 10 mM PMS or PES, 10 µl of 1 M methanol and 100 mM multicomponent buffer pH 9 (consisting of 25 mM citric acid, 25 mM Bis-Tris, 25 mM Tris-HCl and 25 mM CHES) were mixed in a 96 well plate. The plate was incubated for 2 min at 30 °C in the dark. MDH was mixed with 6 µl of 500 mM NH_4Cl and buffer and was added to the assay mix in the plate to start the reaction. The final concentrations per well (200 µl) were: 100 nM MDH, 15 mM NH_4Cl, 50 mM MeOH, 100 µM DCPIP and 1 mM PMS or PES.
For the background control a 96 well plate was prepared as described above except that no MDH was added. The obtained values were path length corrected to 1 cm. For calculating the initial rate, the first 1 min of the slope was used.

6.3 WB Assay

Measurements were performed on an Epoch2 microplate reader at 30 °C and 610 nm. All assay steps were conducted under the exclusion of light. A 2 mM WB stock solution was prepared in MilliQ water as described above and was stored on ice until use. All other stock solutions were prepared in MilliQ water: 1 M methanol, 500 mM NH_4Cl, 20 mM metal. Two different buffers were used: 20 mM Tris-HCl pH 9 (AM1 MDH) and 100 mM multicomponent buffer pH 7.2 (SolV MDH) and pH 9 (AM1 MDH). The general procedure involved the following steps: 100 µl WB in the respective buffer (the concentration of WB was kept constant or was varied depending on the experiment type) and 10 µl 1 M methanol were added to a 96 well plate. The mixture was incubated for 2 min at 30 °C in the microplate reader. Meanwhile MDH was mixed with either NH_4Cl (AM1 MDH) or $EuCl_3$ (SolV MDH) and buffer and was then added to the assay mix to start the reaction. In the case of AM1 MDH the final assay mixture (200 µl) contained 100 nM MDH, 15 mM NH_4Cl, 200 µM WB and 50 mM methanol. For the assay with SolV MDH, 200 nM MDH, 20 µM $EuCl_3$, 200 µM WB and 50 mM methanol were used per well. The specific activity was calculated from the initial rates (slope of the first 30 s (AM1 MDH) or first 5 min (SolV MDH)) using the determined extinction coefficient for the given assay condition (pH, temperature, buffer system, Table S3). Since WB is a one-electron acceptor and two molecules of WB

are needed per molecule of MeOH, the SA was divided by two. The normalized WB SA was similar to the SA determined with PES/PMS.

Ammonia dependence studies were conducted as described above except that the NH_4Cl concentrations was varied.

7 Time-Resolved Laser-Induced Fluorescence Spectroscopy (TRLFS)

All experiments were conducted at the Helmholtz Zentrum Dresden Rossendorf (HZDR) together with Dr. R. Steudtner and Dr. B. Drobot. Measurements were performed in a 3 ml 1 cm-path length cuvette equipped with a screw-on cap at either room temperature (Chelex® and PIPES buffer experiment) or 4 °C (Eu^{3+} and La^{3+} titrations to MDH) with a pulsed Nd:YAG OPO laser system (Powerlite Precision II 9020 laser with a Green Panther EX OPO, Continuum Electro-Optics, San Jose, CA, USA) equipped with a multi-channel optical analysis system consisting of a Kymera 328i spectrograph and an Andor iStar ICCD camera (both Quantum Design GmbH, Darmstadt, Germany). An excitation wavelength of 394 nm was used. The luminescence spectra were recorded in the wavelength range from 500 to 760 nm (grating: 300 lines/mm with a resolution of 0.25 nm). To record the time-dependent luminescence spectra, the delay time between the laser pulse and camera control was sampled in dynamic time intervals (usually between 1 and 301 µs).

For the Chelex® experiment, a 2 mM $EuCl_3$ stock solution (prepared at the HZDR) was diluted to a concentration of 20 µM in MilliQ water that was either treated with Chelex® resin for 2 h or untreated. The pH of the sample was adjusted to either pH 5 or pH 7 using different acids (HCl, H_2SO_4) and NaOH.

For the PIPES titration experiment, two solutions were prepared: 20 µM $EuCl_3$ in MilliQ water pH 7 and 20 µM $EuCl_3$ in 20 mM PIPES pH 7. The pH was adjusted with HCl and NaOH. The solutions were mixed in different ratios and were subsequently analyzed.

For the Eu^{3+} titration experiment, all solutions were prepared in 100 mM NaCl pH 6.5 with added 1 mM MeOH. MDH was re-buffered twice in NaCl solution. The protein concentration was determined with a NanoDrop UV-visible spectrophotometer (Thermo Scientific, Waltham, MA, USA) using the MDH extinction coefficient (equation 4). A concentration of 10 µM MDH was used for the measurement. MDH was titrated with a 3 mM $EuCl_3$ solution in 100 mM NaCl pH 6.5 with 1 mM MeOH. The La^{3+} titration was performed in a similar way, except that MDH was saturated with 15 µM Eu^{3+} first, before a 3 mM $LaCl_3$ solution was added.

8 Isothermal Titration Calorimetry (ITC)

Measurements were performed on a MicroCal VP-ITC instrument (GE Healthcare, Chicago, IL, USA) at the HZDR together with Dr. B. Drobot. MDH was re-buffered twice in 100 mM NaCl pH 7 with 1 mM MeOH. Meanwhile solutions of 3 mM $LaCl_3$, $EuCl_3$ and $LuCl_3$ were prepared in the same medium as applied for re-buffering. The cell temperature was set to 8 °C. The sample chamber was filled with 2 ml of 30 µM MDH whereas the reference chamber contained MilliQ water. The syringe was filled with one of the 3 mM lanthanide solutions. The chambers were allowed to cool to the set temperature. The titration was performed in 28 injections with an injection volume of 10 µl (first injection volume was 5 µl). Data were processed with the VPViewer 2000 software (GE Healthcare, Chicago, IL, USA).

9 Synthesis of *N,N,N′,N′*-tetramethyl-p-phenylenediamine Perchlorate (Wurster's Blue)

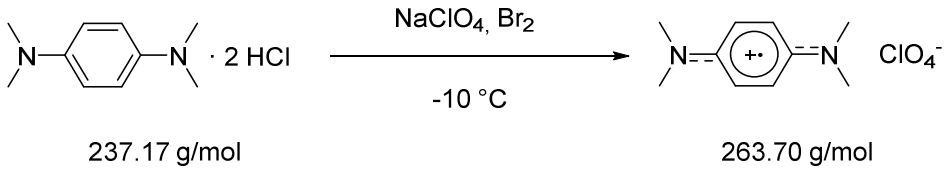

Scheme 9 Synthesis of Wurster's Blue as perchlorate salt using N,N,N',N'-tetramethyl-p-phenylenediamine dihydrochloride.

WB was synthesized according to a modified literature protocol (Scheme 9).[141] First, an aqueous sodium thiosulfate solution (1 M) was prepared for quenching residual or spilled bromine. In a round bottom flask equipped with a pressure equalizing dropping funnel *N,N,N′,N′*-tetramethyl-p-phenylenediamine dihydrochloride (1.0 g, 4.22 mmol) was dissolved in 18 ml MilliQ water at room temperature. A solution of sodium perchlorate (3.65 M in methanol, 28.0 ml, 12.5 g, 102.09 mmol) was added to the clear pale, pink-colored solution in the round bottom flask. Meanwhile, an aqueous bromine solution was prepared by dissolving 100 µl Br_2 in 32 ml of MilliQ water by stirring for about 15 min and was added to the dropping funnel. The flask was then cooled to - 10 °C using isopropanol and dry ice. While maintaining a bath temperature between - 9 °C and - 13 °C the bromine solution (0.063 M, 2.01 mmol) was added dropwise (approx. 1 drop/s) to the reaction mixture in the round bottom flask, gradually resulting in a deep blue solution and a blue precipitate. After warming to 10 °C, the precipitate was filtered off using a sintered glass frit (pore size 4) and washed twice with 10 ml ice-cold methanol and afterwards twice with 2 ml diethyl ether. The deep blue powder was dried *in vacuo* to yield the product (49%) as a blue powder which was shown to be the stable WB radical. Storage at room temperature under nitrogen showed no sign of degradation over weeks. Storage at room temperature for several months, however, is not recommended. Elemental microanalysis showed small impurities of sodium perchlorate, which can be removed by recrystallization via diethyl ether vapor diffusion into a methanolic solution of WB but will introduce additional traces of the MDH substrate methanol. **FT-IR spectroscopy**: $\tilde{\nu}$ = 1540, 1419, 1379, 1341, 1229, 1069, 975, 942, 825 cm^{-1}. **HR-MS (ESI +)**: calculated for $[C_{10}N_2H_{16}]^{\cdot+}$: 164.1314 m/z; found: 164.1308 m/z. **Elemental Analysis**: calculated for $[C_{10}N_2H_{16}]^{\cdot+}$ $[ClO_4]^-$: C 45.55, H 6.12, N 10.62; found: C 45.12, H 5.93, N 10.34.

10 Further Analytical Techniques

10.1 Inductively Coupled Plasma Optical Emission Spectroscopy (ICP-OES)

The metal content of *M. fumariolicum* SolV MDH was determined using ICP-OES at the LMU Munich. The ICP-OES measurements were conducted with a Varian Vista instrument (Palo Alto, CA, USA) with autosampler by J. Obel. MDH samples were digested in 3% nitric acid and heated at 90 °C before analysis.

10.2 Fourier Transform Infrared (FT-IR) Spectroscopy

IR measurements of PMS and PES samples were carried out on a Jasco FT-IR-460Plus (Tokyo, Japan) with an ATR diamond plate in the Group of Prof. Dr. P. Klüfers at the LMU Munich. The Spectra Manager II software version 2.06.00 was used for data processing.

10.3 Nuclear Magnetic Resonance (NMR) Spectroscopy

^{1}H-NMR spectra of formaldehyde, acetaldehyde and GEE were recorded by B. Breitenstein and C. Neumann at the LMU Munich. 1 M aldehyde solutions in MilliQ water and GEE dissolved in MilliQ water of pH 7.2 (at RT or heated for 10 min at 45 °C) were analyzed in D_2O. Spectra were measured at room temperature on an Avance III 400 MHz NMR spectrometer (Bruker, Billerica, MA, USA). Data were processed with the MestreNova software, version 12.0.0 (Mestrelab Research, Santiago de Compostela, Spain).

10.4 Mass Spectrometry (MS)

The synthesized WB compounds were analyzed by electrospray ionization mass spectrometry (ESI-MS). Measurements were performed by Dr. W. Spahl at the LMU, Munich. Spectra were recorded on a Finnigan LTQ FT Ultra Mass Spectrometer (Thermo Scientific, Waltham, MA, USA) using an acetonitrile/water mixture as carrier solvent.

10.5 Elemental Microanalysis

The composition of the synthesized WB compounds and that of the PMS and PES batches was analyzed using elemental microanalyses (C, H, N, S, Cl) at the LMU Munich. Measurements were performed on a vario EL cube (Elementar Analysensysteme, Langenselbold, Germany) by S. Ebert and R. Eicher.

References

V. References

1. Hanson, R. S. & Hanson, T. E. Methanotrophic Bacteria. *Microbiol. Rev.* **60**, 439–471 (1996).
2. IEA. Methane Tracker 2020. (2020) https://www.iea.org/reports/methane-tracker-2020 accessed: 5 May 2020.
3. Kwon, M. *et al.* Novel approaches and reasons to isolate methanotrophic bacteria with biotechnological potentials: recent achievements and perspectives. *Appl. Microbiol. Biotechnol.* **103**, 1–8 (2019).
4. Park, S. & Kim, C. Application and development of methanotrophs in environmental engineering. *J. Mater. Cycles Waste Manag.* **21**, 415–422 (2019).
5. Muenmee, S. *et al.* Microbial consortium involving biological methane oxidation in relation to the biodegradation of waste plastics in a solid waste disposal open dump site. *Int. Biodeterior. Biodegrad.* **102**, 172–181 (2015).
6. Lu, X. *et al.* Methylmercury uptake and degradation by methanotrophs. *Sci. Adv.* **3**, e1700041 (2017).
7. Jahng, D. & Wood, T. K. Trichloroethylene and Chloroform Degradation by a Recombinant Pseudomonad Expressing Soluble Methane Monooxygenase from *Methylosinus trichosporium* OB3b. *Appl. Environ. Microbiol.* **60**, 2473–2482 (1994).
8. Lee, S. W. *et al.* Mixed Pollutant Degradation by *Methylosinus trichosporium* OB3b Expressing either Soluble or Particulate Methane Monooxygenase: Can the Tortoise Beat the Hare? *Appl. Environ. Microbiol.* **72**, 7503–7509 (2006).
9. Semrau, J. D. Bioremediation via methanotrophy: overview of recent findings and suggestions for future research. *Front. Microbiol.* **2**, 1–7 (2011).
10. Wendlandt, K. D. *et al.* Producing poly-3-hydroxybutyrate with a high molecular mass from methane. *J. Biotechnol.* **86**, 127–133 (2001).
11. Anthony, C. *The Biochemistry of Methylotrophs*. (Academic Press, London, UK, 1982).
12. Ochsner, A. M. *et al. Methylobacterium extorquens*: methylotrophy and biotechnological applications. *Appl. Microbiol. Biotechnol.* **99**, 517–534 (2015).
13. Söhngen, N. L. Über Bakterien, welche Methan als Kohlenstoffnahrung und Energiequelle gebrauchen. *Zbl. Bakt., II. Abt.* **15**, 513–517 (1906).
14. Anthony, C. How half a century of research was required to understand bacterial growth on C1 and C2 compounds; the story of the serine cycle and the ethylmalonyl-CoA pathway. *Sci. Prog.* **94**, 109–137 (2011).

15. Wendlandt, K. D. *et al.* The potential of methane-oxidizing bacteria for applications in environmental biotechnology. *Eng. Life Sci.* **10**, 87–102 (2010).
16. Pieja, A. J. *et al.* Methane to bioproducts: the future of the bioeconomy? *Curr. Opin. Chem. Biol.* **41**, 123–131 (2017).
17. Whittenbury, R. *et al.* Enrichment, Isolation and Some Properties of Methane-utilizing Bacteria. *J. Gen. Microbiol.* **61**, 205–218 (1970).
18. Ross, M. O. & Rosenzweig, A. C. A tale of two methane monooxygenases. *J. Biol. Inorg. Chem.* **22**, 307–319 (2017).
19. Kalyuzhnaya, M. G. Methane Biocatalysis: Selecting the Right Microbe in *Biotechnology for Biofuel Production and Optimization* (eds. Eckert, C. A. & Trinh, C. T.) 353–383 (Elsevier Science & Technology, Oxford, UK, 2016).
20. Hou, S. *et al.* Complete genome sequence of the extremely acidophilic methanotroph isolate V4, *Methylacidiphilum infernorum*, a representative of the bacterial phylum Verrucomicrobia. *Biol. Direct* **3**, 26 (2008).
21. van Teeseling, M. C. F. *et al.* Expanding the Verrucomicrobial Methanotrophic World: Description of Three Novel Species of *Methylacidimicrobium* gen. nov. *Appl. Environ. Microbiol.* **80**, 6782–6791 (2014).
22. Islam, T. *et al.* Methane oxidation at 55°C and pH 2 by a thermoacidophilic bacterium belonging to the Verrucomicrobia phylum. *Proc. Natl. Acad. Sci. USA* **105**, 300–304 (2008).
23. Dunfield, P. F. *et al.* Methane oxidation by an extremely acidophilic bacterium of the phylum Verrucomicrobia. *Nature* **450**, 879–882 (2007).
24. Maret, W. The Metals in the Biological Periodic System of the Elements: Concepts and Conjectures. *Int. J. Mol. Sci.* **17**, 66 (2016).
25. Ainscough, E. W. & Brodie, A. M. The Role of Metal Ions in Proteins and other Biological Molecules. *J. Chem. Educ.* **53**, 156–158 (1976).
26. Semrau, J. D. *et al.* Metals and Methanotrophy. *Appl. Environ. Microbiol.* **84**, e02289-17 (2018).
27. Lieberman, R. L. & Rosenzweig, A. C. Crystal structure of a membrane-bound metalloenzyme that catalyses the biological oxidation of methane. *Nature* **434**, 177–182 (2005).
28. Sirajuddin, S. & Rosenzweig, A. C. Enzymatic Oxidation of Methane. *Biochemistry* **54**, 2283–2294 (2015).
29. Murrell, J. C. *et al.* Regulation of expression of methane monooxygenases by copper ions. *Trends Microbiol.* **8**, 221–225 (2000).

30. Anthony, C. Methanol Dehydrogenase, a PQQ-Containing Quinoprotein Dehydrogenase in *Enzyme-Catalyzed Electron and Radical Transfer. Subcellular Biochemistry* (eds. Holzenburg, A. & Scrutton, N. S.) vol. 35, 73–117 (Springer US, Boston, MA, USA, 2000).
31. Hibi, Y. *et al.* Molecular structure of La^{3+}-induced methanol dehydrogenase-like protein in *Methylobacterium radiotolerans*. *J. Biosci. Bioeng.* **111**, 547–549 (2011).
32. Vu, H. N. *et al.* Lanthanide-Dependent Regulation of Methanol Oxidation Systems in *Methylobacterium extorquens* AM1 and Their Contribution to Methanol Growth. *J. Bacteriol.* **198**, 1250–1259 (2016).
33. Farhan Ul Haque, M. *et al.* Cerium Regulates Expression of Alternative Methanol Dehydrogenases in *Methylosinus trichosporium* OB3b. *Appl. Environ. Microbiol.* **81**, 7546–7552 (2015).
34. Ramos, S. J. *et al.* Rare Earth Elements in the Soil Environment. *Curr. Pollut. Reports* **2**, 28–50 (2016).
35. Cotton, S. *Lanthanide and Actinide Chemistry*. (John Wiley & Sons, Ltd., Chichester, UK, 2006).
36. Cheisson, T. & Schelter, E. J. Rare earth elements: Mendeleev's bane, modern marvels. *Science* **363**, 489–493 (2019).
37. Emsley, J. *Nature's Building Blocks: An A-Z Guide to the Elements*. (Oxford University Press, Oxford, UK, 2001).
38. Meier, H. *et al.* Zum Vorkommen von Promethium in der Natur. *Z. Naturforsch.* **25a**, 1945–1954 (1970).
39. Evans, C. H. Interesting and useful biochemical properties of lanthanides. *Trends Biochem. Sci.* **8**, 445–449 (1983).
40. Evans, C. H. *Biochemistry of the Lanthanides*. (Springer US, New York City, NY, USA, 1990).
41. Fricker, S. P. The therapeutic application of lanthanides. *Chem. Soc. Rev.* **35**, 524–533 (2006).
42. Lim, S. & Franklin, S. J. Lanthanide-binding peptides and the enzymes that Might Have Been. *Cell. Mol. Life Sci.* **61**, 2184–2188 (2004).
43. Ganguli, R. & Cook, D. R. Rare earths: A review of the landscape. *MRS Energy Sustain.* **5**, 1–16 (2018).
44. Cotton, S. A. & Harrowfield, J. M. *Lanthanides in Living systems*. *Encyclopedia of Inorganic and Bioinorganic Chemistry* (John Wiley & Sons, Ltd., Chichester, UK, 2012).
45. Jahn, B. & Daumann, L. J. Weder Erden noch selten: Die faszinierende bioanorganische Chemie der Selten-Erd-Elemente. *Chemie Unserer Zeit* **52**, 150–158 (2018).

46. National Comission on the BP Deepwater Horizon Oil Spill and Offshore Drilling. *Deep Water: The Gulf Oil Disaster And The Future Of Offshore Drilling - Report to the President (BP Oil Spill Commission Report)* (2011).
47. Shiller, A. M. *et al.* Light rare earth element depletion during Deepwater Horizon blowout methanotrophy. *Sci. Rep.* **7**, 1–9 (2017).
48. Kessler, J. D. *et al.* A Persistent Oxygen Anomaly Reveals the Fate of Spilled Methane in the Deep Gulf of Mexico. *Science* **331**, 312–315 (2011).
49. Pol, A. *et al.* Rare earth metals are essential for methanotrophic life in volcanic mudpots. *Environ. Microbiol.* **16**, 255–264 (2014).
50. Hektor, H. J. *et al.* Nicotinoprotein methanol dehydrogenase enzymes in Gram-positive methylotrophic bacteria. *J. Mol. Catal. B Enzym.* **8**, 103–109 (2000).
51. Ozimek, P. *et al.* Alcohol oxidase: A complex peroxisomal, oligomeric flavoprotein. *FEMS Yeast Res.* **5**, 975–983 (2005).
52. Duine, J. A. *et al.* PQQ and quinoprotein enzymes in microbial oxidations. *FEMS Microbiol. Rev.* **32**, 165–178 (1986).
53. Anthony, C. & Zatman, L. J. Microbial Oxidation of Methanol. 2. The Methanol-Oxidizing Enzyme of *Pseudomonas* sp. M27. *Biochem. J.* **92**, 614–621 (1964).
54. Chistoserdova, L. Modularity of methylotrophy, revisited. *Environ. Microbiol.* **13**, 2603–2622 (2011).
55. Chistoserdova, L. *et al.* Methylotrophy in *Methylobacterium extorquens* AM1 from a Genomic Point of View. *J. Bacteriol.* **185**, 2980–2987 (2003).
56. Cox, J. M. *et al.* The interaction of methanol dehydrogenase and its electron acceptor, cytochrome c_L in methylotrophic bacteria. *Biochim. Biophys. Acta* **1119**, 97–106 (1992).
57. Harms, N. *et al.* Genetics of C1 metabolism regulation in *Paracoccus dentrificans* in *Microbial Growth on C1 Compounds* (ed. Lidstrom M. E. & Tabita F. R.) 126–132 (Springer Netherlands, Dodrecht, NL, 1996).
58. Skovran, E. *et al.* XoxF Is Required for Expression of Methanol Dehydrogenase in *Methylobacterium extorquens* AM1. *J. Bacteriol.* **193**, 6032–6038 (2011).
59. Chistoserdova, L. Lanthanides: New life metals? *World J. Microbiol. Biotechnol.* **32**, 1–7 (2016).
60. Huang, J. *et al.* Lanthanide-Dependent Methanol Dehydrogenases of XoxF4 and XoxF5 Clades are Differentially Distributed Among Methylotrophic Bacteria and They Reveal Different Biochemical Properties. *Front. Microbiol.* **9**, 1366 (2018).
61. Keltjens, J. T. *et al.* PQQ-dependent methanol dehydrogenases: rare-earth elements make a difference. *Appl. Microbiol. Biotechnol.* **98**, 6163–6183 (2014).

62. Giovannoni, S. J. *et al.* The small genome of an abundant coastal ocean methylotroph. *Environ. Microbiol.* **10**, 1771–1782 (2008).

63. Beck, D. A. C. *et al.* A metagenomic insight into freshwater methane-utilizing communities and evidence for cooperation between the *Methylococcaceae* and the *Methylophilaceae*. *PeerJ* **1**, e23 (2013).

64. Delmotte, N. *et al.* Community proteogenomics reveals insights into the physiology of phyllosphere bacteria. *Proc. Natl. Acad. Sci. USA* **106**, 16428–16433 (2009).

65. Skovran, E. & Martinez-Gomez, N. C. Just add lanthanides. *Science* **348**, 862–863 (2015).

66. Sharp, C. E. *et al.* Distribution and diversity of *Verrucomicrobia* methanotrophs in geothermal and acidic environments. *Environ. Microbiol.* **16**, 1867–1878 (2014).

67. Op den Camp, H. J. M. *et al.* Environmental, genomic and taxonomic perspectives on methanotrophic *Verrucomicrobia*. *Environ. Microbiol. Rep.* **1**, 293–306 (2009).

68. Pol, A. *et al.* Methanotrophy below pH 1 by a new Verrucomicrobia species. *Nature* **450**, 874–878 (2007).

69. Featherston, E. R. *et al.* Biochemical and structural characterization of XoxG and XoxJ and their roles in lanthanide-dependent methanol dehydrogenase activity. *ChemBioChem* **20**, 2360 – 2372 (2019).

70. Versantvoort, W. *et al.* Characterization of a novel cytochrome c_{GJ} as the electron acceptor of XoxF-MDH in the thermoacidophilic methanotroph *Methylacidiphilum fumariolicum* SolV. *Biochim. Biophys. Acta - Proteins Proteomics* **1867**, 595–603 (2019).

71. Jahn, B. *et al.* Similar but not the same: First Kinetic and Structural Analyses of a Methanol Dehydrogenase Containing a Europium Ion in the Active Site. *ChemBioChem* **19**, 1147–1153 (2018).

72. Deng, Y. W. *et al.* Structure and Function of the Lanthanide-Dependent Methanol Dehydrogenase XoxF From the Methanotroph *Methylomicrobium buryatense* 5GB1C. *J. Biol. Inorg. Chem.* **23**, 1037–1047 (2018).

73. Good, N. M. *et al.* Lanthanide-dependent Alcohol Dehydrogenases Require an Essential Aspartate Residue for Metal Coordination and Enzymatic Function. *J. Biol. Chem.* **295**, 8272–8284 (2020).

74. Leopoldini, M. *et al.* The Preferred Reaction Path for the Oxidation of Methanol by PQQ-Containing Methanol Dehydrogenase: Addition-Elimination versus Hydride-Transfer Mechanism. *Chem. Eur. J.* **13**, 2109–2117 (2007).

75. McSkimming, A. *et al.* Functional Synthetic Model for the Lanthanide-Dependent Quinoid Alcohol Dehydrogenase Active Site. *J. Am. Chem. Soc.* **140**, 1223–1226 (2018).

76. Daumann, L. Essential and Ubiquitous: The Emergence of Lanthanide Metallobiochemistry. *Angew. Chemie Int. Ed.* **58**, 12795 –12802 (2019).

77. Good, N. M. *et al.* Contrasting in vitro and in vivo methanol oxidation activities of lanthanide-dependent alcohol dehydrogenases XoxF1 and ExaF from *Methylobacterium extorquens*. *Sci. Rep.* **9**, 4248 (2019).

78. Martinez-Gomeza, N. C. & Skovran, E. Metals in Methanotrophy in *Methane Biocatalysis: Paving the Way to Sustainability* (eds. Kalyuzhnaya, M. G. & Xing, X.-H.) 67–82 (Springer International Publishing, Cham, CH, 2018).

79. Horiike, T. & Yamashita, M. A New Fungal Isolate, *Penidiella* sp. Strain T9, Accumulates the Rare Earth Element Dysprosium. *Appl. Environ. Microbiol.* **81**, 3062–3068 (2015).

80. Ochsner, A. M. *et al.* Use of rare-earth elements in the phyllosphere colonizer *Methylobacterium extorquens* PA1. *Mol. Microbiol.* **111**, 1152–1166 (2019).

81. Cotruvo, J. A. *et al.* Lanmodulin: A Highly Selective Lanthanide-Binding Protein from a Lanthanide-Utilizing Bacterium. *J. Am. Chem. Soc.* **140**, 15056–15061 (2018).

82. Anthony, C. The quinoprotein dehydrogenases for methanol and glucose. *Arch. Biochem. Biophys.* **428**, 2–9 (2004).

83. Fitriyanto, N. A. *et al.* Molecular structure and gene analysis of Ce^{3+}-induced methanol dehydrogenase of *Bradyrhizobium* sp. MAFF211645. *J. Biosci. Bioeng.* **111**, 613–617 (2011).

84. Nakagawa, T. *et al.* A Catalytic Role of XoxF1 as La^{3+}-Dependent Methanol Dehydrogenase in *Methylobacterium extorquens* Strain AM1. *PLoS One* **7**, 1–7 (2012).

85. Chistoserdova, L. & Lidstrom, M. E. Molecular and mutational analysis of a DNA region separating two methylotrophy gene clusters in *Methylobacterium extorquens* AM1. *Microbiology* **143**, 1729–1736 (1997).

86. Bulheller, B. M. & Hirst, J. D. DichroCalc - Circular and linear dichroism online. *Bioinformatics* **25**, 539–540 (2009).

87. PDB database: 4MAE. https://www.rcsb.org/structure/4MAE accessed: 20 April 2020.

88. Chen, Y. H. *et al.* Determination of the Helix and ß Form of Proteins in Aqueous Solution by Circular Dichroism. *Biochemistry* **13**, 3350–3359 (1974).

89. Greenfield, N. J. Using circular dichroism spectra to estimate protein secondary structure. *Nat. Protoc.* **1**, 2876–2890 (2006).

90. Picone, N. & Op den Camp, H. J. M. Role of rare earth elements in methanol oxidation. *Curr. Opin. Chem. Biol.* **49C**, 39–44 (2019).

91. Good, N. M. *et al.* Pyrroloquinoline Quinone Ethanol Dehydrogenase in *Methylobacterium extorquens* AM1 Extends Lanthanide-Dependent Metabolism to Multicarbon Substrates. *J. Bacteriol.* **198**, 3109–3118 (2016).
92. Goodwin, M. G. & Anthony, C. Characterization of a novel methanol dehydrogenase containing a Ba^{2+} ion at the active site. *Biochem. J.* **318**, 673–679 (1996).
93. Goodwin, M. G. *et al.* Reconstitution of the quinoprotein methanol dehydrogenase from inactive Ca^{2+}-free enzyme with Ca^{2+}, Sr^{2+} or Ba^{2+}. *Biochem. J.* **319**, 839–842 (1996).
94. Duine, J. A. *et al.* Enzymology of Quinoproteins in *Advances in Enzymology and Related Areas of Molecular Biology, Volume 59* (ed. Meister, A.) 169–212 (John Wiley & Sons, Inc., New York City, NY, USA, 1987).
95. Cotton, S. A. & Raithby, P. R. Systematics and surprises in lanthanide coordination chemistry. *Coord. Chem. Rev.* **340**, 220–231 (2017).
96. Beardmore-Gray, M. *et al.* The Methanol: Cytochrome c Oxidoreductase Activity of Methylotrophs. *J. Gen. Microbiol.* **129**, 923–933 (1983).
97. Hothi, P. *et al.* Kinetic isotope effects and ligand binding in PQQ-dependent methanol dehydrogenase. *Biochem. J.* **388**, 123–133 (2005).
98. Duine, J. A. & Frank, J. Studies on Methanol Dehydrogenase from *Hyphomicrobium* X. Isolation of an oxidized form of the enzyme. *Biochem. J.* **187**, 213–219 (1980).
99. Tsushima, S. Lanthanide-induced conformational change of methanol dehydrogenase involving coordination change of cofactor pyrroloquinoline quinone. *Phys. Chem. Chem. Phys.* **21**, 21979–21983 (2019).
100. Jordan, N. *et al.* Complexation of Trivalent Lanthanides (Eu) and Actinides (Cm) with Aqueous Phosphates at Elevated Temperatures. *Inorg. Chem.* **57**, 7015–7024 (2018).
101. Good, N. E. *et al.* Hydrogen Ion Buffers for Biological Research. *Biochemistry* **5**, 467–477 (1966).
102. Day, D. J. & Anthony, C. Methanol Dehydrogenase from *Methylobacterium extorquens* AM1. **188**, 210–216 (1990).
103. Dales, S. L. & Anthony, C. The interaction of methanol dehydrogenase and its cytochrome electron acceptor. *Biochem. J.* **312**, 261–265 (1995).
104. Kalimuthu, P. *et al.* Electrocatalysis of a Europium-Dependent Bacterial Methanol Dehydrogenase with its Physiological Electron Acceptor Cytochrome c_{GJ}. *Chem. – A Eur. J.* **25**, 8760–8768 (2019).
105. Dijkstra, M. *et al.* Studies on electron transfer from methanol dehydrogenase to cytochrome c_L, both purified from *Hyphomicrobium* X. *Biochem. J.* **257**, 87–94 (1989).

106. Anthony, C. Bacterial Oxidation of Methane and Methanol in *Advances in Microbial Physiology, Volume 27* (eds. Rose, A. H. & Tempest, D. W.) 113–210 (Academic Press, London, UK, 1986).

107. Frank, J. & Duine, J. A. Methanol Dehydrogenase from *Hyphomicrobium* X. *Methods Enzymol.* **188**, 202–209 (1990).

108. Armstrong, J. M. The molar extinction coefficient of 2,6-dichlorophenol indophenol. *Biochim. Biophys. Acta* **86**, 194–197 (1964).

109. Frank, J. *et al.* Kinetic and spectral studies on the redox forms of methanol dehydrogenase from *Hyphomicrobium* X. *Eur. J. Biochem.* **174**, 331–338 (1988).

110. Duine, J. A. *et al.* Purification and Properties of Methanol dehydrogenase from *Hyphomicrobium* X. *Biochim. Biophys. Acta* **524**, 277–287 (1978).

111. Duine, J. A. *et al.* Glucose Dehydrogenase from *Acinetobacter calcoaceticus*: A 'Quinoprotein'. *FEBS Lett.* **108**, 443–446 (1979).

112. Chistoserdova, L. & Kalyuzhnaya, M. G. Current Trends in Methylotrophy. *Trends Microbiol.* **26**, 703–714 (2018).

113. Anthony, C. & Zatman, L. J. The microbial oxidation of methanol. Purification and properties of the alcohol dehydrogenase of Pseudomonas sp. M27. *Biochem. J.* **104**, 953–959 (1967).

114. Zheng, Y. *et al.* Physiological Effect of XoxG(4) on Lanthanide-Dependent Methanotrophy. *mBio* **9**, e02430-17 (2018).

115. Huang, J. *et al.* Rare earth element alcohol dehydrogenases widely occur among globally distributed, numerically abundant and environmentally important microbes. *ISME J.* **13**, 2005–2017 (2019).

116. Melin, A. D. & Lohmeier-Vogel, E. M. Using Cytochome C to Monitor Electron Transport and Inhibition in Beef Heart Submitochondrial Particles. *Biochem. Mol. Biol. Educ.* **32**, 39–44 (2004).

117. Hollywood, K. A. *et al.* Monitoring the Succinate Dehydrogenase Activity Isolated from Mitochondria by Surface Enhanced Raman Scattering. *J. Phys. Chem. Part C* **114**, 7308–7313 (2010).

118. VanderJagt, D. J. *et al.* Ascorbate in Plasma as Measured by Liquid Chromatography and by Dichlorophenolindophenol Colorimetry. *Clin. Chem.* **32**, 1004–1006 (1986).

119. Dawson, R. M. C. *et al. Data for Biochemical Research (third edition)* (Oxford Science Publications, Oxford, UK, 1986).

120. Bessey, O. A. & King, G. The Distribution of Vitamin C in Plant and Animal Tissues, and Its Determination. *J. Biol. Chem.* **103**, 687–698 (1933).

121. Konidari, C. N. *et al.* Kinetic and mechanistic study of the reaction of 2,6-dichlorophenol-indophenol and cysteine. *Talanta* **39**, 863–868 (1992).

122. Naumann, R. *et al.* Voltammetric measurements of the kinetics of enzymatic reduction of 2,6-dichlorophenolindophenol in normal and neoplastic hepatocytes using glucose as substrate. *Biochim. Biophys. Acta* **847**, 96–100 (1985).

123. Fukada, H. & Takahashi, K. Enthalpy and heat capacity changes for the proton dissociation of various buffer components in 0.1 M potassium chloride. *Proteins Struct. Funct. Genet.* **33**, 159–166 (1998).

124. Grady, J. K. *et al.* Radicals from 'Good's' buffers. *Anal. Biochem.* **173**, 111–115 (1988).

125. Hoffman, E. A. *et al.* Formaldehyde Crosslinking: A Tool for the Study of Chromatin Complexes. *J. Biol. Chem.* **290**, 26404–26411 (2015).

126. Wu, C. H. *et al.* Sequence-Specific Capture of Protein-DNA Complexes for Mass Spectrometric Protein Identification. *PLoS One* **6**, e26217 (2011).

127. Ferreira, C. M. H. *et al.* (Un)suitability of the use of pH buffers in biological, biochemical and environmental studies and their interaction with metal ions - a review. *RSC Adv.* **5**, 30989–31003 (2015).

128. El-Roudi, O. M. *et al.* Potentiometric Studies on the Binary Complexes of N-[Tris(hydroxymethyl)methyl]glycine with Th^{4+}, Ce^{3+}, La^{3+}, and UO_2^{2+} and Medium Effects on a Th-Tricine Binary Complex. *J. Chem. Eng. Data* **42**, 609–613 (1997).

129. Ghosh, R. & Quayle, J. R. Phenazine Ethosulfate as a Preferred Electron Acceptor to Phenazine Methosulfate in Dye-Linked Enzyme Assays. *Anal. Biochem.* **99**, 112–117 (1979).

130. Wu, M. L. *et al.* XoxF-Type Methanol Dehydrogenase from the Anaerobic Methanotroph "*Candidatus* Methylomirabilis oxyfera". *Appl. Environ. Microbiol.* **81**, 1442–1451 (2015).

131. King, T. E. Reconstitution of Respiratory Chain Enzyme Systems. XI. Use of Artificial Electron Acceptors in the Assay of Succinate-Dehydrogenase Enzymes. *J. Biol. Chem.* **238**, 4032–4036 (1963).

132. Hester, R. E. & Williams, K. P. J. Free radical studies by resonance Raman spectroscopy. The 5,10-dihydrophenazine and 5-methyl-10-hydrophenazine radical cations. *J. Raman Spectrosc.* **13**, 91–95 (1982).

133. Harris, T. K. & Davidson, V. L. A New Kinetic Model for the Steady-State Reactions of the Quinoprotein Methanol Dehydrogenase from *Paracoccus denitrificans*. *Biochemistry* **32**, 4362–4368 (1993).

134. Dijkstra, M. *et al.* Methanol oxidation under physiological conditions using methanol dehydrogenase and a factor isolated from *Hyphomicrobium* X. *FEBS Lett.* **227**, 198–202 (1988).

135. Endres, H. *et al.* Crystal and Molecular Structure of Bis(N,N,N',N'-tetramethyl-1,4-diaminobenzeniumyl) [Wurster's Blue Cation]-tetracyanoplatinate(II)-mono-hydrate. *Z. Naturforsch. B* **34**, 140–144 (1979).

136. Steigman, J. & Cronkright, W. Formation of Wurster's blue in benzene at 25 deg. *J. Am. Chem. Soc.* **92**, 6736–6743 (1970).

137. Steigman, J. & Cronkrigh, W. Acid-base reactions of N,N,N',N'-tetramethyl-p-phenylenediamine with carboxylic acids in benzene at 25 deg. *J. Am. Chem. Soc.* **92**, 6729–6736 (1970).

138. Franzen, V. N,N,N',N'-Tetraäthyl-p-phenylendiamin zum Nachweis kurzlebiger organischer radikale in Lösung. *Chem. Ber.* **88**, 1697–1703 (1955).

139. Sakata, T. & Nagakura, S. Spectroscopic Behavior of Würster's Blue Perchlorate and N-Ethylphenazyl Crystals. *Bull. Chem. Soc. Jpn.* **42**, 1497–1503 (1969).

140. Michaelis, L. *et al.* The Free Radicals of the Type of Wurster's Salts. *J. Am. Chem. Soc.* **61**, 1981–1992 (1939).

141. Michaelis, L. & Granick, S. The Polymerization of the Free Radicals of the Wurster Dye Type: The Dimeric Resonance Bond. *J. Am. Chem. Soc.* **65**, 1747–1755 (1943).

142. Albrecht, A. C. & Simpson, W. T. Spectroscopic Study of Wurster's Blue and Tetramethyl-p-phenylenediamine with Assignments of Electronic Transitions. *J. Am. Chem. Soc.* **77**, 4454–4461 (1955).

143. Hothi, P. *et al.* Effects of Multiple Ligand Binding on Kinetic Isotope Effects in PQQ-dependent Methanol Dehydrogenase. *Biochemistry* **42**, 3966–3978 (2003).

144. Reddy, S. Y. & Bruice, T. C. Mechanisms of ammonia activation and ammonium ion inhibition of quinoprotein methanol dehydrogenase: A computational approach. *Proc. Natl. Acad. Sci. USA* **101**, 15887–15892 (2004).

145. Jahn, B. *et al.* Understanding the chemistry of the artificial electron acceptors PES, PMS, DCPIP and Wurster's Blue in methanol dehydrogenase assays. *J. Biol. Inorg. Chem.* **25**, 199–212 (2020).

146. McIlwain, H. The phenazine series. Part VI. Reactions of alkyl phenazonium salts; the phenazyls. *J. Chem. Soc.* 1704–1711 (1937).

147. Arun, P. *et al.* Rapid sodium cyanide depletion in cell culture media: Outgassing of hydrogen cyanide at physiological pH. *Anal. Biochem.* **339**, 282–289 (2005).

148. Yamagiwa, T. *et al.* A Stable *in Vitro* Method for Assessing the Toxicity of Potassium Cyanide and Its Antidote. *Tokai J. Exp. Clin. Med.* **38**, 114–122 (2013).

149. Mostafa, A. M. *et al.* Renal metabolism of acrylonitrile to cyanide: *In vitro* studies. *Pharmacol. Res.* **40**, 195–200 (1999).

150. Anthony, C. The c-type cytochromes of methylotrophic bacteria. *Biochtmica Biophys. Acta,* **1099**, 1–15 (1992).

151. Wehrmann, M. *et al.* Functional Role of Lanthanides in Enzymatic Activity and Transcriptional Regulation of Pyrroloquinoline Quinone-Dependent Alcohol Dehydrogenases in *Pseudomonas putida* KT2440. *mBio* **8**, 1–14 (2017).

152. Daumann, L. J. *et al.* Promiscuity comes at a price: Catalytic versatility vs efficiency in different metal ion derivatives of the potential bioremediator GpdQ. *Biochim. Biophys. Acta - Proteins Proteomics* **1834**, 425–432 (2013).

153. Xiao, Z. & Wedd, A. G. The challenges of determining metal-protein affinities. *Nat. Prod. Rep.* **27**, 768–789 (2010).

154. Sule, N. *et al.* Probing the metal ion selectivity in methionine aminopeptidase via changes in the luminescence properties of the enzyme bound europium ion. *J. Inorg. Biochem.* **106**, 84–89 (2012).

155. Masuda, S. *et al.* Lanthanide-Dependent Regulation of Methylotrophy in *Methylobacterium aquaticum* Strain 22A. *mSphere* **3**, e00462-17 (2018).

156. Seitz, M. *et al.* The Lanthanide Contraction Revisited. *J. Am. Chem. Soc.* **129**, 11153–11160 (2007).

157. Shannon, R. D. Revised Effective Ionic Radii and Systematic Studies of Interatomic Distances in Halides and Chalcogenides. *Acta Crystallogr.* **A32**, 751–767 (1976).

158. Harris, T. K. & Davidson, V. L. Replacement of enzyme-bound calcium with strontium alters the kinetic properties of methanol dehydrogenase. *Biochem. J.* **300**, 175–182 (1994).

159. Schmitz, R. A. *et al.* The thermoacidophilic methanotroph *Methylacidiphilum fumariolicum* SolV oxidizes subatmospheric H_2 with a high-affinity, membrane-associated [NiFe] hydrogenase. *ISME J.* **14**, 1223–1232 (2020).

160. Collins, R. N. *et al.* Applications of Time-Resolved Laser Fluorescence Spectroscopy to the Environmental Biogeochemistry of Actinides. *J. Environ. Qual.* **40**, 731–741 (2011).

161. Stumpf, T. & Fanghänel, T. A Time-Resolved Laser Fluorescence Spectroscopy (TRLFS) Study of the Interaction of Trivalent Actinides (Cm(III)) with Calcite. *J. Colloid Interface Sci.* **249**, 119–122 (2002).

162. Bader, M. *et al.* Association of Eu(III) and Cm(III) onto an extremely halophilic archaeon. *Environ. Sci. Pollut. Res.* **26**, 9352–9364 (2019).

163. Richter, C. *et al.* Macroscopic and spectroscopic characterization of uranium(VI) sorption onto orthoclase and muscovite and the influence of competing Ca^{2+}. *Geochim. Cosmochim. Acta* **189**, 143–157 (2016).

164. Moulin, C. *et al.* Europium complexes investigations in natural waters by time-resolved laser-induced fluorescence. *Anal. Chim. Acta* **396**, 253–261 (1999).

165. Binnemans, K. Interpretation of europium(III) spectra. *Coord. Chem. Rev.* **295**, 1–45 (2015).

166. Horrocks, W. D. & Sudnick, D. R. Time-Resolved Europium(III) Excitation Spectroscopy: A Luminescence Probe of Metal Ion Binding Sites. *Science* **206**, 1194–1197 (1979).

167. Bowen, L. M. *et al.* Lanthanide spectroscopic studies of the dinuclear and Mg(II)-dependent *Pvu*II restriction endonuclease. *Biochemistry* **43**, 15286–15292 (2004).

168. Frey, M. W. *et al.* Elucidation of the metal-binding properties of the Klenow fragment of *Escherichia coli* polymerase I and bacteriophage T4 DNA polymerase by lanthanide(III) luminescence spectroscopy. *Chem. Biol.* **3**, 393–403 (1996).

169. Feig, A. L. *et al.* Probing the binding of Tb(III) and Eu(III) to the hammerhead ribozyme using luminescence spectroscopy. *Chem. Biol.* **6**, 801–810 (1999).

170. Rhee, M. J. *et al.* Laser-induced lanthanide luminescence as a probe of metal ion-binding sites of human Factor Xa. *J. Biol. Chem.* **259**, 7404–7408 (1984).

171. Martinez-Gomez, N. C. *et al.* Lanthanide Chemistry: From Coordination in Chemical Complexes Shaping Our Technology to Coordination in Enzymes Shaping Bacterial Metabolism. *Inorg. Chem.* **55**, 10083–10089 (2016).

172. Chikkamath, S. *et al.* Sorption of Eu(III) on Fe-montmorillonite relevant to geological disposal of HLW. *Radiochim. Acta* **106**, 971–983 (2018).

173. Raj, D. B. A. *et al.* Highly Luminescent Poly(Methyl Methacrylate)-Incorporated Europium Complex Supported by a Carbazole-Based Fluorinated β-Diketonate Ligand and a 4,5-Bis(diphenylphosphino)-9,9-dimethylxanthene Oxide Co-Ligand. *Inorg. Chem.* **49**, 9055–9063 (2010).

174. Song, L. *et al.* Fluorescence Quenching of a Europium Coordination Compound for the Detection of Trace Amounts of Water: Uncovering the Response Mechanism by Structural Confirmation. *Eur. J. Inorg. Chem.* 2264–2271 (2015).

175. Brown, M. A. *et al.* Aqueous Complexation and Interactions of Selected Trivalent Lanthanides With Citric Acid at Varying Ionic Strengths in *Actinide and Fission Product Partitioning and Transmutation* (OECD) (2012).

176. Blanchard, J. S. Buffers for Enzymes. *Methods Enzymol.* **104**, 404–414 (1984).

177. Good, N. E. & Izawa, S. Hydrogen Ion Buffers. *Methods Enzymol.* **24**, 53–68 (1972).

178. McNemar, L. S. *et al.* Terbium(III) Luminescence Study of the Spatial Relationship of Tryptophan Residues to the Two Metal Ion Binding Sites of *Escherichia coli* Glutamine Synthetase. *Biochemistry* **30**, 3417–3421 (1991).

179. Anthony, C. & Williams, P. The structure and mechanism of methanol dehydrogenase. *Biochim. Biophys. Acta - Proteins Proteomics* **1647**, 18–23 (2003).

180. Saboury, A. A. A review on the ligand binding studies by isothermal titration calorimetry. *J. Iran. Chem. Soc.* **3**, 1–21 (2006).

181. Hansen, L. D. *et al.* Enzyme-catalyzed and binding reaction kinetics determined by titration calorimetry. *Biochim. Biophys. Acta - Gen. Subj.* **1860**, 957–966 (2016).

182. Clugston, S. L. *et al.* Investigation of metal binding and activation of *Escherichia coli* glyoxalase I: Kinetic, thermodynamic and mutagenesis studies. *Biochem. J.* **377**, 309–316 (2004).

183. Czyrko, J. *et al.* Metal-cation regulation of enzyme dynamics is a key factor influencing the activity of S-adenosyl-L-homocysteine hydrolase from *Pseudomonas aeruginosa*. *Sci. Rep.* **8**, 11334 (2018).

184. Drobot, B. *et al.* Cm^{3+}/Eu^{3+} induced structural, mechanistic and functional implications for calmodulin. *Phys. Chem. Chem. Phys.* **21**, 21213–21222 (2019).

185. Lumpe, H. *et al.* Impact of the lanthanide contraction on the activity of a lanthanide-dependent methanol dehydrogenase - a kinetic and DFT study. *Dalt. Trans.* **47**, 10463–10472 (2018).

186. Luque, I. & Freire, E. Structure-based prediction of binding affinities and molecular design of peptide ligands. *Methods Enzymol.* **295**, 100–122 (1998).

187. Warren, J. C. *et al.* The effect of structure-disrupting ions on the activity of myosin and other enzymes. *J. Biol. Chem.* **241**, 309–316 (1966).

188. Sinha, R. & Khare, S. K. Protective role of salt in catalysis and maintaining structure of halophilic proteins against denaturation. *Front. Microbiol.* **5**, 1–6 (2014).

189. Pomper, B. K. & Vorholt, J. A. Characterization of the formyltransferase from *Methylobacterium extorquens* AM1. *Eur. J. Biochem.* **269**, 4769–4775 (2001).

190. Marx, C. J. *et al.* Formaldehyde-Detoxifying Role of the Tetrahydromethanopterin-Linked Pathway in *Methylobacterium extorquens* AM1. *J. Bacteriol.* **185**, 7160–7168 (2003).

191. Chistoserdova, L. *et al.* Identification of a Fourth Formate Dehydrogenase in *Methylobacterium extorquens* AM1 and Confirmation of the Essential Role of Formate Oxidation in Methylotrophy. *J. Bacteriol.* **189**, 9076–9081 (2007).

192. Good, N. M. *et al.* Investigation of lanthanide-dependent methylotrophy uncovers complementary roles for alcohol dehydrogenase enzymes. *bioRxiv* (2018).

193. Bogart, J. A. *et al.* DFT Study of the Active Site of the XoxF-Type Natural, Cerium-Dependent Methanol Dehydrogenase Enzyme. *Chem. Eur. J.* **1**, 1743–1748 (2015).

194. Grosse, S. *et al.* Purification and properties of methanol dehydrogenase from *Methylosinus* sp. WI 14. *J. Basic Microbiol.* **38**, 189–196 (1998).

195. Grosse, S. *et al.* Purification and properties of methanol dehydrogenase from *Methylocystis* sp. GB 25. *J. Basic Microbiol.* **37**, 269–279 (1997).

196. Schmidt, S. *et al.* Functional investigation of methanol dehydrogenase-like protein XoxF in *Methylobacterium extorquens* AM1. *Microbiology* **156**, 2575–2586 (2010).

197. Frank, J. *et al.* On the mechanism of inhibition of methanol dehydrogenase by cyclopropane-derived inhibitors. *Eur. J. Biochem.* **184**, 187–195 (1989).

198. Duine, J. A. *et al.* Quinoproteins in the dissimilation of C1 compounds in *Microbial Growth on C1 Compounds* (eds. Verseveld, H. W. & Duine, J. A.) 105–113 (Springer Netherlands, Dodrecht, NL, 2012).

199. Dijkstra, M. *et al.* Inactivation of quinoprotein alcohol dehydrogenases with cyclopropane-derived suicide substrates. *Eur. J. Biochem.* **140**, 369–373 (1984).

200. Greenzaid, P. *et al.* A Nuclear Magnetic Resonance Study of the Reversible Hydration of Aliphatic Aldehydes and Ketones. I. Oxygen-17 and Proton Spectra and Equilibrium Constants. *J. Am. Chem. Soc.* **89**, 749–756 (1967).

201. Medvedeva, A. S. *et al.* Spontaneous hydration of the carbonyl group in substituted propynals in aqueous medium. *Russ. J. Org. Chem.* **49**, 828–831 (2013).

202. Itoh, S. *et al.* Model Studies on Calcium-Containing Quinoprotein Alcohol Dehydrogenases. Catalytic Role of Ca^{2+} for the Oxidation of Alcohols by Coenzyme PQQ (4,5-Dihydro-4,5-dioxo-1H-pyrrolo[2,3-*f*]quinoline-2,7,9-tricarboxylic Acid). *Biochemistry* **37**, 6562–6571 (1998).

203. Cleland, W. W. The use of isotope effects to determine enzyme mechanisms. *Arch. Biochem. Biophys.* **433**, 2–12 (2005).

204. Roston, D. *et al.* Isotope effects as probes for enzyme catalyzed hydrogen-transfer reactions. *Molecules* **18**, 5543–5567 (2013).

205. Sen, A. & Kohen, A. Enzymatic tunneling and kinetic isotope effects: Chemistry at the crossroads. *J. Phys. Org. Chem.* **23**, 613–619 (2010).

206. Truhlar, D. G. Tunneling in enzymatic and nonenzymatic hydrogen transfer reactions. *J. Phys. Org. Chem.* **23**, 660–676 (2010).

207. Hammes-Schiffer, S. Hydrogen tunneling and protein motion in enzyme reactions. *Acc. Chem. Res.* **39**, 93–100 (2006).

208. Nagel, Z. D. & Klinman, J. P. Tunneling and Dynamics in Enzymatic Hydride Transfer. *Chem. Rev.* **110**, PR41–PR67 (2010).

209. Warshel, A. *et al.* Electrostatic basis for enzyme catalysis. *Chem. Rev.* **106**, 3210–3235 (2006).

210. Scheiner, S. Calculation of isotope effects from first principles. *Biochim. Biophys. Acta - Bioenerg.* **1458**, 28–42 (2000).

211. Kohen, A. Kinetic isotope effects as probes for hydrogen tunneling, coupled motion and dynamics contributions to enzyme catalysis. *Prog. React. Kinet. Mech.* **28**, 119–156 (2003).

212. Francis, K. & Gadda, G. On the use of noncompetitive kinetic isotope effects to investigate flavoenzyme mechanism in *Methods in Enzymology* (ed. Palfey, B.) vol. 620, 115–143 (Academic Press, Boston, MA, USA, 2019).

213. Gu, H. & Zhang, S. Advances in kinetic isotope effect measurement techniques for enzyme mechanism study. *Molecules* **18**, 9278–9292 (2013).

214. Wang, L. *et al.* Quantum delocalization of protons in the hydrogen-bond network of an enzyme active site. *Proc. Natl. Acad. Sci. USA* **111**, 18454–18459 (2014).

215. Spencer, H. T. *et al.* Kinetic Scheme for Thymidylate Synthase from *Escherichia coli*: Determination from Measurements of Ligand Binding, Primary and Secondary Isotope Effects, and Pre-Steady-State Catalysis. *Biochemistry* **36**, 4212–4222 (1997).

216. Knapp, M. J. *et al.* Temperature-dependent isotope effects in soybean Lipoxygenase-1: Correlating hydrogen tunneling with protein dynamics. *J. Am. Chem. Soc.* **124**, 3865–3874 (2002).

217. Nagel, Z. D. *et al.* Active Site Hydrophobic Residues Impact Hydrogen Tunneling Differently in a Thermophilic Alcohol Dehydrogenase at Optimal vs. Non-Optimal Temperatures. *Biochemistry* **51**, 4147–4156 (2012).

218. Kohen, A. *et al.* Enzyme dynamics and hydrogen tunnelling in a thermophilic alcohol dehydrogenase. *Nature* **399**, 496–499 (1999).

219. Schowen, B. K. & Schowen, R. L. Solvent Isotope Effects on Enzyme Systems in *Methods in Enzymology* vol. 87, 551–606 (1982).

220. Venkatasubban, K. S. & Schowen, R. L. The proton inventory technique. *Crit. Rev. Biochem. Mol. Biol.* **17**, 1–44 (1984).

221. Elrod, J. P. *et al.* Protonic Reorganization and Substrate Structure in Catalysis by Serine Proteases. *J. Am. Chem. Soc.* **102**, 3917–3922 (1980).

222. Fitzpatrick, P. F. Combining Solvent Isotope Effects with Substrate Isotope Effects in Mechanistic Studies of Alcohol and Amine Oxidation by Enzymes. *Biochim. Biophys. Acta* **1854**, 1746–1755 (2015).

223. Klinman, J. P. Acid base catalysis in the yeast alcohol dehydrogenase reaction. *J. Biol. Chem.* **250**, 2569–2573 (1975).

224. Koushik, S. V. *et al.* The catalytic mechanism of kynureninase from *Pseudomonas fluorescens*: Insights from the effects of pH and isotopic substitution on steady-state and pre-steady-state kinetics. *Biochemistry* **37**, 1376–1382 (1998).

225. Zheng, Y. J. *et al.* Catalytic mechanism of quinoprotein methanol dehydrogenase: A theoretical and x-ray crystallographic investigation. *Proc. Natl. Acad. Sci. USA* **98**, 432–434 (2001).

226. Zhang, X. *et al.* Mechanism of methanol oxidation by quinoprotein methanol dehydrogenase. *Proc. Natl. Acad. Sci. USA* **104**, 745–749 (2007).

227. Cook, P. F. & Cleland, W. W. pH Variation of Isotope Effects in Enzyme-Catalyzed Reactions. 1. Isotope- and pH-Dependent Steps the Same. *Biochemistry* **20**, 1797–1805 (1981).

228. Cook, P. F. & Cleland, W. W. pH Variation of Isotope Effects in Enzyme-Catalyzed Reactions. 2. Isotope-Dependent Step Not pH Dependent. Kinetic Mechanism of Alcohol Dehydrogenase. *Biochemistry* **20**, 1805–1816 (1981).

229. Liu, H. & Warshel, A. Origin of the temperature dependence of isotope effects in enzymatic reactions: The case of dihydrofolate reductase. *J. Phys. Chem. B* **111**, 7852–7861 (2007).

230. Kohen, A. & Klinman, J. P. Enzyme Catalysis: Beyond Classical Paradigms. *Acc. Chem. Res.* **31**, 397–404 (1998).

231. Laemmli, U. K. Cleavage of Structural Proteins during the Assembly of the Head of Bacteriophage T4. *Nature* **227**, 680–685 (1970).

232. Nick Pace, C. *et al.* How to measure and predict the molar absorption coefficient of a protein. *Protein Sci.* **4**, 2411–2423 (1995).

233. Eulen, H. v. *et al.* Reduktone und Endiol-Umlagerungen in saurer und alkalischer Lösung. *Liebigs Ann. Chem.* **581**, 198–210 (1953).

234. Steyn-Parvé, E. P. & Beinert, H. On the Mechanism of Dehydrogenation of Fatty Acyl Derivatives of Coenzyme A. VI. Isolation and Properties of Stable Enzyme-Substrate Complexes. *J. Biol. Chem.* **233**, 843–853 (1958).

235. Basford, R. E. & Huennekens, F. M. Studies on Thiols. I. Oxidation of Thiol Groups by 2,6-Dichlorophenol Indophenol. *J. Am. Chem. Soc.* **77**, 3873–3877 (1955).

236. Crane, F. L. *et al.* On The Mechanism of Dehydrogenase of Fatty Acyl Derivatives of Coenzyme A. I. The General Fatty Acyl Coenzyme A Dehydrogenase. *J. Biol. Chem.* **218**, 701 (1956).

237. Duine, J. A. *et al.* Monomeric and Dimeric Quinoprotein Alcohol Dehydrogenase from Alcohol-grown *Pseudomonas* BB1. *J. Gen. Microbiol.* **131**, 3163–3169 (1985).

Appendix

VI. Appendix

1 Materials

1.1 MDH Samples

Table 12 MDH samples that have been used in the experimental part of this work. AM1 La-MDH was kindly provided by the Group of Prof. Dr. N.C. Martinez-Gomez.

MDH sample	Purification year	Buffer
SolV La-MDH	2016	10 mM KP pH 7, 1mM MeOH
SolV Eu-MDH 4th	2016	10 mM PIPES pH 7.2, 1mM MeOH
AM1 La-MDH	2018	25 mM Tris-HCl pH 8, 150 mM NaCl, 1mM MeOH
SolV Eu-MDH 1st	2019	10 mM PIPES pH 7.2, 1mM MeOH
SolV Eu-MDH 2nd	2019	10 mM PIPES pH 7.2, 1mM MeOH
SolV Pr-MDH	2019	10 mM PIPES pH 7.2, 1mM MeOH

1.2 Buffers

Table 13 Buffers that have been used in the experimental part of this work to analyze assay components and measure MDH activity.

Buffer	Purity	Supplier
1,4-Piperazinediethanesulfonic acid (PIPES)	BioPerformance, ≥ 99 %	Sigma-Aldrich (St. Louis, MO, USA)
1,4-Piperazinediethanesulfonic acid (PIPES)		ICN Biomedicals (Aurora, OH, USA)
2,2-Bis(hydroxymethyl)-2,2',2''-nitrilotriethanol (Bis-Tris)	BioXtra, ≥ 98%	Sigma-Aldrich (St. Louis, MO, USA)
2-Amino-2-(hydroxymethyl)propane-1,3-diol (Tris)	ultrapure, ≥ 99.9%	Sigma-Aldrich (St. Louis, MO, USA)
2-Amino-2-(hydroxymethyl)propane-1,3-diol hydrochloride (Tris-HCl)	molecular biology grade	Alfa Aesar (Ward Hill, MA, USA)
2-(Cyclohexylamino)ethanesulfonic acid (CHES)	≥ 99%	Sigma-Aldrich (St. Louis, MO, USA)
2-(N-Morpholino)ethanesulfonic acid (MES)	≥ 99.5%	Sigma-Aldrich (St. Louis, MO, USA)

Buffer	Purity	Supplier
3-(Cyclohexylamino)-1-propanesulfonic acid (CAPS)	BioXtra, ≥ 99%	Sigma-Aldrich (St. Louis, MO, USA)
3-Morpholino-2-hydroxypropanesulfonic acid (MOPSO)	≥ 99%	Sigma-Aldrich (St. Louis, MO, USA)
3-(N-Morpholino)propanesulfonic acid (MOPS)	≥99.5%	Sigma-Aldrich (St. Louis, MO, USA)
Sodium citrate tribasic dihydrate	BioUltra, ≥ 99.5%	Sigma-Aldrich (St. Louis, MO, USA)
Potassium phosphate tribasic (KP)	reagent grade, ≥ 98%	Sigma-Aldrich (St. Louis, MO, USA)

1.3 Electron Acceptors and Dyes

Table 14 Electron acceptors and dyes that have been used for the assay optimization and investigation of MDH enzymes in this work.

Compound	Purity	Supplier	Note
2,6-Dichlorophenol indophenol sodium salt hydrate (DCPIP)	≥ 90%	Sigma-Aldrich (St. Louis, MO, USA)	-
***N,N,N´,N´*-Tetramethyl-p-phenylenediamine (TMPD)**	99%	Sigma-Aldrich (St. Louis, MO, USA)	-
***N,N,N´,N´*-Tetramethyl-p-phenylenediamine dihydrochloride (TMPDD)**	≥ 97%	Sigma-Aldrich (St. Louis, MO, USA)	-
Phenazine methosulfate	≥ 90%	Sigma-Aldrich (St. Louis, MO, USA)	Lot# 125M4099V (PMS1), Lot# 057M4019V (PMS2); yellow
Phenazine methosulfate	98%	abcr (Karlsruhe, Germany)	Lot# 1385955 (PMS3); grey yellow
Phenazine ethosulfate	≥ 95%	Sigma-Aldrich (St. Louis, MO, USA)	Lot# MKCD9943 (PES1); brown, opened for eleven months Lot# MKCD9943 (PES2); brown, opened for seven months Lot# MKCD9943 (PES3); brown, opened for five months Lot# MKCG3495 (PES4); orange, opened for six months

1.4 Chemicals and Reagents

Table 15 Chemicals and reagents that have been used in the experimental part of this work.

Chemical/Reagent	Purity	Supplier
β-Mercaptoethanol	for synthesis	Merck (Darmstadt, Germany)
Acetaldehyde	≥99.5%	Sigma-Aldrich (St. Louis, MO, USA)
Ammonium chloride	-	VWR (Radnor, PA, USA)
Ammonium persulfate (APS)	For electrophoresis, ≥ 98%	Sigma-Aldrich (St. Louis, MO, USA)
Barium chloride dihydrate	99%	Grüssing (Filsum, Germany)
Bromine	puriss. p.a. ≥ 99%	Sigma-Aldrich (St. Louis, MO, USA)
Bromophenol blue sodium salt	for electrophoresis	GE Healthcare (Chicago, IL, USA)
Calcium chloride dihydrate	pure	AppliChem (Darmstadt, Germany)
Chelex® 100 sodium salt	50-100 mesh (dry)	Sigma-Aldrich (St. Louis, MO, USA)
Coomassie Brilliant Blue (CBB) G250	C.I. 42655	Sigma-Aldrich (St. Louis, MO, USA)
Cyclopropanol	-	abcr (Karlsruhe, Germany)
Deuterium chloride (35 wt. % in D_2O)	≥99 atom % D	Sigma-Aldrich (St. Louis, MO, USA)
Deuterium oxide	99.9 atom % D	Sigma-Aldrich (St. Louis, MO, USA)
Diethylether	99.5% ACS	Bernd Kraft (Duisburg, Germany)
Ethanol	BioReagent	Fisher Chemicals (Waltham, MA, USA)
Europium(III) chloride hexahydrate	99.99%	Sigma-Aldrich (St. Louis, MO, USA)
Glycine	for analysis	Merck Millipore (Burlington, MA, USA)
Glycine ethyl ester hydrochloride	99%	Alfa Aesar (Ward Hill, MA, USA)
Glycerol	extra pure, 99+%	Fisher Chemicals (Waltham, MA, USA)
Lanthanum(III) chloride heptahydrate	99.99%	Sigma-Aldrich (St. Louis, MO, USA)
Lutetium(III) chloride hexahydrate	99.9%	chemPUR (Karlsruhe, Germany)
Methanol	HPLC grade	Fisher Chemicals (Waltham, MA, USA)
Methanol-d^4 (MeOD)	99.8%	Deutero (Kastellaun, Germany)
N,N,N′,N′-Tetramethylethylenediamine (TEMED)	molecular biology, ≥99% (GC)	Sigma-Aldrich (St. Louis, MO, USA)
n-Propanol	BioReagent	Fisher Chemicals (Waltham, MA, USA)
Paraformaldehyde	95-100.5%	Sigma-Aldrich (St. Louis, MO, USA)
Polyacrylamide (PAA), (37.1:1)	40% acrylamide/bisacrylamide	Carl Roth (Karlsruhe, Germany)

Chemical/Reagent	Purity	Supplier
Potassium cyanide	96%	VWR (Radnor, PA, USA)
Praseodymium(III) chloride hydrate	99.99%	Sigma-Aldrich (St. Louis, MO, USA)
Pyrroloquinoline quinone (PQQ)	-	Purified from capsules by Dr. H. Lumpe
Sodium chloride	for analysis	Bernd Kraft (Duisburg, Germany)
Sodium dodecylsulfate (SDS)	molecular biology, ≥98.5% (GC)	Sigma-Aldrich (St. Louis, MO, USA)
Sodium deuteroxide (40 wt. % in D_2O)	99 atom % D	Sigma-Aldrich (St. Louis, MO, USA)
Sodium perchlorate monohydrate	reagent grade	Fisher Chemicals (Waltham, MA, USA)
Ytterbium(III) chloride hexahydrate	99.9%	abcr (Karlsruhe, Germany)

1.5 Solutions

Table 16 Composition of solutions that have been used in the experimental part of this work.

Solution	Composition
Coomassie Brilliant Blue Stain, 2 l 0.25% CBB, 40% methanol, 10% acetic acid	5 g CBB G250 800 ml methanol, 200 ml acetic acid, MilliQ water
Coomassie destain solution, 1 l 20% ethanol, 10% acetic acid	200 ml ethanol, 100 ml acetic acid, MilliQ water
Formaldehyde solution	10 mg PFA 1 ml MilliQ water 1 drop 1 M NaOH 55-60 °C, water bath
SDS running buffer (1x), 0.5 l	50 ml 10x SDS running buffer, 450 ml MilliQ water
SDS running buffer (10x), 2 l 250 mM Tris, 1.92 M Glycine, 1% SDS, pH 8.3	60 g Tris 288 g Glycine 20 g SDS MilliQ water

Solution	Composition
SDS sample buffer (4x), 10 ml 250 mM Tris-Cl pH 6.8, 8% SDS, 40% glycerol, 20% β-mercaptoethanol, 0.02% bromophenol blue	0.3 g Tris 0.8 g SDS 4 ml Glycerol 2 ml β-mercaptoethanol 0.4 ml 0.5% w/v bromophenol blue MilliQ water

1.6 Equipment

Table 17 Consumables that have been used in the experimental part of this work.

Consumable	Manufacturer
96 well plate	Corning (Corning, NY, USA)
Capillaries (BLAUBRAND, intraMARK, 50 µl)	BRAND (Wertheim, Germany)
Centrifugal filter units (30 kDa, Amicon® Ultra-4)	Merck Millipore (Burlington, MA, USA)
Centrifugal filter units (30 kDa, Vivaspin 500)	Sartorius (Göttingen, Germany)
Wax seal plates	Hirschmann Laborgeräte (Eberstadt Germany)
Hypodermic needle	B. Braun (Puchheim, Germany)
Sterile filter units (0.45 µM)	VWR (Radnor, PA, USA)
Syringe (0.5 ml)	Henke-Sass, Wolf (Tuttlingen, Germany)
Syringe (10 ml, 20 ml)	B. Braun (Puchheim, Germany)
Syringe filter (25 mm, 0.45 µm, nylon membrane)	VWR (Radnor, PA, USA)

Table 18 Instruments and components that have been used in the experimental part of this work.

Instrument or component	Manufacturer
Avance III 400 MHz NMR spectrometer	Bruker (Billerica, MA, USA)
Andor iStar ICCD camera	Quantum Design (Darmstadt, Germany)
Äkta purifier (FPLC with UV-visible detector, collector and SP-sepharose column)	GE Healthcare (Chicago, IL, USA)
Cary60 UV-visible spectrometer	Agilent Technologies (Santa Clara, CA, USA)
Cary single cell Peltier element	Agilent Technologies (Santa Clara, CA, USA)
Centrifuge (Megafuge 8R)	Thermo Fisher (Waltham, MA, USA)

Instrument or component	Manufacturer
Circular dichroism spectropolarimeter (J-810)	Jasco (Tokyo, Japan)
Dry block heater	IKA (Staufen im Breisgau, Germany)
Electrophoresis devices (Mini-PROTEAN®)	BioRad (Hercules, CA, USA)
EMXnano EPR spectrometer	Bruker (Billerica, MA, USA)
Epoch2 microplate reader	BioTek Instruments (Winooski, VT, USA)
Finnigan LTQ FT Ultra Mass Spectrometer	Thermo Scientific (Waltham, MA, USA)
FT/IR-460Plus with ATR diamond plate	Jasco (Tokyo, Japan)
Gel documentation system (ChemiDoc MP)	BioRad (Hercules, CA, USA)
Kymera 328i spectrograph	Quantum Design (Darmstadt, Germany)
Lambda 750 spectrophotometer	PerkinElmer (Waltham, MA, USA)
Magnetic stirrer MR-Hei standard	Heidolph (Schwabach, Germany)
MicroCal VP-ITC instrument	GE Healthcare (Chicago, IL, USA)
Nd:YAG OPO laser system (Powerlite Precision II 9020 laser with Green Panther EX OPO)	Continuum Electro-Optics (San Jose, CA, USA)
pH meter	Mettler-Toledo (Columbus, OH, USA)
Quartz SUPRASIL cuvette (1 cm, 2mm)	Hellma Analytics (Mühlheim, Germany)
Shaker (multi reax)	Heidolph (Schwabach, Germany)
Synergy HTX microplate reader	BioTek Instruments (Winooski, VT, USA)
TrayCell® with 10x cap	Hellma Analytics (Mühlheim, Germany)
vario EL cube	Elementar Analysensysteme (Langenselbold, Germany)
Vista ICP-OES	Varian (Palo Alto, CA, USA)
Water system Millipore® Synergy® UV	Merck Millipore (Burlington, MA, USA)

1.7 Software

Table 19 Software that has been used for data processing during this work.

Software	**Manufacturer**
Cary WinUV	Agilent Technologies (Santa Clara, CA, USA)
Gen5	BioTek Instruments (Winooski, VT, USA)
Kaleidagraph	Synergy Software (Reading, PA, USA)
MestreNova	MestreLab Research (Santiago de Compostela, Spain)

2 Supplementary Figures

2.1 SolV MDH Derivatives

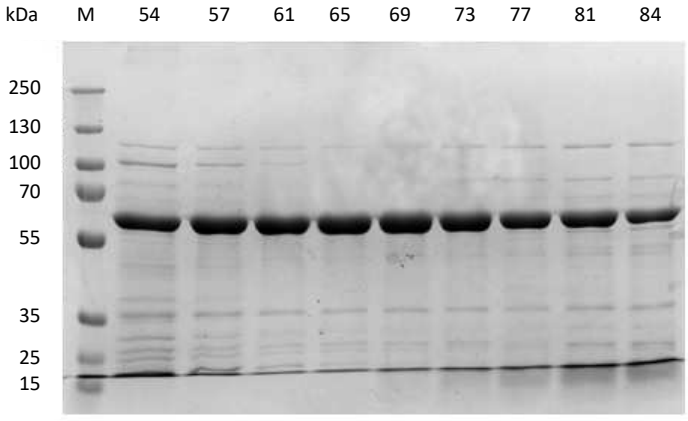

Figure S1 SDS-PAGE of onefold purified Eu-MDH. Peak fractions 58-80 containing a band at 63 kDa (SolV MDH monomer) were pooled and denoted as Eu-MDH 1st. Conditions: 10% Tris-Gel, 7.5 µg/lane, 100 mA. M = prestained PageRuler Plus. Numbers indicate purification fractions.

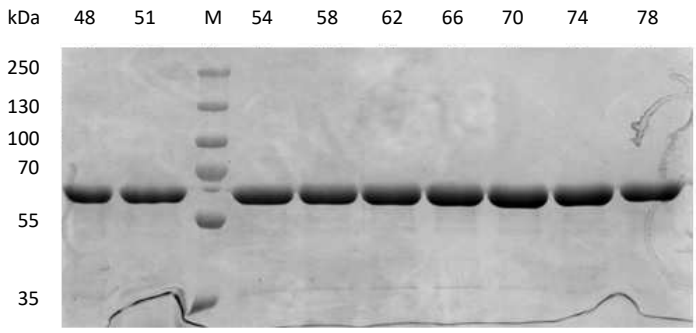

Figure S2 SDS-PAGE of twofold purified Eu-MDH. All fractions containing a band at 63 kDa (SolV MDH monomer) were pooled and denoted as Eu-MDH 2nd. Conditions: 10% Tris-Gel, 7.5 µg/lane, 100 mA. M = prestained PageRuler Plus. Numbers indicate purification fractions.

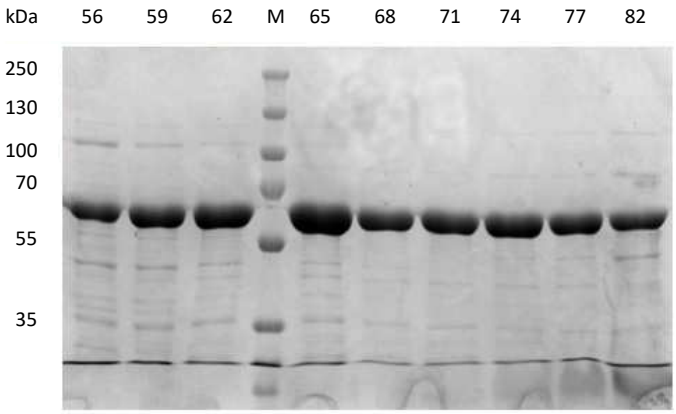

Figure S3 SDS-PAGE of purified Pr-MDH. Peak fractions 59-74 containing a band at 63 kDa (SolV MDH monomer) were pooled and used for experiments. Conditions: 10% Tris-Gel, 7.5 µg/lane, 100 mA. M = prestained PageRuler Plus. Numbers indicate purification fractions.

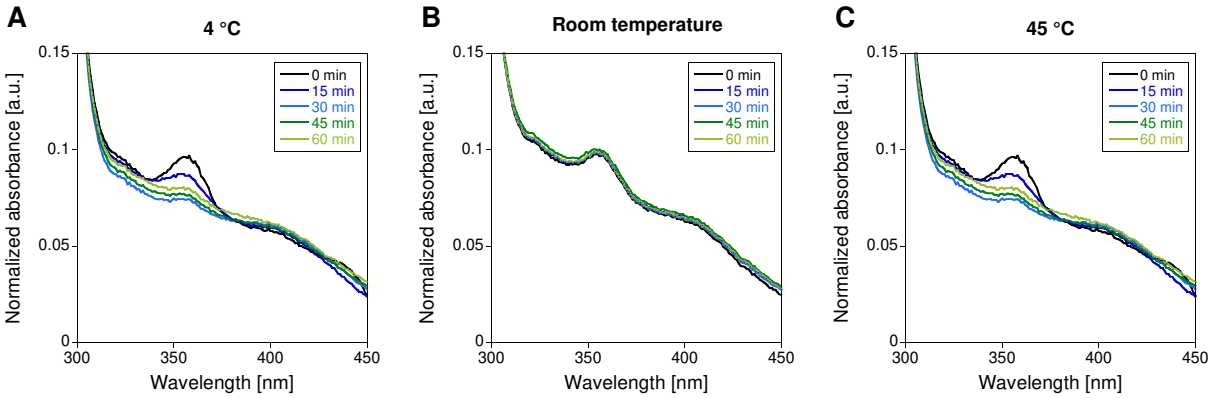

Figure S4 UV-visible absorption spectra of differently treated Eu-MDH 1st in 20 mM PIPES pH 7.2. The PQQ fingerprint was recorded every 15 min during the incubation of Eu-MDH at either 4 °C (A), room temperature (B) or 45 °C (C). Spectra were recorded in a 1 mm-path length CD-cuvette at a Cary60 spectrophotometer. Spectra were baseline corrected and normalized to the A_{280nm} peak.

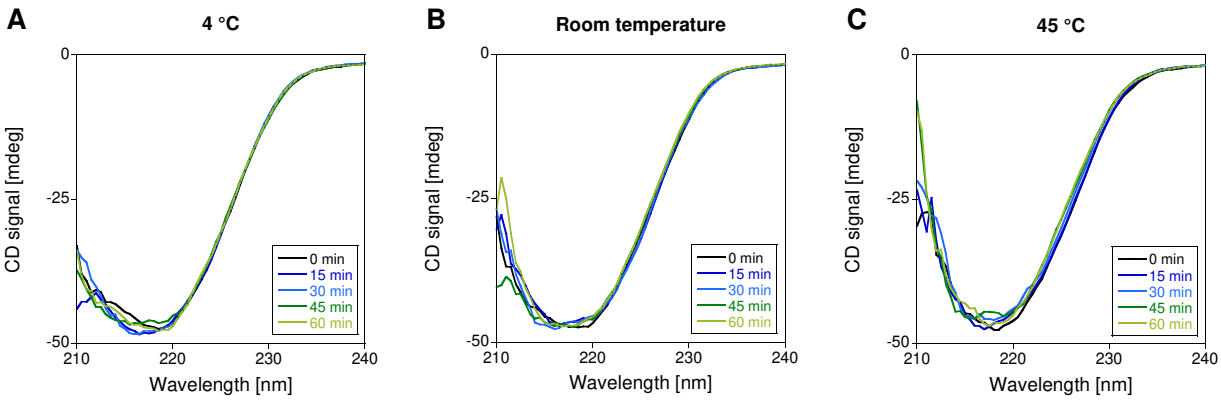

Figure S5 CD spectra of differently treated Eu-MDH 1st in 20 mM PIPES pH 7.2. Spectra were recorded every 15 min at a Jasco J-810 CD spectrometer during the incubation of Eu-MDH at either 4 °C (A), room temperature (B) or 45 °C (C) in a 1 mm-path length CD-cuvette.

2.2 Assay Optimization

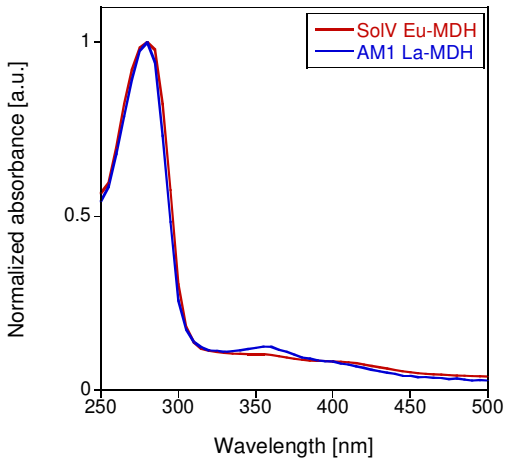

Figure S6 Normalized absorbance spectra of SolV Eu-MDH (red) vs. AM1 La-MDH untagged (blue) both in 20 mM PIPES pH 7.2 and after washing. Spectra were recorded at room temperature at a Cary60 spectrophotometer. Here the PQQ to total protein ratios (355/280) were 0.10486 for Eu-MDH and 0.12629 for La-MDH.

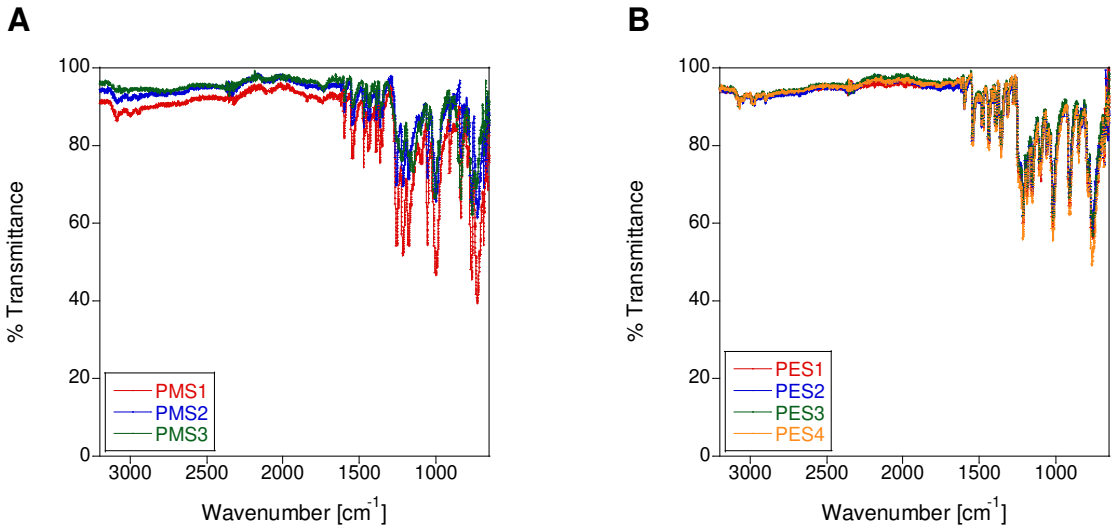

Figure S7 FT-IR spectra of different PMS (A) and PES (B) batches. It can be observed, that the abcr® sample (>98% purity, PMS3) is missing a peak at 1435 cm^{-1}, shows additional and red-shifted peaks in the region of 1030-780 cm^{-1} and a different signature between 1300-1100 cm^{-1} and 750-650 cm^{-1} compared to the FT-IR spectra of Sigma-Aldrich® samples PMS1 and PMS2 (>90% purity).

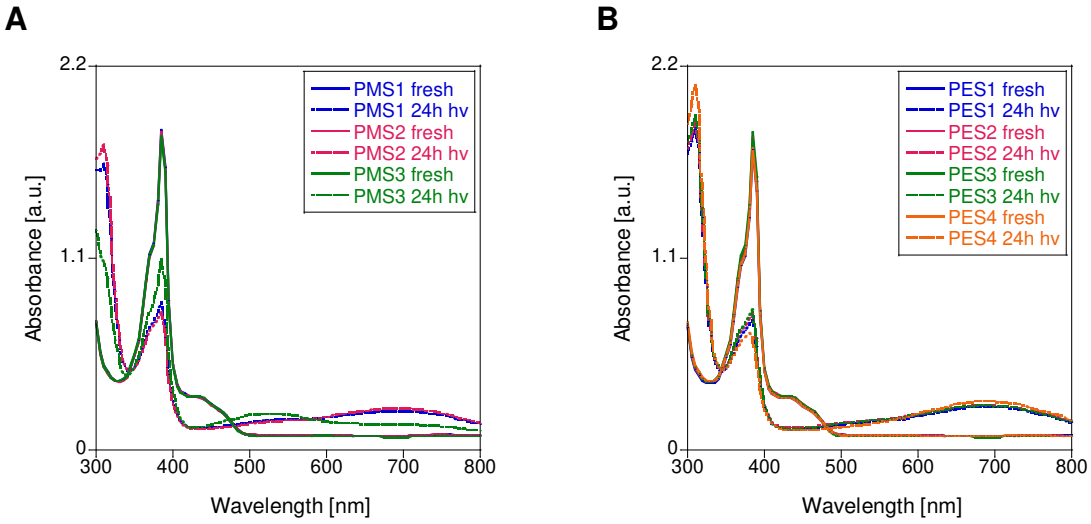

Figure S8 UV-vis spectra of different PMS (A) and PES (B) batches at RT. Conditions were as follows: 125 µM phenazine species in MilliQ before (continuous line) and after daylight exposure for 24 h (dotted line), Epoch2 plate reader (not baseline corrected). The UV-vis spectrum of the light-exposed abcr® sample (PMS3) exhibits an entirely different spectrum and a blue shift of the peak at 700 nm to 520 nm compared to PMS1 and PMS2.

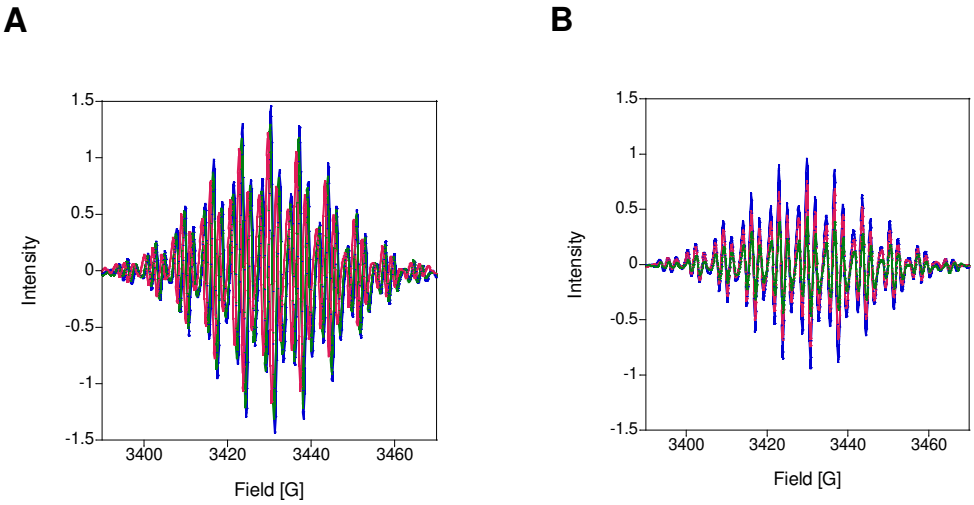

Figure S9 EPR spectra of 200 µM WB in 100 mM multicomponent buffer. Blue line: fresh sample, pink line: heated sample for 30 min at 30 °C, green line: heated sample for 30 min at 45 °C, both under exclusion of light. (A) pH 7.2 (B) pH 9. Spectra were collected on an EMXnano EPR spectrometer at room temperature and in the dark.

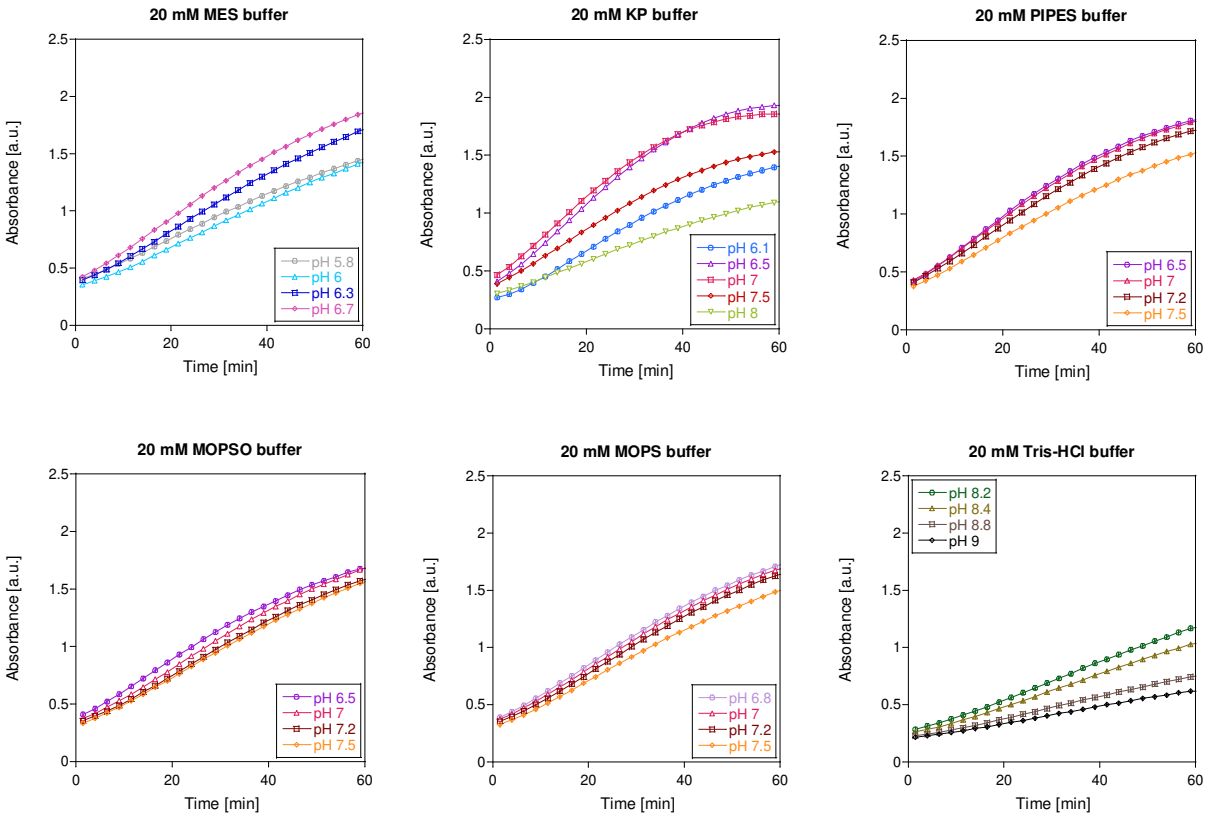

Figure S10 pH-dependence of in situ WB formation from N,N,N',N'-tetramethyl-p-phenylenediamine (TMPD) in different buffers. Conditions were as follows: 200 µM TMPD in 20 mM buffer of different pH, heated for 1 h at 45 °C. Absorbance at 610 nm was monitored with an Epoch2 plate reader. Triplicates with standard deviation are shown. Data were path length corrected.

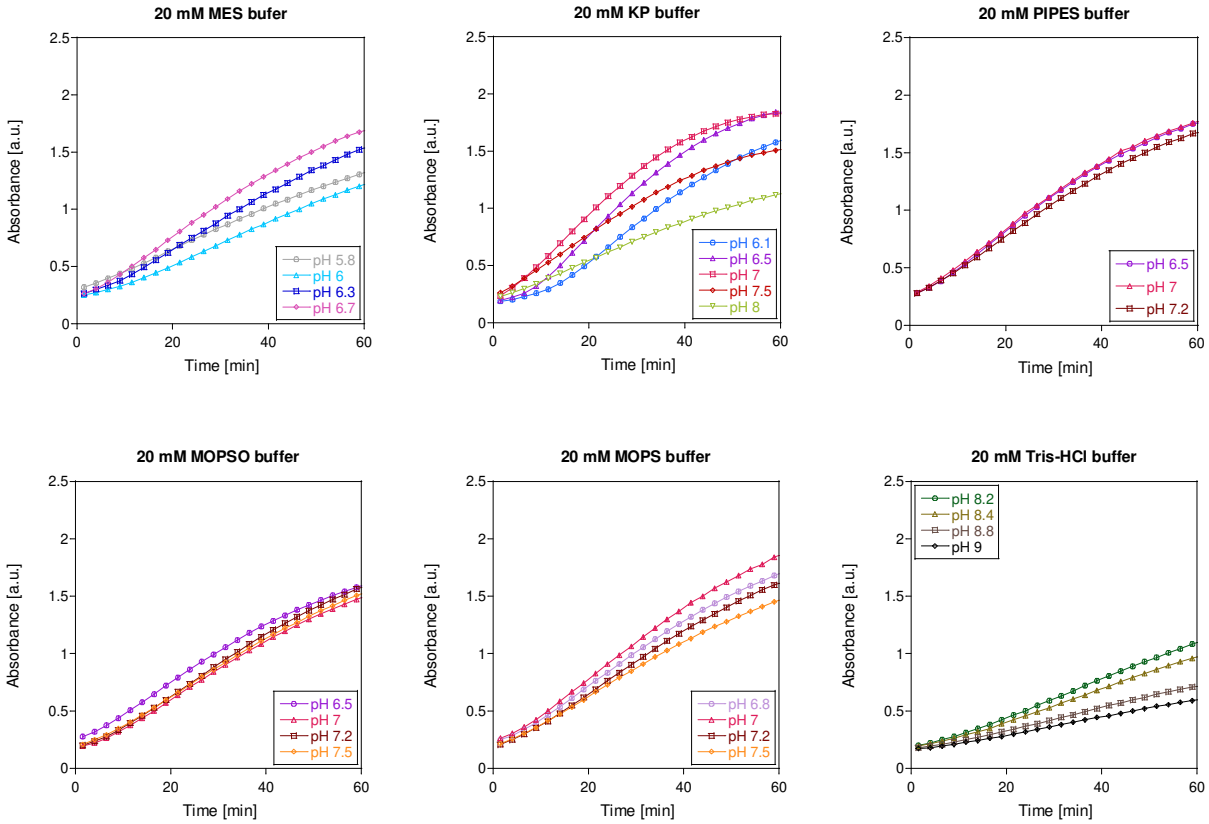

Figure S11 pH-dependence and in situ WB formation from N,N,N′,N′-tetramethyl-p-phenylenediamine dihydrochloride (TMPDD) in different buffers. Conditions were as follows: 200 µM TMPDD in 20 mM buffer of different pH, heated for 1 h at 45 °C. Absorbance at 610 nm was monitored with an Epoch2 plate reader. Triplicates with standard deviation are shown. Data were path length corrected.

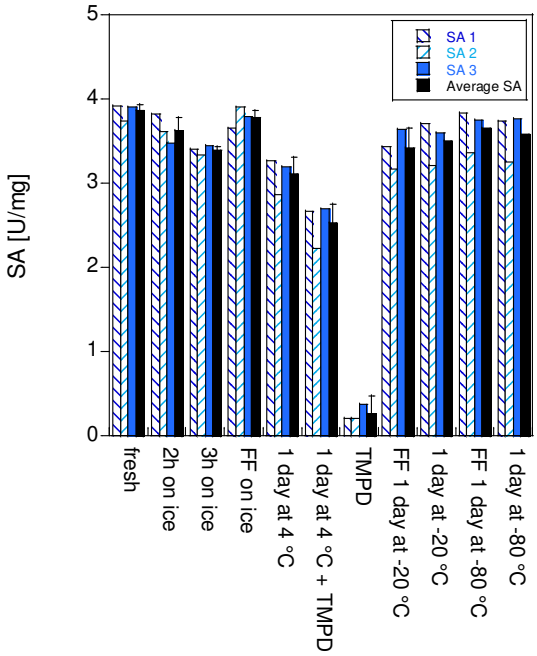

Figure S12 Influence of WB storage conditions on the specific activity (SA, in µmol min^{-1} mg^{-1}) of His-tagged AM1 La-MDH. WB samples were either stored on ice over a prolonged time or under different conditions with and without flash freezing (FF) the samples. The assay conditions were as follows: 100 mM multicomponent buffer pH 9, 100 nM AM1 La-MDH, 200 µM WB, 15 mM NH_4Cl, 50 mM MeOH. Total volume in wells was 200 µl. The WB concentration was adjusted to 200 µM for each condition. Data were collected using an Epoch2 plate reader with automatic path length correction to 1 cm at 30 °C and 610 nm. Technical duplicates were conducted by the same pair of hands. Initial rates (first 30 s of the assay) were used for calculating the SA.

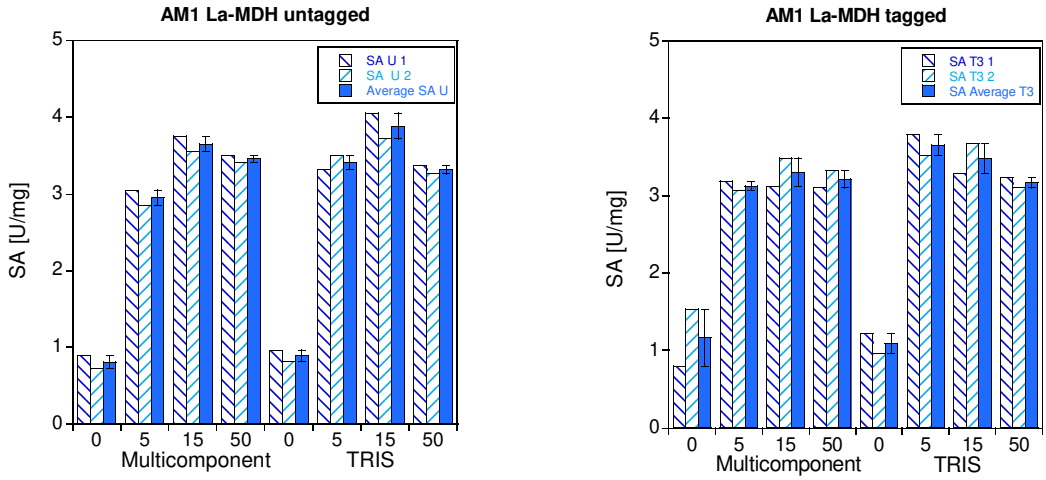

Figure S13 Ammonia-dependence of AM1 La-MDH in 100 mM multicomponent and 25 mM Tris buffer pH 9. The specific activity (SA, in µmol min^{-1} mg^{-1}) of untagged (U) and His-tagged (T3) La-MDH was determined using WB. The conditions were as follows: 200 µM WB and increasing concentrations of NH_4Cl (0, 5, 15 and 50 mM), 50 mM MeOH. The total volume in wells was 222 µl. Data were collected at 30 °C and 610 nm using an Epoch2 plate reader. All SA are technical replicates. SA1 and SA2 were determined by different pairs of hands.

2.3 Impact of Metals & Substrate Kinetics

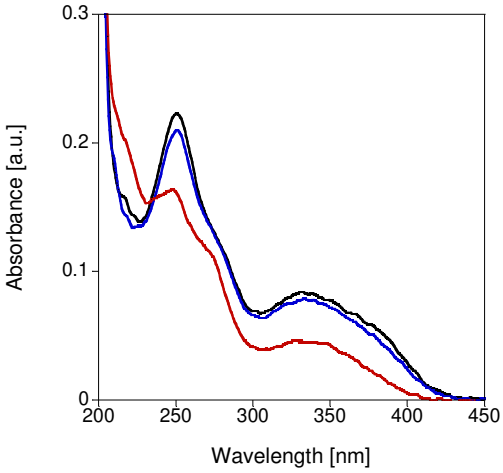

Figure S14 UV-visible spectra of 10 µM PQQ with 10 µM Eu in 100 mM NaCl pH 6.5 + 1 mM MeOH. Black: before laser exposure. Blue: after low energy laser power exposure. Red: after high energy laser exposure.

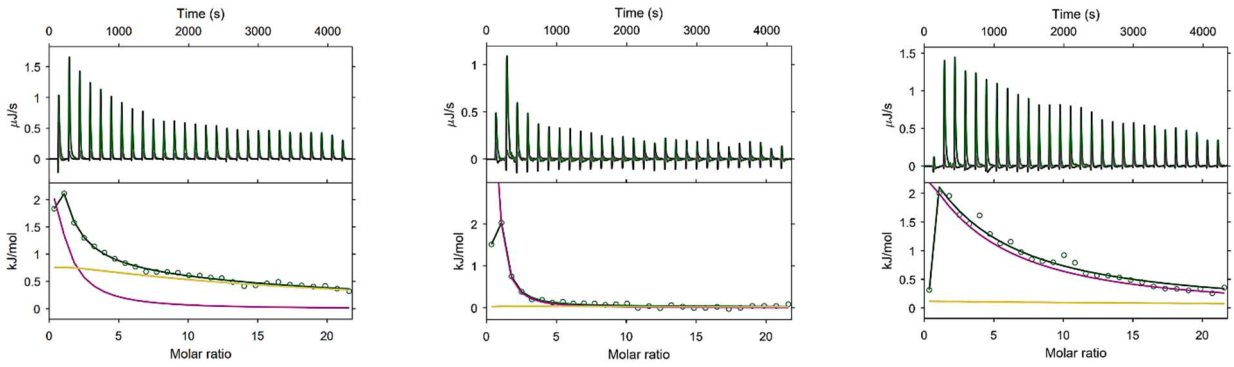

Figure S15 ITC thermogram (upper panel) and integrated data (lower panel) of the Ln^{3+} titration to 30 µM Eu-MDH with about 70% of Eu occupation. From left to right: Eu^{3+}, La^{3+}, Lu^{3+}. Figures were kindly provided by Dr. B. Drobot.

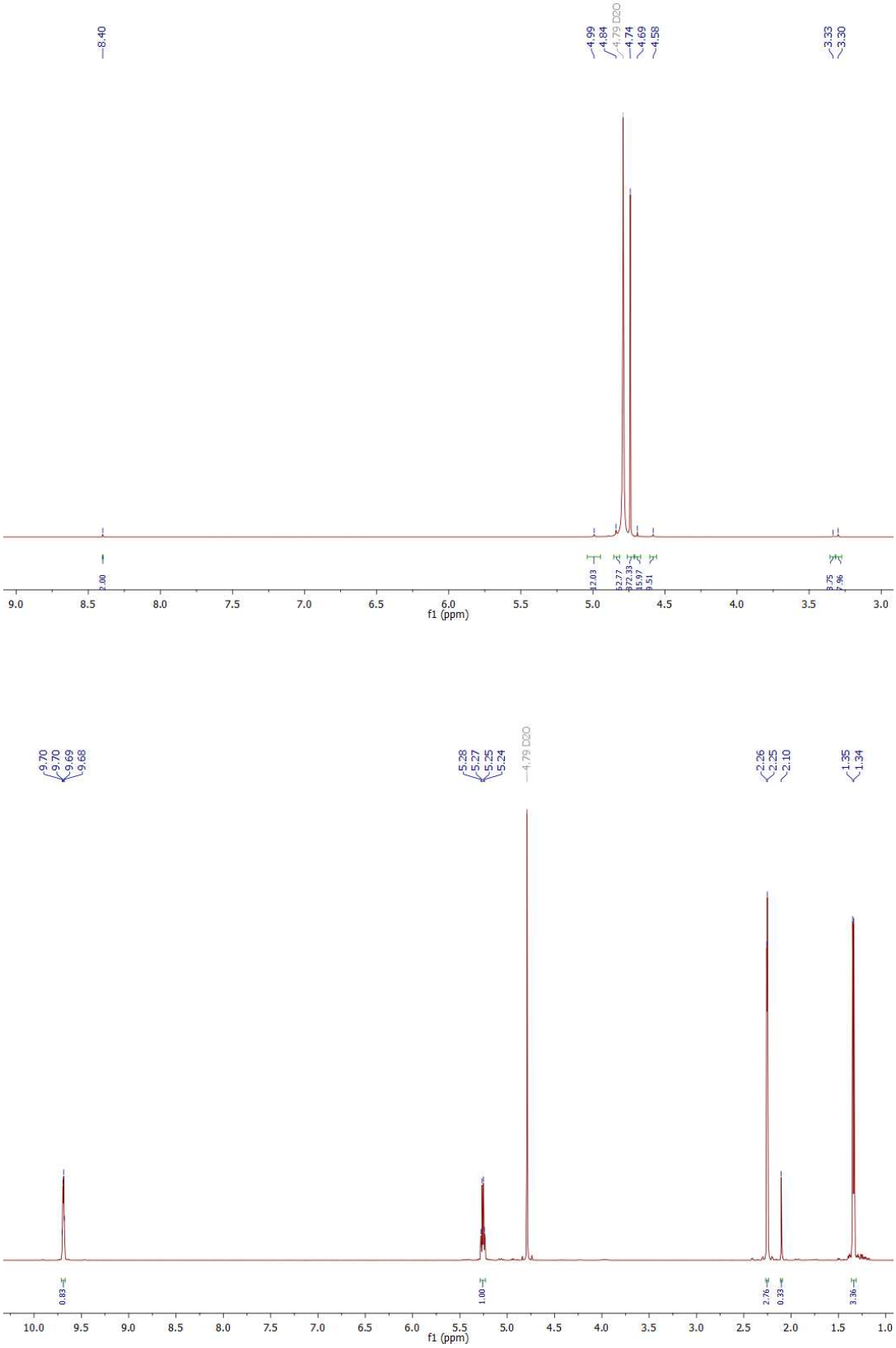

Figure S16 ^{1}H-NMR spectra of formaldehyde (upper spectrum) and acetaldehyde (lower spectrum) water mixtures in D_2O at room temperature.

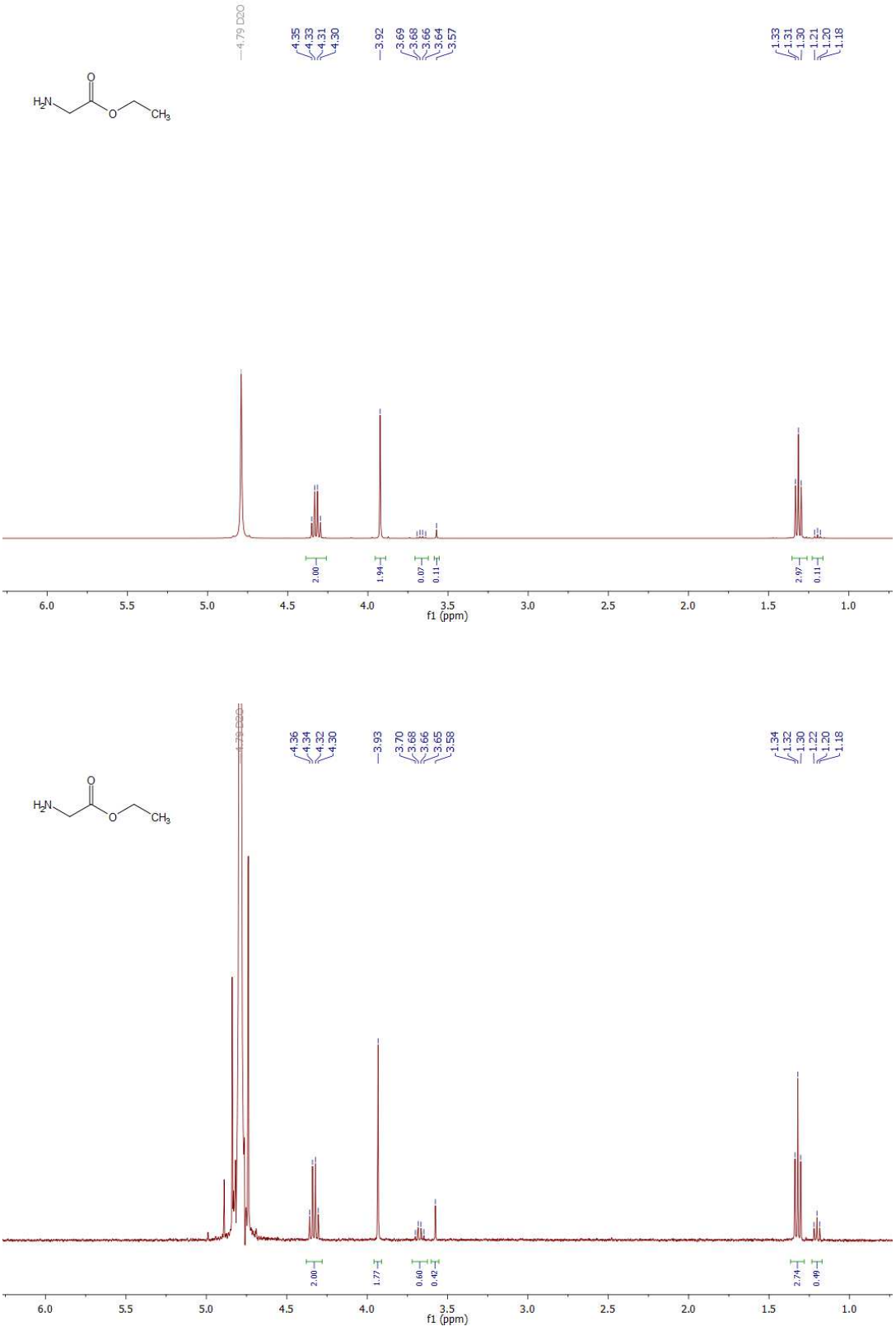

Figure S17 ^{1}H-NMR spectra of GEE in D_2O at pH 7. Samples were either stored at room temperature (upper spectrum) or heated at 45 °C for 10 min (lower spectrum).

3 Supplementary Tables

Table S1 Extinction coefficients of DCPIP in different buffer systems, at different pH values and temperatures that have been reported in the literature. a) Multicomponent buffer: 2.5 mM citric acid, 2.5 mM Bis-Tris, 2.5 mM Tris and 2.5 mM CHES.[104] *b) Corrected pH of buffer at 45 °C.*[123]

Extinction coefficient ε_{600nm} [$mM^{-1} \cdot cm^{-1}$]	**Buffer system**	**pH**	**Temperature [°C]**
14.0[108]	Phosphate	6.05	26
6.6[233]	-	6.05	-
18.5[234]	Phosphate	6.50	21
20.6[108]	Phosphate	7	26
19.1[195,196,235]	Phosphate	7	-
21.0[234]	Phosphate	7	20 – 30
17.8[234]	Phosphate	7	20
16.1[236]	Phosphate	7	30
18.5[71]	PIPES	7.2	45
19.1	Tris-HCl	8	30
21.5[49]	-	8	-
21.8[108]	-	8	26
21.9[108]	-	8.3	26
21.9[60]	Tris-HCl	8.5/9	26
19.0[155]	Tris-HCl	9	30
21.0[32,91]	Tris-HCl	9	30
21.5[49]	Tris-HCl	8	-
21.9[60]	Tris-HCl	9	26
22.0[133]	CHES	9	30
7.8 ± 0.2	Multicomponent buffer[a)]	5.3[b)]	45
11.3 ± 0.3	Multicomponent buffer[a)]	5.7 [b)]	45
14.4 ± 0.5	Multicomponent buffer[a)]	6.4[b)]	45
17.9 ± 0.5	Multicomponent buffer[a)]	6.7[b)]	45
18.8 ± 0.5	Multicomponent buffer[a)]	7.1[b)]	45
19.7 ± 0.5	Multicomponent buffer[a)]	7.4[b)]	45
19.7 ± 0.4	Multicomponent buffer[a)]	8.7[b)]	45

Table S2 Elemental analysis results of PMS and PES solids. The Lot# is provided in the materials section.

Phenazine species	Sample #	N [%]	C [%]	H [%]	S [%]
PMS	theoretical values	9.14	54.89	4.61	10.47
	1	8.97	54.71	4.70	10.45
	2	9.21	55.04	4.45	10.22
	3	9.32	54.05	4.41	10.58
PES	theoretical values	8.38	57.47	5.43	9.59
	1	8.25	57.25	5.49	9.77
	2	8.31	57.28	5.44	9.55
	3	8.32	57.61	5.44	9.56
	4	8.35	57.56	5.49	9.46

Table S3 Extinction coefficients of WB in different buffer systems, at different pH values and temperature. a) Multicomponent buffer: 2.5 mM citric acid, 2.5 mM Bis-Tris, 2.5 mM Tris and 2.5 mM CHES. b) Multicomponent buffer: 25 mM citric acid, 25 mM Bis-Tris, 25 mM Tris and 25 mM CHES.

Wavelength [nm]	Extinction coefficient ε_{610nm} [$mM^{-1} \cdot cm^{-1}$]	Buffer system	pH	Temperature [°C]
560	12.30[133]	100 mM CHES	9	30
600	9.00[237]	64 mM sodium borate	9	22
600	9.00[98]	100 mM tetrasodium pyrophosphate	9	22.5
610	9.75 ± 0.48	Multicomponent buffer[a)]	6.2	30
610	9.60 ± 0.34	Multicomponent buffer[a)]	7.0	30
610	9.53 ± 0.34	Multicomponent buffer[a)]	7.5	30
610	9.51 ± 0.26	Multicomponent buffer[a)]	8.1	30
610	8.82 ± 0.37	Multicomponent buffer[a)]	9.0	30
610	9.67 ± 0.41	Multicomponent buffer[b)]	7.0	30
610	8.17 ± 0.41	Multicomponent buffer[b)]	9.0	30
612	12.70[109]	50 mM MOPSO/ 50 mM CHES	7/9	20
640	2.14[107]	100 mM sodium tetraborate	9	-
640	2.78[133]	100 mM CHES	9	30
652	1.07[109]	50 mM MOPSO/ 50 mM CHES	7/9	20

Table S4 Molar extinction coefficients of DCPIP at 600 nm in either 10 mM multicomponent (MC) buffer (2.5 mM citric acid, 2.5 mM Bis-Tris, 2.5 mM Tris and 2.5 mM CHES) or 100 mM NaCl. Data were collected on an Epoch2 plate reader with path length correction and used for the calculation of the SA of SolV MDH.

Buffer system	pH	Temperature [°C]	ε_{600nm} [$mM^{-1} \cdot cm^{-1}$]
10 mM MC	5.8	45	12.44 ± 0.15
	6.2	45	15.40 ± 0.37
	6.7	45	18.85 ± 0.47
	7	45	19.79 ± 0.22
	7.2	25	20.05 ± 0.04
	7.2	30	19.84 ± 0.11
	7.2	35	19.55 ± 0.02
	7.2	40	19.33 ± 0.2
	7.2	45	19.09 ± 0.25
	7.2	49	18.81 ± 0.03
	7.6	45	20.98 ± 0.54
	8	45	21.29 ± 0.40
	8.5	45	20.63 ± 0.19
100 mM NaCl	7	45	15.52 ± 0.01

4 List of Abbreviations

A	Arrhenius pre-exponential factor
A_{280nm}	Absorbance at 280 nm
ADH	Alcohol dehydrogenase
AM1	*Methylorubrum extorquens* strain AM1
APS	Ammonium persulfate
ATP	Adenosine triphosphate
c	Concentration
CBB	Calvin-Benson-Bassham
CAPS	Cyclohexylamine-based buffer
CD	Circular dichroism
CHES	Cyclohexylamine-based buffer
cm	Centimeter
CN	Coordination number
d	Path length of cell
DCPIP	Dichlorophenol indophenol
DFT	Density functional theory
$[E_0]$	Total enzyme concentration
E_a	Activation energy
EA	Electron acceptor
EPR	Electron paramagnetic resonance
ESI	Electrospray ionization
EtOH	Ethanol
Eu-MDH	Europium-containing methanol dehydrogenase
ε	Molar extinction coefficient
FAD	Flavin adenine dinucleotide
FF	Flash frozen in liquid nitrogen
FPLC	Fast protein liquid chromatography
FT-IR	Fourier transform infrared (spectroscopy)
G	Gauss
GEE	Glycine ethyl ester
GWP	Global warming power

h	Hour
HEPES	Piperazine-based buffer
HREE	Heavy rare earth elements (Gd-Lu)
HR-MS	High resolution mass spectrometry
ICP-MS	Inductively coupled plasma mass spectrometry
ICP-OES	Inductively coupled plasma optical emission spectrometry
ITC	Isothermal titration calorimetry
K_{assoc}	Metal association constant
k_{cat}	Turnover number
K_d	Metal binding constant
k_D	Rate constant of reaction with heavy isotope
k_H	Rate constant of reaction with light isotope
K_i	Inhibition constant
K_m	Michaelis-Menten constant, measure for affinity
k_n	Rate constant of reaction with mixed isotopes
kDa	Kilodalton
KIE	Kinetic isotope effect
kJ	Kilojoule
KP	Potassium phosphate buffer
La-MDH	Lanthanum-containing methanol dehydrogenase
Ln	Lanthanide
LREE	Light rare earth elements (La-Eu)
M	Molar
mA	Milliampere
MC	Multicomponent buffer
MDH	Methanol dehydrogenase
MeOD	Deuterated methanol (d^3-MeOD)
MeOH	Methanol
MES	Morpholine-based buffer
MHz	Megahertz
min	Minute
MMO (pMMO/sMMO)	Methane monooxygenase (particulate/soluble)
mg	Milligram
ml	Milliliter

mm	Millimeter
mM	Millimolar
MOPS	Morpholine-based buffer
MOPSO	Morpholine-based buffer
MoxF	Old name for the big subunit of the Ca^{2+}-dependent methanol dehydrogenase
mV	Millivolt
MW	Molecular weight
MxaI	Small subunit of the Ca^{2+}-dependent methanol dehydrogenase
MxaF	Big subunit of the Ca^{2+}-dependent methanol dehydrogenase
*mxa*G	Gene encoding cytochrome c_L, the electron acceptor of the Ca^{2+}-dependent methanol dehydrogenase
µg	Microgram
µl	Microliter
µM	Micromolar
µs	Microsecond
NAD(P)	Nicotinamide adenine dinucleotide (phosphate)
Nd:YAG	Neodymium-doped yttrium aluminum garnet
nm	Nanometer
nM	Nanomolar
NMR	Nuclear magnetic resonance
OPO	Optical parametric oscillator
PAA	Polyacrylamide/bisacrylamide
PARAFAC	Parallel factor (analysis)
PDB	Protein Data Bank
PES	Phenazine ethosulfate
PIPES	Piperazine-based buffer
PMS	Phenazine methosulfate
ppm	Parts per million
PQQ	Pyrroloquinoline quinone
PQQH	Semiquinone form of pyrroloquinoline quinone
Pr-MDH	Praseodymium-containing methanol dehydrogenase
psi	Pound-force per square inch
R	Gas constant
REE	Rare earth elements

RNA	Ribonucleic acid
rpm	Revolutions per minute
RT	Room temperature
RuMP	Ribulose monophosphate
s	Second
[S]	Substrate concentration
SA	Specific enzymatic activity
SEM	Standard error of the mean
SDS-PAGE	Sodium dodecyl sulfate polyacrylamide gel electrophoresis
SolV	*Methylacidiphilum fumariolicum* strain SolV
SP-sepharose	Sulphopropyl sepharose resin
SSF	Sample specific factor
TEMED	Tetramethylethylenediamine
TMPD	*N,N,N',N'*-tetramethyl-p-phenylenediamine
TMPDD	*N,N,N',N'*-tetramethyl-p-phenylenediamine dihydrochloride
TRLFS	Time-resolved laser-induced fluorescence spectroscopy
U	(Enzyme) unit
UV	Ultraviolet
v_0	Initial velocity of enzyme
v_{max}	Maximal velocity of an enzyme under the given condition
WB	Wurster's blue
*xox*F	Gene encoding the lanthanide-dependent methanol dehydrogenase
XoxF	Lanthanide-dependent methanol dehydrogenase
XoxG	C-type cytochrome, the electron acceptor of the lanthanide-dependent methanol dehydrogenase

5 Publications

5.1 Original Publications Published as Part of This Thesis and Statement of Contribution

Understanding the chemistry of the artificial electron acceptors PES, PMS, DCPIP and Wurster's Blue in methanol dehydrogenase assays

Bérénice Jahn, Niko S. W. Jonasson, Hurina Hu, Helena Singer, Arjan Pol, Nathan M. Good, Huub J. M. Op den Camp, N. Cecilia Martinez-Gomez, Lena J. Daumann*

J. Biol. Inorg. Chem. **25**, 199–212 (2020).

Bérénice Jahn (Ludwig-Maximilians-University Munich, supervisor: Prof. Dr. Lena Daumann) measured all UV-visible absorption and EPR spectra and additionally IR spectra of the PMS and PES samples. Bérénice Jahn performed enzyme activity assays as well as wrote the main part of the manuscript together with Prof. Dr. Lena Daumann and synthesized Wurster´s blue compounds together with Helena Singer (Ludwig-Maximilians-University Munich, supervisor: Prof. Dr. Lena Daumann). Niko Jonasson (Ludwig-Maximilians-University Munich, supervisor: Prof. Dr. Lena Daumann) measured mass spectra together with Hurina Hu (Ludwig-Maximilians-University Munich, practical student of Bérénice Jahn) and wrote the respective part of the manuscript. Hurina Hu additionally synthesized a Wurster´s blue sample and pyocyanin and measured NMR spectra. Dr. Arjan Pol (Radboud University Nijmegen, Netherlands, group of Prof. Dr. Huub J. M. Op den Camp) cultivated *M. fumariolicum* SolV and purified the MDH enzyme together with Prof. Dr. Lena Daumann. Dr. Nathan Good (Michigan State University, East Lansing, MI, USA, group of Dr. N. Cecilia Martinez-Gomez) cultivated *M. extorquens* AM1 and purified the MDH enzyme. Each author also revised the manuscript.

Similar but Not the Same: First Kinetic and Structural Analyses of a Methanol Dehydrogenase Containing a Europium Ion in the Active Site

Bérénice Jahn, Arjan Pol, Henning Lumpe, Thomas R. M. Barends, Andreas Dietl, Carmen Hogendoorn, Huub J. M. Op den Camp, Lena J. Daumann*

ChemBioChem **19**, 1147–1153 (2018).

Bérénice Jahn (Ludwig-Maximilians-University Munich, supervisor: Prof. Dr. Lena Daumann) performed all enzyme activity assays and wrote the main part of the manuscript together with Prof. Dr. Lena Daumann. Dr. Arjan Pol (Radboud University Nijmegen, Netherlands, group of Prof. Dr. Huub J. M. Op den Camp) cultivated *M. fumariolicum* SolV and purified the Eu-MDH enzyme together with Prof. Dr. Lena Daumann, who also conducted the UV-visible absorption measurements of the enzyme. Dr. Henning Lumpe (Ludwig-Maximilians-University Munich, supervisor: Prof. Dr. Lena Daumann) performed DFT calculations and wrote the respective part of the methods section and edited the related images and supporting information. Andreas Dietl (Max-Planck Institute for Medical Research, Heidelberg, Germany, supervisor: Dr. Thomas R. M. Barends) grew MDH protein crystals, performed X-ray diffraction analysis and interpreted the data with the help of his supervisor. Carmen Hogendoorn (Radboud University Nijmegen, Netherlands, supervisor: Prof. Dr. Huub J. M. Op den Camp) performed the SolV growth experiments in the presence of different lanthanides. Each author also revised the manuscript.

5.2 Original Publications That Are Not Part of This Thesis

One Enzyme Three Techniques: Photochemistry of Europium-dependent Methanol Dehydrogenase
Preliminary authors: Bérénice Jahn, Nader A. Danaf, Björn Drobot, Robin Steudtner, Arjan Pol, Don C. Lamb, Michael Seitz, Huub J. M. Op den Camp, Lena J. Daumann*
Manuscript in preparation

Weder Erden noch selten. Die faszinierende bioanorganische Chemie der Selten-Erd-Elemente
Bérénice Jahn and Lena J. Daumann*
Chem. Unserer Zeit **52**, 150–158 (2018).

5.3 Original Publications Published Prior to This Thesis

Micropatterning as a tool to identify regulatory triggers and kinetics of actin-mediated endothelial mechanosensing
Florian A. Gegenfurtner, Bérénice Jahn, Helga Wagner, Christoph Ziegenhain, Wolfgang Enard, Ludwig Geistlinger, Joachim O. Rädler, Angelika M. Vollmar, Stefan Zahler
J. Cell Sci. **131**(10), jcs212886 (2018).

5.4 Poster Presentations

The Surprising Bioinorganic Chemistry of Rare Earth Elements - Spectroscopic Models for the Characterization of REE-dependent Methanol Dehydrogenases

Henning Lumpe, Bérénice Jahn, Violeta Vetsova, Patrick Grassl, Sina Witzel, Arjan Pol, Huub J. M. Op den Camp, Lena Daumann

13. Koordinationschemie-Tagung **2017**, March 5-7, Potsdam, Germany

Investigation of the Mechanistic Role of Rare Earth Elements in Methanol Dehydrogenases

Bérénice Jahn, Surbhi Jain, Arjan Pol, Carmen Hogendoorn, Huub J. M. Op den Camp, Lena J. Daumann

14. Koordinationschemie-Tagung **2018**, March 11-13, Heidelberg, Germany

The Features of the Europium(III)-containing Methanol Dehydrogenase Investigated Employing its Luminescence Properties

Nader A. Danaf, Bérénice Jahn, Arjan Pol, Huub J. M. Op den Camp, Michael Seitz, Lena J. Daumann, Don C. Lamb

15. Koordinationschemie-Tagung **2019**, March 3-5, Munich, Germany

5.5 Oral Presentations

Activity Studies of the First Europium(III)-containing Methanol Dehydrogenase Using an Improved Assay Protocol

Bérénice Jahn, Arjan Pol, Huub J. M. Op den Camp, Lena J. Daumann

15. Koordinationschemie-Tagung **2019**, March 3-5, Munich, Germany

6 Disclosure of Participation

The following people mentioned underneath, contributed in the practical laboratory work of this thesis, as part of their research internships:

Bettina Motycka performed Michaelis-Menten kinetics with La-MDH and La^{3+} titrations.

Isabel Müller and **Sosena Mesfin** performed pre-experiments that are not presented in this thesis.

Hurina Hu synthesized a sample of the WB dye which was used in parts of this work.

Sebastian Preussger performed Michaelis-Menten kinetics of Eu-MDH with alcohols and recorded CD spectra of the lanthanide derivatives of MDH.

The following people mentioned underneath contributed to this work, as part of a cooperation:

Dr. Arjan Pol assisted in MDH purification together with **Helena Singer** at the Radboud University in Nijmegen, Netherland.

Dr. Björn Drobot and **Dr. Robin Steudtner** measured TRLFS spectra of Chelex®-treated solutions, PIPES and MDH samples at the HZDR in Dresden, Germany. **Dr. Björn Drobot** additionally assisted in ITC measurements.

7 Acknowledgements

Zuallererst möchte ich mich bei Frau Prof. Dr. Lena Daumann für die Betreuung meiner Doktorarbeit bedanken. Vielen Dank Lena, dass Du mir das Vertrauen geschenkt hast, in Deinem Arbeitskreis promovieren zu dürfen. Du hattest immer ein offenes Ohr für mich und hast mich unterstützt, wann immer ich es gebraucht habe. Die Zeit im AK Daumann war eine schöne und lehrreiche Zeit. Vielen Dank für die zahlreichen Möglichkeiten, die Du mir in Form von Weiterbildungen, Konferenzbesuchen und Forschungsaufenthalten bei Kooperationspartnern gegeben hast.

Ein weiterer großer Dank geht an Herrn PD Dr. Dietmar Martin. Vielen Dank, dass Sie das Zweitgutachten meiner Arbeit übernommen haben und den damit verbundenen zeitlichen Aufwand.

Des Weiteren möchte ich mich bei Herrn Prof. Dr. Huub Op den Camp, Herrn Prof. Dr. Hans-Christian Böttcher, Herrn Prof. Dr. Stefan Schwarzer und Frau Prof. Dr. Bettina Lotsch für das Mitwirken in der Prüfungskommission bedanken.

Prof. Dr. Huub Op den Camp und Dr. Arjan Pol danke ich für die schöne und erfolgreiche Kooperation und die lehrreiche Zeit an der Radboud Universität in Nimwegen. Ich habe die Zeit in Holland sehr genossen.

Dr. Robin Steudtner und Dr. Björn Drobot danke ich für die interessante Kooperation und guten Gespräche am HZDR und der TU Dresden. Vielen Dank, dass ich so nett aufgenommen wurde.

Prof. Dr. Don Lamb und Nader Danaf danke ich für die interessanten Einblicke in die Fluoreszenzspektroskopie und langen Gespräche im Rahmen unserer Kooperation.

Dr. N. Cecilia Martinez-Gomez und Dr. Nathan Good danke ich für die Bereitstellung der AM1 MDH und die erfolgreiche Kooperation.

Ein großer Dank geht an den AK Daumann und alle ehemaligen Mitglieder. Danke für die schöne Zeit und netten Gespräche und die vielen Hilfestellungen und Diskussionsrunden rund um meine Arbeit. Danken möchte ich in diesem Zusammenhang v.a. Helena und Violeta für die tolle Freundschaft; Helena für ihre hilfsbereite und nette Art und die schöne Zeit in und außerhalb des Labors und Violeta

für ihr immer offenes Ohr. Außerdem möchte ich Henning und Tri für die nette Atmosphäre im Labor danken. Ich werde es vermissen. Ein besonderer Dank gilt auch Lauren, die sich die Zeit genommen hat, meine Arbeit gründlich Korrektur zu lesen.

Des Weiteren danke ich meinen Praktikanten und meinem Bacheloranten für die motivierende Projektarbeit, die Unterstützung im Labor und die netten Gespräche, namentlich: Bettina Motycka, Isabel Müller, Sosena Mesfin, Hurina Hu und Sebastian Preussger.

Ein besonderer Dank gilt meinen Eltern, die mich in all meinen Entscheidungen unterstütz und bekräftigt haben, und mir die Freiheit gegeben haben, meinen Weg so zu gehen, wie ich es wollte. Ohne euch wäre ich nicht der Mensch geworden, der ich heute bin. Vielen Dank für Eure bedingungslose Liebe und Unterstützung. Des Weiteren möchte ich meiner Babcia danken, die immer für mich da war.

Last but not least, möchte ich Max für seine immerwährende Unterstützung danken. Vielen Dank, dass Du immer für mich da bist und für die schöne Zeit, die wir schon verbracht haben, und noch verbringen werden.